AWARD NUMBER: W81XWH-16-C-0123

TITLE: Modeling Metabolic Exhaustion of the Auditory System

PRINCIPAL INVESTIGATOR: Philemon Chan, PhD

CONTRACTING ORGANIZATION: L3 Applied Technologies, Inc.
SAN DIEGO, CA 92121

REPORT DATE: NOVEMBER 2019

TYPE OF REPORT: FINAL

PREPARED FOR: U.S. Army Medical Research and Materiel Command
Fort Detrick, Maryland 21702-5012

REPORT DOCUMENTATION PAGE		*Form Approved* *OMB No. 0704-0188*
Public reporting burden for this collection of information is estimated to average 1 hour per response, including the time for reviewing instructions, searching existing data sources, gathering and maintaining the data needed, and completing and reviewing this collection of information. Send comments regarding this burden estimate or any other aspect of this collection of information, including suggestions for reducing this burden to Department of Defense, Washington Headquarters Services, Directorate for Information Operations and Reports (0704-0188), 1215 Jefferson Davis Highway, Suite 1204, Arlington, VA 22202-4302. Respondents should be aware that notwithstanding any other provision of law, no person shall be subject to any penalty for failing to comply with a collection of information if it does not display a currently valid OMB control number. **PLEASE DO NOT RETURN YOUR FORM TO THE ABOVE ADDRESS.**		
1. REPORT DATE NOVEMBER 2019	**2. REPORT TYPE** Final Report	**3. DATES COVERED** 15AUG2016 - 18AUG2019
4. TITLE AND SUBTITLE Modeling Metabolic Exhaustion of the Auditory System		**5a. CONTRACT NUMBER** W81XWH-16-C-0123
		5b. GRANT NUMBER
		5c. PROGRAM ELEMENT NUMBER
6. AUTHOR(S) Zagadou, B., Chan, P., Ho, K.		**5d. PROJECT NUMBER**
		5e. TASK NUMBER
		5f. WORK UNIT NUMBER
7. PERFORMING ORGANIZATION NAME(S) AND ADDRESS(ES) L3 ATI 10180 Barnes Canyon Road San Diego, California 92121-2724		**8. PERFORMING ORGANIZATION REPORT NUMBER**
9. SPONSORING / MONITORING AGENCY NAME(S) AND ADDRESS(ES) U.S. Army Medical Research and Materiel Command Fort Detrick, Maryland 21702-5012		**10. SPONSOR/MONITOR'S ACRONYM(S)**
		11. SPONSOR/MONITOR'S REPORT NUMBER(S)
12. DISTRIBUTION / AVAILABILITY STATEMENT Approved for public release; distribution is unlimited.		
13. SUPPLEMENTARY NOTES		

14. ABSTRACT

This report describes the results of the two-year project sponsored by the US Army Medical Research and Development Command (USAMRDC) to develop a metabolic exhaustion (ME) model of the auditory system to account for the effect of complex noise exposures on dose accumulation for the development of auditory damage risk criteria. Using chinchilla auditory temporary threshold shift (TTS) data from exposure to complex noise, a ME model was developed that predicts the effects of complex noise exposure on TTS. The complex impulse noise was composed of multiple impulses of unequal intensities and unequal inter-pulse intervals(IPI), and in some cases including the presence of high-intensity background noise. The chinchilla ME model was validated with data comparison and provided an understanding of the mechanism of injury by damage accumulation inside the cochlea. The chinchilla model was adapted to construct the human ME model using cochlear tissue stiffness data measured from chinchilla and human cadaver ears.

The ME model is based on a mechanistic description of the energy deficit occurring within the outer hair cells (OHC) inside the cochlea as a result of complex noise exposure. The straining energy of the OHC caused by the noise exposure exceeding a threshold leads to increase in metabolic demand while supply is insufficient that can cause damage. An electroacoustic model of the cochlea including the OHC was developed that calculates the OHC energy deficit (OHC-ED) as the integrated difference between the rate of work of stress within the OHC and available power supply. The OHC-ED was correlated to TTS data to establish the dose-response curve for complex noise exposure.

The major findings of this study are summarized as follows. There was a good correlation between the OHC-ED predictions and TTS data from chinchillas. The dose-response curve was established with a good fit and relative tight confidence band, considering the small data sample size. The ME model showed that the energy supply was low in general, explaining the high injury rate observed in the complex noise exposure experiment. For the relatively high-level impulses considered in this study, the energy deficit was practically equal to the energy demand. The relatively short IPI also contributed to the low energy supply. The ME model suggests that the effect of IPI on the order of 1 second on injury is not significant, but the effect of moderately high intensity background noise is significant. The chinchilla ME model is also able to track the effect of very long IPI on the order of minutes on injury. The chinchilla ME model developed in this project provides a good foundation for understanding noise-induced auditory exhaustion from multiple shots in humans for which data are still currently lacking.

In addition, an empirical dose accumulation algorithm in the ME regime for complex noise with IPI on the orders of seconds was developed following the previous approach for the Auditory 4.5 model, and the protective effects from acoustic reflex were explored for exposure conditions representatives of flashbangs with findings documented.

15. SUBJECT TERMS Impulse noise, auditory injury, biomechanics, cochlea, outer hair cells, metabolic exhaustion, energy deficit					
16. SECURITY CLASSIFICATION OF:			17. LIMITATION OF ABSTRACT	18. NUMBER OF PAGES	19a. NAME OF RESPONSIBLE PERSON USAMRMC
a. REPORT U	b. ABSTRACT U	c. THIS PAGE U	U	121	19b. TELEPHONE NUMBER *(include area code)*
					Standard Form 298 (Rev. 8-98) Prescribed by ANSI Std. Z39.18

Table of Contents

Figures

Tables

Part 1: Modeling Metabolic Exhaustion of the Auditory System

1.1 Introduction

Sponsored by the U. S. Army Medical Research and Material Command (USAMRMC), L3 Applied Technologies, Inc. (L3 ATI) completed the previous project to improve and validate the Auditory Hazard Assessment Algorithm for Humans (AHAAH) (Price and Kalb 1991; Zagadou et al., 2016). Critical improvements were made to the middle ear and the integrated cochlear energy (ICE) was used as the damage correlate. The ICE-based model was validated against the Blast Overpressure Project (BOP) human walk-up data and the German rifle data and recommended for use as the new biomechanically-based auditory standard against blast injury. The AHAAH-based ICE model still only simulates mechanical damage and do not address damage accumulation from complex noise with unequal impulses at unequal intervals.

There is very limited research addressing dose accumulation mechanism for predicting auditory injury risk. The Panel of the American Institute of Biological Sciences (AIBS) recommended the development of a metabolic exhaustion (ME) model (Wightman et al., 2010) to address the fundamental mechanism of temporary damage, recovery and permanent damage progression so that dose accumulation can be calculated correctly from exposures to a complex mixture of noise in real life. This capability is necessary to meet the modern day military needs in impulse noise injury assessments that far exceed the capabilities provided by traditional approaches including the current ICE model and AHAAH. In fact, the dose accumulation algorithm in the current MIL-STD-1474E assumes multiple impulses are presented at equal intensities and equal intervals; however, the spacing between impulses is not specified. For occupational training, the shot intervals could vary from seconds for small arms firings to perhaps minutes for large weapon exercises. Operational conditions involve a complex mixture of irregular impulses including blasts riding on top of intense continuous noises that are far too challenging for any existing injury assessment methods. The current biomechanically-based auditory models need to be generalized to predict the accumulative effect and recovery from cellular exhaustion.

Animal data show complex injury trends from complex noise exposure. Henderson, Subramaniam et al. (1991) showed that the effect of impact noise combined with a continuous noise does not follow the simple additive rule. The inter-pulse interval (IPI) can have a greater effect at low sound pressure levels (~125 dB) versus higher levels (~137 dB) (Henderson, Subramaniam et al. 1991). The mixing of IPI exacerbates injury in chinchillas (Danielson, Henderson et al. 1991). A ME model is needed to capture the dose accumulation mechanism to include the effect of silence and recovery on damage in cochlear tissues.

The objective of this 2-year project was to develop a ME model to account for the effect of complex noise exposures on auditory injury. An energy deficit model of the hair cells inside the cochlea was developed using data from chinchilla exposures to complex noise, including multiple, moderate level blasts with unequal intensity and unequal IPI riding on top of continuous background noise. The chinchilla complex noise exposure data were collected at the University of California San Diego (UCSD). The chinchilla ME model was validated with data comparison and provided an understanding of the mechanism of injury by damage accumulation inside the cochlea. The chinchilla ME model was adapted to construct the human model. Cochlear tissue stiffness data were collected at Boston University (BU) and Massachusetts Ear and Eye Infirmary (MEEI) using both chinchilla and human cadaver ears, respectively. This report is organized in sections including the introduction, methods, results, discussion, and conclusion, respectively. Key accomplishments and reportable outcomes are listed before the conclusion.

1.2 Construction of Metabolic Exhaustion Model

This section describes the cochlear model developed to study metabolic exhaustion within the cochlear cells resulting from complex noise exposures. The cochlear model is the platform for the ME model, and hence an accurate representation of cochlear mechanics is critical. In the following, the anatomical simplifications and electroacoustic analog of the cochlea model, cochlear equations, and solutions implementation in MATLAB are described.

1.2.1 Construction of Electroacoustic Analog

1.2.1.1 Description of Cochlear Electroacoustic Analog

Figure 1 illustrates the analogy between the anatomically simplified cochlear cross-section components and their electro-acoustic representation. The electro-acoustic model represents a generic model formulation for cochlear mechanics that can be adapted to study various species including humans, provided material properties are available.

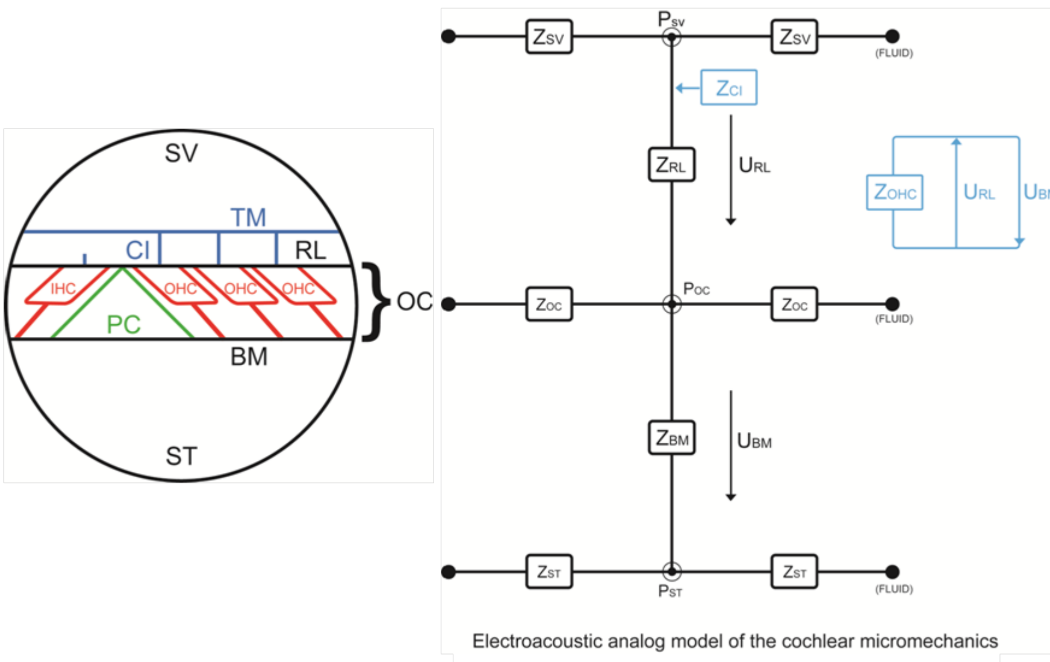

a) **b)**

Figure 1. Electroacoustic analog of the cochlear cross section. a) Simplified anatomy of the cochlear cross section. b) Electroacoustic analog of the cross section (1 section, Δx shown).

Figure 1a shows a simplified cochlear cross-section including the fluid compartments and the dominant cochlear structures. The fluid compartments are the scala vestibuli (SV), scala tympani (ST), and organ of Corti (OC). The represented cellular components are the basilar membrane

(BM), tectorial membrane (TM), reticular lamina (RL), pillar cells (PC), cilia (CI), and inner and outer hair cells (IHC and OHC).

Figure 1b shows one unit of the analog model composed of two adjacent cross-sections spanning a distance, Δx, along the cochlea. In the analog model, SV, ST, and OC fluids are modeled as fluid lines and represented by their impedances, Z_{SV}, Z_{OC}, and Z_{ST}, respectively. The fluid pressures, P_{SV}, P_{OC}, and P_{ST} are shown as nodes between two contiguous representative cross-sections. The RL and BM components are modeled as parallel impedances, Z_{RL} and Z_{BM}. All components are dependent on the longitudinal distance, x, from the base of the cochlea. The BM and RL volumes velocities (U_{RL}, U_{BM}) are indicated by the arrows in the analog model. The OHC is represented by its impedance Z_{OHC} and the OHC volume velocity (U_{OC}) is the difference between the volume velocity of the BM and RL (U_{RL}-U_{BM}). The cilia displacement is considered proportional to the RL displacement since the base of the tectorial membrane is hinged on the bony shelf.

1.2.1.2 Description of Cochlear Equations

The basic equations for the electro-acoustic model of the cochlear micromechanics for a pure tone with angular frequency ω vibrating the stapes are given by the following differential equations.

$$\frac{d^2 P_{SV}}{dx^2} = \frac{Z_{SV}}{(\Delta x)^2} U_{RL} \tag{1}$$

$$\frac{d^2 P_{ST}}{dx^2} = -\frac{Z_{ST}}{(\Delta x)^2} U_{BM} \tag{2}$$

$$\frac{d^2 P_{OC}}{dx^2} = \frac{Z_{OC}}{(\Delta x)^2} (U_{RL} - U_{BM}) \tag{3}$$

$$P_{SV} - P_{OC} = \left(Z_{RL} + Z_{OHC} - i\frac{g_{OHC}}{\omega} e^{\left(-\frac{k\cdot x}{L}\right)}\right) U_{RL} - Z_{OHC} U_{BM} \tag{4}$$

$$P_{OC} - P_{ST} = \left(-Z_{OHC} + i\frac{g_{OHC}}{\omega} e^{\left(-\frac{k\cdot x}{L}\right)}\right) U_{RL} + (Z_{BM} + Z_{OHC}) U_{BM} \tag{5}$$

The unknown variables for the cochlear fluid and cellular components are the pressures and volume velocities denoted by the P and U, respectively, where the subscritpts indicate the fluid or structure component of the cochlea. For example, P_{SV} and P_{ST} indicate the pressure in SV and ST, respectively, and U_{RL} is the volume velocity of the RL. L is the total length of the cochlea. The model input is the stapes volume velocity, and the outputs are P and U along the cochlear length.

The cochlear amplifier (CA) is represented by an exponential term with amplitude g_{OHC}, modeling the OHC gain, and a spatial decay term described by the space constant L/k, where k is a constant. The active OHC force is assumed to be proportional to the RL volume velocity.

From Eq. 1 to 3, the fluid impedance for SV, ST, and OC are each represented by its mass component only, i.e., Z = i·ω·ρ·Δx/A, were A represents the area of the ST, SV and OC, respectively, with ρ being the density of cochlear fluids set equal to that of water.

The BM impedance is given by:

$Z_{BM} = R_{BM} + i\,(\,\omega L_{BM} - 1/(\omega C_{BM}\,)$, where

$R_{BM} = \sqrt{L_{BM}/C_{BM}}/Q$

$L_{BM} = 1/(C_{BM} \cdot (2\pi \cdot CF)^2)$ and Q represents the resonance quality factor, whose value is chosen to match the BM response from the model to experimental data.

The impedances for the OHC and RL are defined based on the BM impedance.

The following boundary conditions (BC) must be satisfied for Eqs. 1-5. At the basal end (x = 0), the BCs involves the stapes volume velocity as the input to the model, and the round window volume velocity is equal to the stapes volume velocity. At the apical end (x = L), the SV and ST pressures must be equal. The OC is closed at the basal and apical ends.

In the actual simulations, additional terms were added to Eqs. 1-5 to include the effects of the longitudinal variation of the area of the scalae and fluid viscosity.

1.2.1.3 Solution Implementation in MATLAB

1.2.1.3.1 *Discretized Equations*

The solution of the cochlear equations was implemented using MATLAB software. The five electro-acoustic differential equations were non-dimensionalized and discretized using the finite difference (FD) method. Using FD, the spatial derivative of the variable at a given node in the model is approximated using the values of the variable at the neighboring nodes. The cross-sections are thus connected along the length of the model, and the end nodes are used to set the BCs in the model.

The cochlear length is divided in N = 400 sections with length Δx = L/N. The discrete equations lead to a matrix equation, Eq. 6, that is solved using direct matrix inversion in MATLAB. The resulting matrix equations were solved for the pressure P and velocity U for all components of the cochlea model.

$$AX=B \qquad (6)$$

- $X = [X_1\ X_2 \ldots X_j \ldots X_{N+1}]$ is the vector solution or unknown
- $X_j = [P_{ST}\ P_{SV}\ P_{OC}\ U_{RL}\ U_{BM}]^{(j)}$, for each node j
- $B = B(\omega)$ is the forcing term at the stapes (the input)
- $A = A(\omega)$ is the frequency-dependent matrix of coefficient

Since the matrix Eq. 6 is dependent on the frequency, ω, the solution for a pure tone stimulus can be easily calculated. To obtain the solution for an arbitrary stimulus transmitted to the stapes, the electroacoustic model response for all the frequencies contained in the stimulus signal must be calculated. The details of the procedure are described next.

1.2.1.3.2 *Cochlear Response Calculation*

To calculate the cochlea response for arbitrary stapes velocity input, a frequency domain solution of the electroacoustic equations is sought that requires the modal response (mode) of the cochlear model. The modal response of the cochlea is defined as the frequency response to the unit stapes volume velocity. To obtain the frequency response of the cochlea for arbitrary stapes velocity input, the modal response is multiplied by the stapes volume velocity in the frequency domain. The time domain response is obtained by converting the response back to time domain using inverse Fourier transform (IFFT).

The procedure is summarized by the following set of equations.

$$U_s(\omega) = 1 \implies Y_{mode}(x,\omega) \qquad (Y_{mode}\text{: Cochlear mode}) \qquad (7)$$

$$U_s(\omega) \neq 1 \implies Y(x,t) = IFFT[U_s(\omega) \cdot Y_{mode}(x,\omega)] \qquad (Y\text{: Cochlear solution}) \qquad (8)$$

$$U_s(\omega) = FFT\big(U_s(t)\big) \qquad (U_s\text{: Stapes response}) \qquad (9)$$

The cochlear solution, Y represents the volume velocity (U) or the pressure (P) for the cochlear component of interest.

The number of cochlear modes (Nm) required for the calculation of the cochlear response to an arbitrary stapes volume velocity is given by the product of duration (Td) of the time signal and the Nyquist frequency (Nf) (half of the signal sampling rate, fs), i.e., Nm = Nf*Td. Hence, Nm can be very large for a long duration pressure-time waveform sampled at a high rate, which is typical for impulse noise pressure trace, and mode calculations can be time consuming.

In practice, the number of modes will be limited by the upper limit of hearing, at least for the OHC variables of interest, and the computation time can be reduced considerably. In addition, the cochlear modes are calculated only once and used for subsequent calculation of cochlear response for arbitrary stapes input. A parallelized computation method was used to speed up the mode calculation.

The passive mode ($g_{OHC} = 0$) was used to calculate all of the cochlear variables needed to quantify the energy deficit within the OHC as a result of the multiple noise exposure, as described in the following section.

1.2.2 Description of Cellular Energy Deficit Model

The main assumption of the cellular deficit model is that the straining energy of the cochlear tissues exceeding a threshold leads to increase in metabolic demand while the supply is insufficient that can cause damage. The energy deficit model is illustrated in Figure 2 and formulated in Eqs. 10-11.

Figure 2 displays the diagram for the power within a given cellular component versus the rate of work (W) by sound-induced stress. The power required (Pr) to maintain the cellular function is increased during the sound exposure while the power supply (Ps) reaches its maximum at the critical power from sound-induced stress (Wc). The time integral of the difference determines the energy deficit (D) that is related to the threshold shift experienced post-exposure.

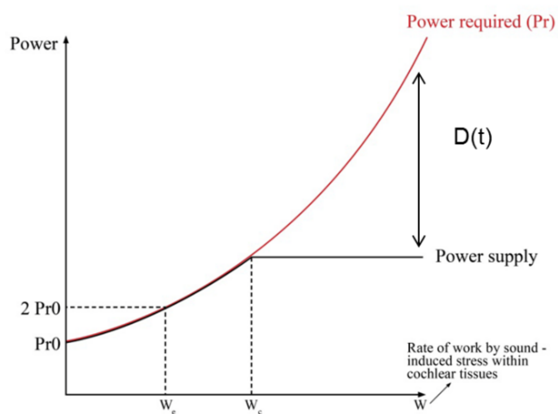

Figure 2. Diagram of cochlear cellular energy deficit model

The cellular energy deficit equation is given in Eq. 10:

$$D = \wp_{r0} \int_{base}^{apex} \int_0^T \left[\left(\frac{W(x,t)}{W_e(x,t)} \right)^\beta - \left(\frac{W_c(x,t)}{W_e(x,t)} \right)^\beta \right] dt dx \tag{10}$$

$$W(x,t) = U(x,t) \cdot P(x,t) \tag{11}$$

- $\wp r_0$ = 5.6 µCal/min
- W_c: critical power from noise-induced stress
- W_e: normalization factor
- P: pressure
- U: volume velocity
- T = total duration of exposure
- *x*: cochlear location
- *t*: time variable
- β: free parameter

W is calculated along the cochlear length using the electro-acoustic model described in the previous section, and D is calibrated using animal injury data from complex noise exposures.

The following adjustments were made to account for the differences between chinchilla and other species. The power required at rest, $\wp_{r0}$ given in micro-calorie per minute (µCal/min) ranges from 5.6 to 7.8 for guinea pig; the lower bound was used for chinchilla. The critical power, W_c is calculated as the cochlear model response to pink noise exposure at 75 dBA, while the normalization factor W_e is obtained from pink noise at 65 dBA. Since the dB levels were specified for humans, W_e and W_c were reduced by a factor of 10 for chinchilla.

The OHC, which is the most susceptible cochlear component to damage is used to calculate D. Therefore, all W calculations refer to the OHC. In practice, the mean value for W_e was chosen. Also, the discrete locations along the cochlear length, x were selected to be the critical bands of the cochlea. Eq. 10, is thus simplified to yield Eq. 12.

$$D = \frac{\wp_{r0}}{\langle W_e^\beta \rangle} \sum_{i=1}^{23} \int_0^T \left[W^\beta(x_i,t) - W_c^\beta(x_i,t) \right] dt \tag{12}$$

This alternate formula was used to calculate D for all the results that are presented later in the result section. The OHC energy, E_{OHC}, as identified in the first term of Eq. 12 is also calculated for comparison.

1.2.3 Middle and Outer Ear Models

1.2.3.1 Chinchilla Middle Ear Transfer Function

The available chinchilla measurement data from literature was used to construct the outer ear to middle ear transfer function (TF). The TFs from the free field (FF) to the eardrum and eardrum to the stapes were cascaded and used to transfer the complex noise to the stapes through the middle ear and to calculate the stapes velocity that is used as the input to the ME cochlear model.

The TF from the FF to eardrum (TFOE) was obtained by combining the data from (Murphy & Davis, 1998) and (Koka, Jones, Thornton, Lupo, & Tollin, 2011). Figure 3 shows the combined TFOE.

For the middle ear the stapes velocity TF (SVTF) data from (Robles, Temchin, Fan, & Ruggero, 2015) was used. Figure 4 shows the plot for SVTF, and Figure 5 shows the resulting open-ear to stapes velocity TF (TF_{OE2ST}) from the cascaded TFOE and SVTF.

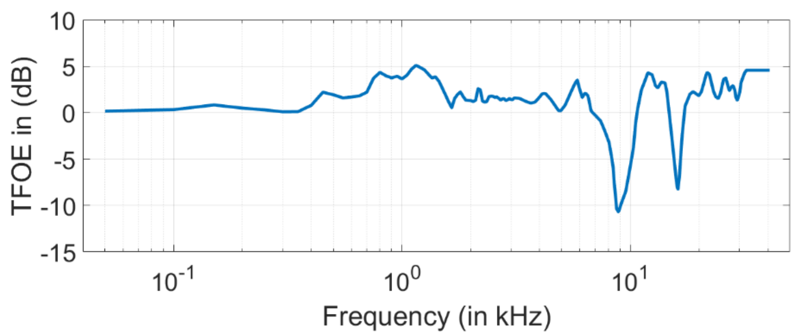

Figure 3. Combined TFOE from Murphy et al. (1998) and Koka et al. (2010)

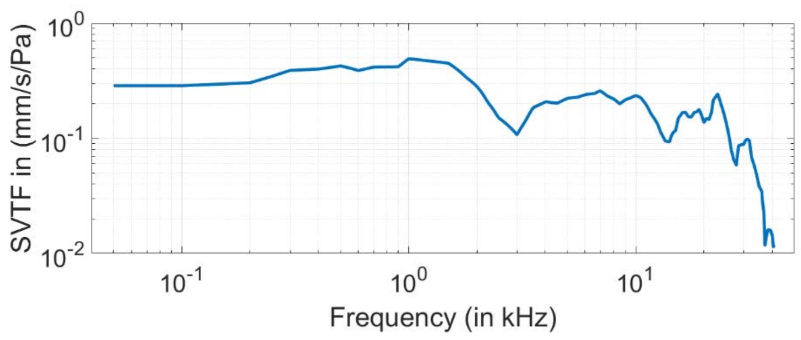

Figure 4. Chinchilla SVTF from Robles et al 2015.

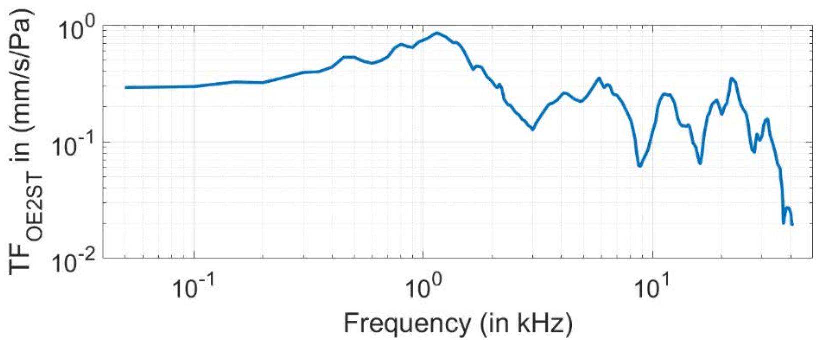

Figure 5. Chinchilla open-ear-to-stapes velocity TF (TF_{OE2ST})

1.2.3.2 Human middle model

Because the ME cochlear model is a standalone model that takes its input at the stapes, it can be easily connected to the AHAAH-ICE model to determine the OHC energy deficit. Hence, to calculate the OHC-ED for humans, the outer and middle ear electroacoustic models previously developed in (Zagadou, Chan, Ho, & Shelley, 2016) are used to connect the middle ear to the human ME cochlear model via the stapes. The stapes velocity is first calculated by transferring the free field pressure through the outer and middle ear to generate the stapes velocity-time waveform, which is then converted to volume velocity using the stapes footplate area. Time domain Fourier transformation is used to obtain the frequency response for the stapes volume velocity, as described in Eq. 9. The time domain cochlear variable solutions corresponding to the stapes volume velocity are then determined using Eqs 7-8.

1.3 Cochlear Tissue Stiffness Measurements

Cochlear tissue stiffness measurement experiments were performed at Boston university (BU) and Massachusetts Eye and Ear Infirmary (MEEI) to collect chinchilla and cadaver cochlear tissue data under approved Institutional Animal Care and Use Committee (IACUC) and Human Research Protection (HRPO), respectively. The cochlear tissue stiffness data collected provided the BM compliance values for the generic electroacoustic model described previously that were adapted for chinchillas and humans, respectively. The BM point stiffness test set up and the measurement approach are described in the following.

1.3.1 BM Point Stiffness Test Set Up

The point stiffness measurement technique is illustrated in Figure 6. The technique applies a displacement to the BM and measures force via the deflection of a beam to derive tissue point stiffness. Figure 6 shows the probe system, composed of piezo drivers and a probe force sensor approaching the BM. A precision micromanipulator is used to control the force-probe positioning on the preparation.

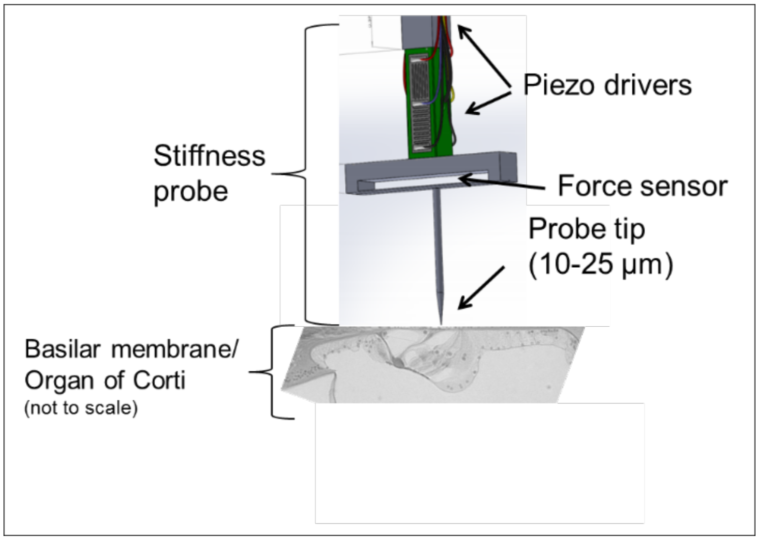

Figure 6. Illustration of point stiffness technique

Figure 7 shows the complete experiment set up for the point stiffness measurement used for chinchilla and human temporal bones. The point stiffness tests setup is the same for chinchilla and human specimens. In Figure 7a and b, the specimen is approached by a force probe using the micromanipulator system. The point stiffness was measured for the basal, middle, and apical turns of the chinchilla and human cochleae, respectively. In each turn, point stiffness measurements were performed at several radial locations to determine the radial stiffness variation.

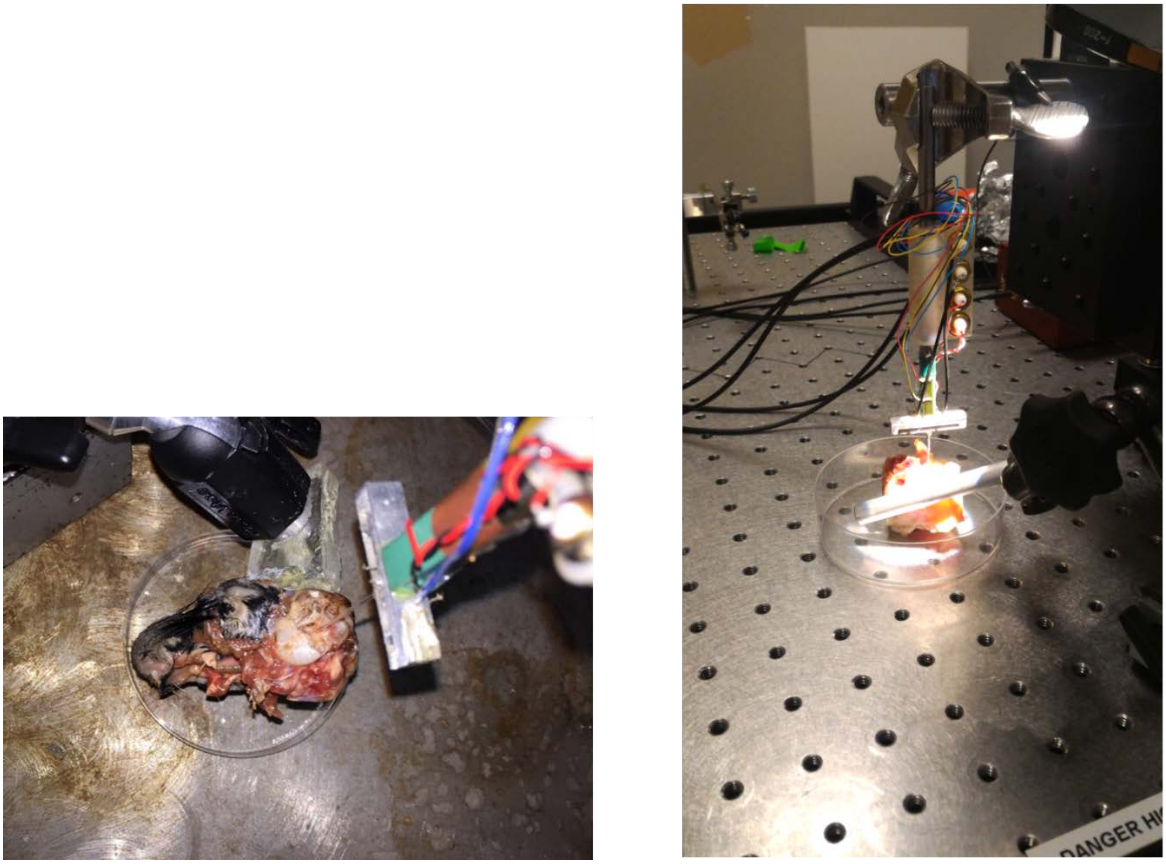

a) Chinchlla　　　　　b) Human

Figure 7. BM point stiffness test set up. a) Set up at BU showing chinchilla specimen approached by force-probe using micromanipulator system b) Set up at MEEI shownning human temporal bone specimen approached by force-probe using micromanipulator system

1.3.2 Measurement Approach

1.3.2.1 Chinchilla

Point stiffness measurements were made in a total of 33 longitudinal locations using 27 animals (14 in turn one, 11 in turn two, and 7 in turn three). At each longitudinal location, radial measurements were made approximately every 20-30um across the width of the BM. In the second and third turn preparations it usually was not possible to span the whole width of the BM because the openings in the bone were kept small enough to prevent damage to the spiral ligament. Three of the turn one locations were measured on frozen-thawed ears to examine the effect of freezing on stiffness. There was no significant change in stiffness from the freeze thaw cycle.

The point in the static displacement progression when the phase approached -90 degrees was considered as the physiologically relevant point stiffness. The value when the probe lost contact during retraction was also used as a measure of point stiffness. The stiffness values at initial and final contact were used to determine point stiffness.

The approach for the cochlear turn preparation is described as follows.

The experiments were performed in accordance with the protocol approved by the Boston University animal science review board. Point stiffness measurements were made on extracted Chinchilla (Chinchilla lanigera) cochleae. The animal was administered an initial dose of ketamine (100 mg/kg) plus xylazine (10 mg/kg) intraperitoneally, followed by supplemental doses (25% of initial dose) depending on the animal's reflexes. Following the absence of any reflex, the animal was decapitated and its temporal bones excised and placed in oxygenated culture medium (Leibovitz L-15). Most of the bulla, the tympanic membrane and the middle ear ossicles were then removed to expose the cochlea. The cochlea was then transferred into fresh medium to prevent possible blood clot formation on the organ of Corti (OC) when the structure was opened.

Removing the round window membrane in a chinchilla can dislodge the BM. Care was exercised to cut the round window where it attaches near the BM. Pulling it off will dislodge the BM leading to a large reduction in stiffness. Second and third turn preparations were made by thinning the bone around the scalae with a razor blade then cleaving the cochlea into single turn segments.

Figure 8 shows a photomicrograph of the measurement probe in action at a basal location on the BM. The probe tip is rounded and has a diameter of approximately 20 μm. In the base of a chinchilla, the widths of the BM between the inner osseous lamina and spiral ligament have been consistently 200 μm. In the preparation shown in Figure 8, the bone apical to the round window is carefully removed by chipping with a scalpel and forceps. Once the bone is sufficiently removed the prep is irrigated with fresh media and placed in a new dish. Then, the round window is removed with a tungsten hook. Performing the steps in this order reduces the chance of bone debris from damaging the BM.

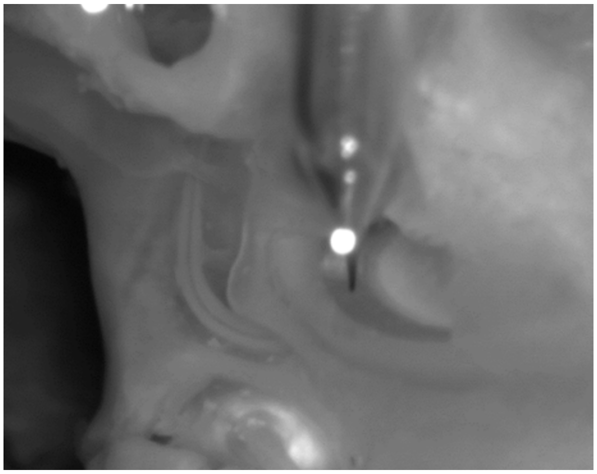

Figure 8. Photomicrograph of probe measuring a basal location on the BM.

Figure 9 shows a photograph of a second turn preparation. The Dieter's cells and OHCs are visible in this experiment. The probe is directly on top of the third row of Dieter's cells. Making these preparations is very difficult. The chinchilla cochlea bone is very brittle and it tends to shatter. To counteract this, the bone has to be deeply scored before attempting to separate the turns. The turn to be separated is scored with a scalpel to the point where it is thinned. Then, the preparation is irrigated and transferred to a clean dish of culture medium to prevent contamination with bone dust. Then, a scalpel is used to crack the cochlea along the score line.

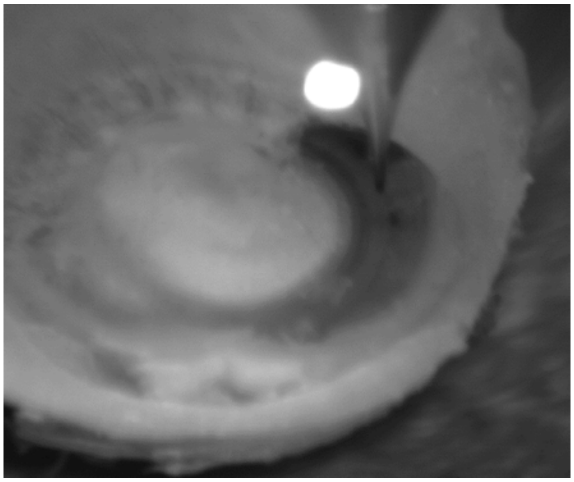

Figure 9. Photograph of a second turn preparation.

1.3.2.2 Human temporal bones

Point stiffness measurements were made on 1 frozen bone that has been used in multiple experiments (measurements 1 mm from base CF = 17.7 kHz) and 3 freshly thawed temporal bones

(6 measurements 1 mm from the base (CF = 17.7 kHz), 3 measurements at 12 mm (CF = 3.2 kHz) from the base, and 3 measurements at 19 mm from the base (CF = 1 kHz)). Multiple measurements were made in the radial direction for each longitudinal location measured to determine the radial pattern of the stiffness. The approach is described as follow.

The temporal bones were prepared using a facial recess approach, similar to (Nakajima et al., 2009). For the measurements 1 mm from the base, the bone surrounding the round window membrane (RWM) was drilled, and the RWM was removed with a sharp blade. For the more apical measurement locations, the underside of the cochlea was removed using a dental burr until scala tympani of the first turn was nearly exposed. A scalpel was used to carefully open a 1 mm^2 hole in the thinned bone at the respective measurement location. Thus, measurement in the base (through the RWM area) was achieved, 12 mm from the base and 19 mm from the base, which covers about 60% of the total length of the cochlea. Figure 10 shows the first turn preparation of a human cochlea.

Figure 10. First-turn preparation of a human cochlea.

1.4 Development of Complex Noise Generation Equipment

This project requires a noise generation system capable of producing complex sequences of impulse noise of equal and unequal intensity and presentation intervals, including impulses riding on top of continuous background noise that will be used to perform chinchilla experiments. Two complex noise generation systems were developed for this purpose. The L3 Automated Rapid Fire Shock Tube (ARFST) system was used and calibrated to produce multiple blasts with unequal intensity levels and unequal IPI. To produce the intense continuous background noise, a continuous noise generation system (CNGS) was developed using a loudspeaker. All noise generation equipment was fabricated at the L3 facility in San Diego and delivered to University of California at San Diego (UCSD) for use in animal testing. All equipment was calibrated and tested on site before delivery to the UCSD laboratory. The ARFST system and the CNGS are described in this section. The details of the calibration of the two noise generation systems can be found in Appendix A.

1.4.1 ARFST System Description

1.4.1.1 ARFST System Apparatus

The ARFST system shown in Figure 11 is a pneumatically and electrically controlled device consisting of two separate shock tubes each working with a large rotating disk which automatically cycles between shots to replace the burst diaphragm. The device uses two tubes that alternate shots to reduce the time interval between shots. An automated shock tube with a rotating wheel design has an inherent time delay due to the mechanics of the system. Having two symmetric systems built into one apparatus cuts the delay time in half. Both tubes are made with a 4.5-inch long compression chamber and a 16-inch long expansion section. The system requires a high pressure helium line with pressure set to 100 psi. A compressed air source is also required to operate all of the pneumatic components. This pneumatic pressure required to maintain proper motion and chamber sealing is 150 psi.

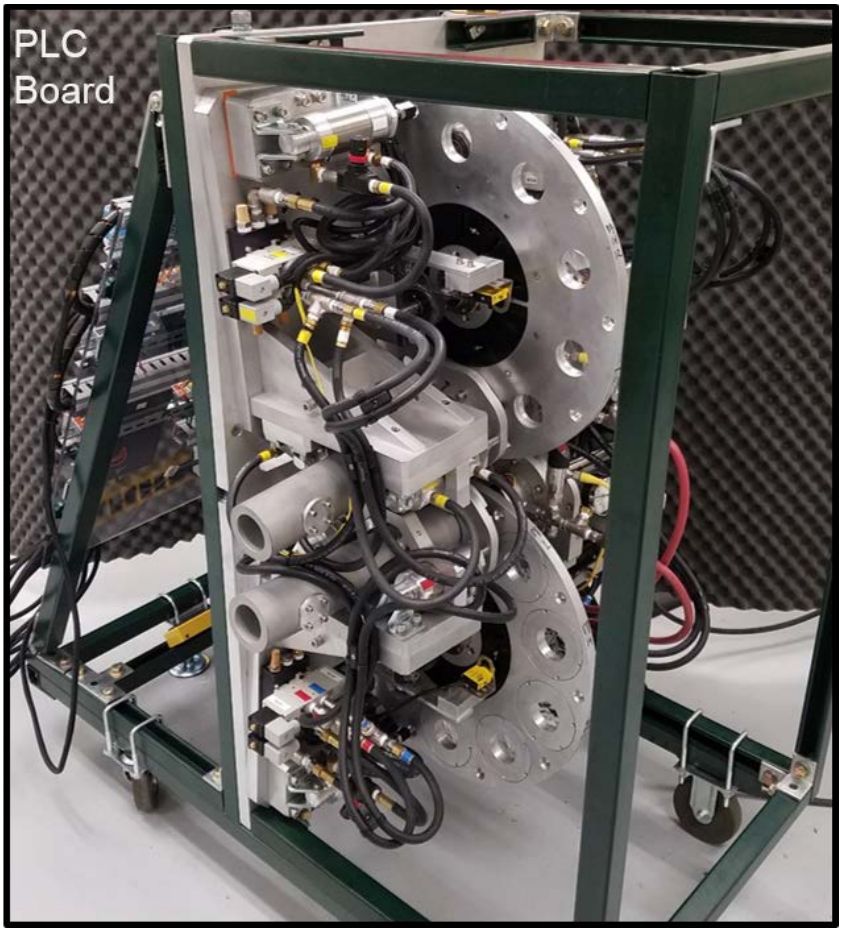

Figure 11. Automated Rapid Fire Shock Tube (ARFST) system.

1.4.1.2 Control of the ARFST System

Control of the ARFST is done using the commercial 0BA8 LOGO! Logic Module from Siemens. The Siemens 0BA8 allows for a maximum of 24 digital inputs, 20 digital outputs, 8 analog inputs, and 8 analog outputs. In addition, its program memory allows for a maximum of 400 function blocks, 50 message texts, and 64 digital and analog flags. The device is programmed using Siemens proprietary software, LOGO!Soft Comfort and the firmware is uploaded over an Ethernet connection with a PC. This programmable logic controller (PLC) was chosen for its robust design and its intended use in small automation projects, such as the ARFST.

The PLC completely controls every mechanical operation of the ARFST. The user is able to program the function of the shock tube through the PLC control module box. Through the keypad on the module, the user can input the number of shots desired (1-10), the thickness of each diaphragm used, and the time delay between successive shots. The shock tube is capable of shooting diaphragms with thicknesses of 0.5, 1.0, 1.5, 2.0, and 2.5 milli-inches (mil). To account for the variable thicknesses and desired shot time intervals, a correlation equation was built into the PCL control unit to ensure steady blast intervals.

1.4.1.3 Operation of ARFST system

For a better understanding of the ARFTS and its automation procedure, a parts diagram can be seen in Figure 12. When a sequence of shots is initiated, power is applied to the motor and the rotating diaphragm wheel (3) then rotates to the first Mylar diaphragm (11) to be ruptured. Once the optical switch (7) senses the wheel is in the proper position, the brake to the motor is applied momentarily, stopping the wheel from rotating further. Power is then removed from the motor, allowing the wheel to be freely rotated. At this time, the clocking plunger momentarily fires, ensuring that the diaphragm is properly aligned with the centerline of the compression chamber (1). The pneumatic chamber clamps close (8), sealing the chamber, and the helium release valve is opened. The chamber is then filled with helium until the chamber reaches a predefined pressure value. This pressure value corresponds to approximately 90% of the maximum pressure at which the diaphragm naturally ruptures, ensuring that the diaphragm will never rupture on its own. Once this value is reached, a pneumatic harpoon fires, puncturing the diaphragm, and sending the pressure wave through the expansion chamber (2) and out of the shock tube exit (10).

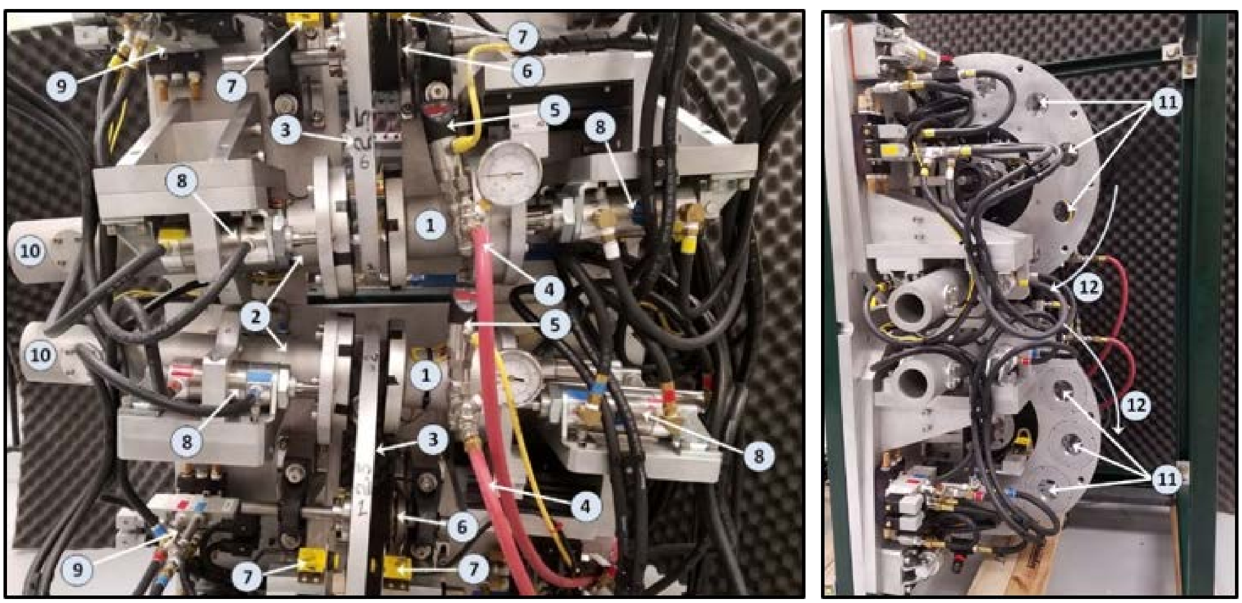

a) **b)**

Figure 12. Part Diagram of the ARFST system: a) Side view b) Front view. System Components: (1) Compression Chamber, (2) Expansion Chamber, (3) Rotating Diaphragm Wheel, (4) Helium Supply Line, (5) Pressure Transducer, (6) Electric Motor Gearing to Wheel, (7) Optical Encoder for Wheel Alignment, (8) Pneumatic Clamps, (9)

Pneumatic Control Solenoids, (10) Tube Exit, (11) Mylar Diaphragm Loading Slots, (12) Wheel Rotation, (13) Wheel Clocking Mechanism, (14) Clocking Alignment Index Points

1.4.1.4 Safety features of the ARFST system

Within the ARFST programmed logic there are a number of safety features that prevent mechanical damage to the machine as well as injury to the user. One of these safety features is implemented during the start of the program. When the program is first run, the chambers open, the harpoon is retracted, and the wheel is allowed to spin freely without causing the optical switch to inadvertently trigger any part of the system. The user must hold the F1 key on the keypad to start the program to enable the optical switch input. Once the program has started, at no time should the machine be touched by the user. If a situation occurs where the machine must be shut down immediately, the emergency stop switch located on top of the machine may be activated.

Another safety feature is a check to ensure that the rotating diaphragm wheel is properly aligned before the chamber can be closed or the harpoon can fire. This ensures that the harpoon will not contact any part of the wheel and damage it. The system will detect mismatch between selected and installed diaphragm thickness, and automatically shut down with an error message appearing on the remote. This will prevent an erroneous test from continuing.

1.4.2 CNGS System Description

The CNGS is comprised of a laptop, white noise sound file, sound amplifier, and loudspeaker as shown in Figure 13.

- The laptop is used to play the sound file.
- A white noise sound file is used to create the continuous noise segments required for our purpose.
- The sound amplifier used is a stereo line/Microphone mixer with two output line that can be used to connect to two speakers. One channel of the Stereo line/Microphone mixer was used to connect to the loudspeaker.
- The loudspeaker is a Dynaudio AIR 6 Digital Master Studio Monitor capable of producing > 126 dB PPL at 1m, with frequency response of 40 Hz-22 kHz (+/- 3dB).
- A standard sound level meter (CEL240 Type 2) was used to measure the peak pressure level (PPL) to ensure the desired dB level output by the CNGS is reached.

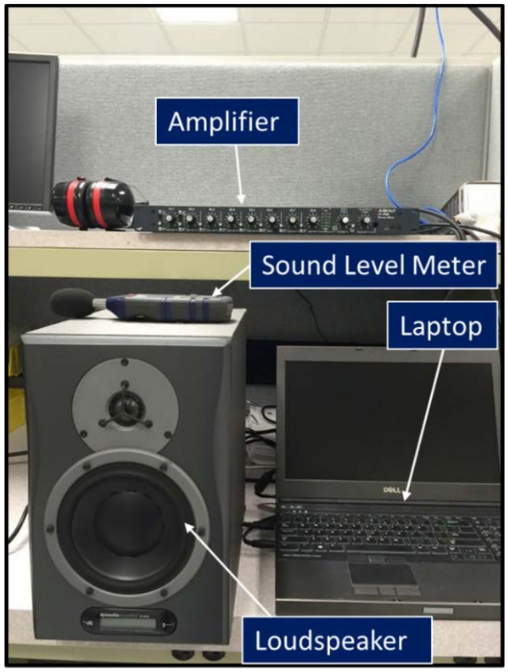

Figure 13. CNGS Components

1.5 Chinchilla Complex Noise Exposure Experiment

Chinchilla complex noise exposure experiment was performed for model validation. The complex noise exposure test matrix was designed using three impulse peak pressure levels (PPLs), three different IPIs, 10 impulses per test condition (TC), and 2 different levels of background noise. The test matrix was designed guided by literature and previous data trend as described below.

1.5.1 Complex Noise Exposure Test Matrix

1.5.1.1 Guidance from Previous Data

Literature data suggested the existence of three apparent regimes for the effects of IPI on the exposure dose accumulation (Danielson, Henderson, Gratton, Bianchi, & Salvi, 1991; Henderson, Subramaniam, Gratton, & Saunders, 1991):

- The acoustic reflex (AR) regime characterized by very short IPI, IPI < 250 ms
- The ME regime corresponding to moderate IPI, 250 ms < IPI < 60 secs
- An extended ME regime for long IPI, IPI >> 60 secs

The current project focused on the moderate IPI. In this ME regime, literature data suggests that IPI has a stronger effect on injury for low level impulses and that the effect of combined unequal impulse above and below the critical level can be significant for dose accumulation. Gas anesthesia (isoflurane) has been found to have some protective effect against temporary threshold shift (TTS), potentially reducing TTS by 10 to 40 dB in anesthetized animals (Ruebhausen, Brozoski, & Bauer, 2012).

Based on these results the following guidelines were adopted.

1. Use a fixed IPI for level greater than 137 dB
2. IPI between 3 and 20 secs will tend to produce low injury
3. Exposure levels should not be greater than the critical level of 150 dB for chinchilla
4. Increase the exposure level by 10 dB to compensate for gas anesthesia when used

Hence, the sound exposure levels satisfying the literature-based guidelines for ME study were:

- 3 impulse levels: L1, L2, L3 = 125, 135, 145 dB PPL, respectively
- 2 continuous noise levels: Lc1, Lc2 = 90, 100 dB PPL, respectively

Because the exposures from the literature were not actual impulses, but synthetized impacts, pulse, or impulse noise, additional information from previous chinchilla tests were integrated into the design. Based on previous chinchilla tests with shock tube noise exposures, higher exposures are required to create meaningful TTS. At 2 feet standoff with 160-180 dB PPL and N = 1 to 8 independent shots (IPI ~1-2 min), the resulting TTS_2 was between 10 and 48 dB.

Therefore, the literature-based exposure levels were increased by 15 dB for the impulses to yield the final exposure levels for the ME test matrix:

- 3 impulse levels: L1, L2, L3 = 140, 150, 160 dB PPL, respectively
- 2 continuous noise levels: Lc1, Lc2 = 90, 100 dB PPL, respectively

1.5.1.2 Description of the ME Test Matrix

The ME test matrix for the chinchilla complex noise exposure is shown in Table 1, with a schematic illustration of the multiple shots provided in column 7. For each TC, the multiple shots sequence is composed of 10 shots given at constant or varied IPI. In column 7, each spikes represents 1 shot, and the height is proportional to the exposure peak level (L). The spacing between adjacent spikes is proportional to the IPI. The shot sequences with colored underlines represent the addition of background continuous noise, with two colors representing two distinct level of the continuous background noise, respectively.

The ME test matrix is composed of 2 test series with a total of 24 TCs (Table 1). In Series 1, two or three levels are combined, and the 10 impulses are given at a constant IPI (t1 or t3). The first 6 TCs of Series 1 (Series 1-a) are without continuous background noise. In the last 6 TCs of Series 1 (Series 1-b), t3 is used as the IPI in place of t1 in 3 tests (TC 10-12), and each TC contains a continuous or intermittent background noise. In Series 2, the IPI is varied between the 10 impulses in addition to varying the levels, and the first 6 tests (TC 13-18, Series 2-a) are without background noise while the last 6 (TC 19-24, Series 2-b) contain continuous or intermittent background noise. Five animals are used for each TC (n=5).

In addition to allowing the construction of a dose-response curve against cochlear injury, the test matrix was also designed to help elucidate the effects of the complex noise features, including the IPI, shot sequence, and background continuous noise. Cross comparison of TC 1-4 and TC 13-16 will determine the possible effects of the IPI on outcomes, while cross comparing TC 2 and 6 and TC 4 and 5, respectively will determine the effect of shot sequence. To assess the effect of the background continuous noise on outcomes, cross comparison between TC 1-3 and TC 7-9 on one hand, and Series 2-a and -b on the other hand will be performed.

Table 1. Metabolic exhaustion test matrix

Series	Test Condition	Peak Pressure Level (L)	N	IPI (t)	Number of Animal	Schematic Description of Multiple Shots	Total Impulses
1-a	1	L1, L2	10	t1	5	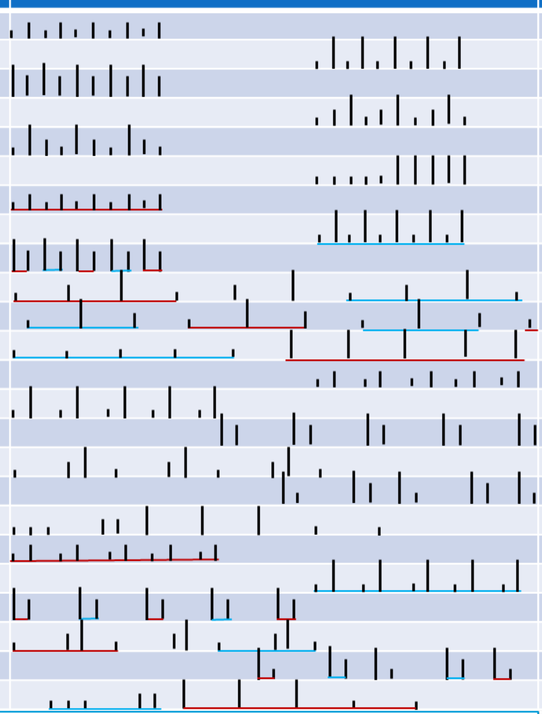	5L1+5L2
	2	L1, L3	10	t1	5		5L1+5L3
	3	L3, L2	10	t1	5		5L3+5L2
	4	L1, L2, L3	10	t1	5		4L1+3L2+3L3
	5	L1, L3, L2	10	t1	5		4L1+3L2+3L3
	6	L1, L3	10	t1	5		5L1+5L3
1-b	7	L1, L2	10	t1	5		5L1+5L2
	8	L1, L3	10	t1	5		5L1+5L3
	9	L3, L2	10	t1	5		5L3+5L2
	10	L1, L2, L3	10	t3	5		4L1+3L2+3L3
	11	L1, L3, L2	10	t3	5		4L1+3L2+3L3
	12	L1, L3	10	t3	5		5L1+5L3
2-a	13	L1, L2	10	t1, t2	5		5L1+5L2
	14	L1, L3	10	t1, t2	5		5L1+5L3
	15	L3, L2	10	t1, t3	5		5L3+5L2
	16	L1, L2, L3	10	t3, t1, t2	5		4L1+3L2+3L3
	17	L3, L1, L2	10	t1, t3, t2	5		5L3+3L1+2L2
	18	L1, L2, L3	10	t1, t2, t3	5		5L1+2L2+3L3
2-b	19	L1, L2	10	t1, t2	5		5L1+5L2
	20	L1, L3	10	t1, t2	5		5L1+5L3
	21	L3, L2	10	t1, t3	5		5L3+5L2
	22	L1, L2, L3	10	t3, t1, t2	5		4L1+3L2+3L3
	23	L3, L1, L2	10	t1, t3, t2	5		5L3+3L1+2L2
	24	L1, L2, L3	10	t1, t2, t3	5		5L1+2L2+3L3

Peak pressure level (L) L1, L2 and L3 = 140, 150 and 160 dB, respectively.
Interpulse interval (IPI) t1, t2 and t3 = 3, 9 and 20 seconds, respectively.

Continuous noise
Lc1 = 100 dB   Lc2 = 90 dB

1.5.2 Noise Exposure Experiment Set Up

Before the actual blast exposure tests were conducted, a variety of tests were performed that included the calibration of firing sequence of the ARFST system and mapping of the microphone position to the desired PPLs. A detailed description of these calibration tests can be found in Appendix A. The mapping of microphone position was performed to find the optimal distance to the test target, given the three Mylar thickness sizes used and the desired blast levels for metabolic exhaustion study. The optimal radial distance was found to be 8ft from the exit and 10º from the tube centerline, which was subsequently used for all tests performed for this project to position the test animal and microphone as shown in Figure 14.

Figure 14 shows the chinchilla blast exposure experiment set up. The room was covered with foam to minimize sound reflection. As shown, the ARFST system is in the back hidden by the insulating foam; only the tube exit is visible. The chinchilla (target) is placed in a custom made holder in front of the tube exit, at 29 inches above the floor representing the average height of the two tubes.

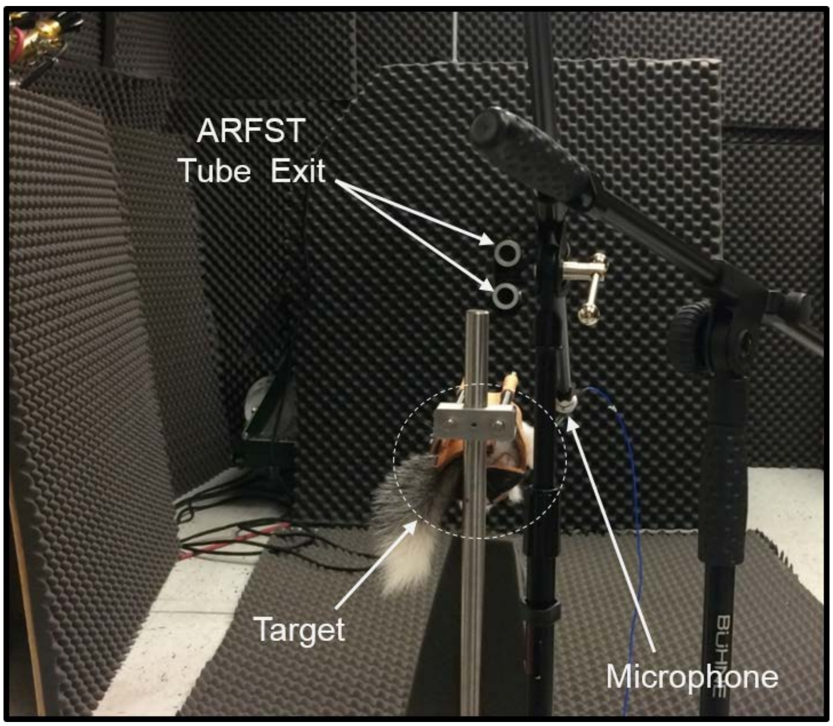

Figure 14. Chinchilla complex noise exposure experiment set up. ARFST in the back with tube exit shown. Chinchilla in front with head towards tube exit (10º off tube centerline at 8ft). Microphone positioned near chinchilla ear.

The set up when the continuous background noise is added to the blast sequence is shown in Figure 15. Figure 15 shows the components of Figure 14 with the addition of the loudspeaker. The loudspeaker is suspended at an angle, above the chinchilla (target) using chains and hooks on a horizontal bar and centered to align in the vertical plan with the shock tube exits. The loudspeaker output is controlled by a computer program as explained below.

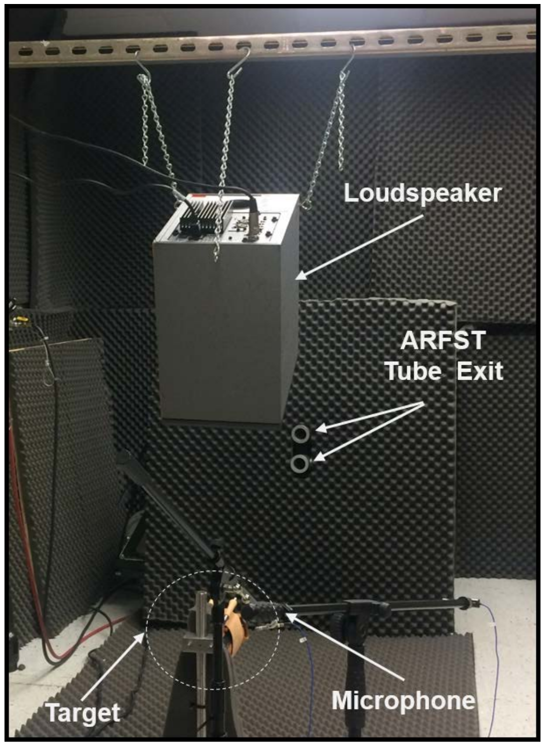

Figure 15. Complex noise exposure experiment set up with ARFST and CNGS. Loudspeaker of the CNGS is suspended on top of target and functions in synchrony with the ARFST system.

A computer program was created to synchronize the continuous noise produced by the CNGS and the blast generated by the ARFST system such that both noise generation systems are triggered simultaneously and run in parallel during testing. As shown in the test matrix (Table 1), the continuous noise sequence is composed of either a continuous noise throughout the total duration of the exposure or an intermittent noise with periods of ON and OFF sound, with one of two intensity levels selected during the ON-period. The program encodes all the continuous noise sequences of the test matrix, including the duration and intensity level of the tone segment. Given a TC, the continuous noise sequence is triggered by the first blast of the ARFST system and stays on for the duration of the blast sequence to generate the complex noise.

1.5.3 Blast Waveforms Recording and Processing

The blast waveforms recorded at the microphones positioned near the chinchilla ear were saved on the Synergy data acquisition system and processed using MATLAB to visualize the waveforms and to reconstruct the mixture of blast and continuous background noise. The microphone positioned near the chinchilla ear was used to record the blast waveforms for Series 1-a and 2-a. To collect the blast and the continuous background noise (Series 1-b and 2-b), two different microphones were used because of the differing characteristics of the exposures. A high sensitivity microphone (Microphone 2) was used to collected the background noise, while the low sensitivity microphone (Microphone 1) is used to collect the blast. In this case, recordings were performed simultaneously. The pair of recordings from each TC were merged to generate the complex mixture of noise for data analysis and input to the ME model. Pressure data from Microphone 2, which contains the background noise was used as the baseline waveform, and the clipped pressure data from the blasts due to the limited range of Microphone 2 were replaced by those from Microphone 1.

1.5.4 ABR measurements

The standard auditory brainstem recording (ABR) method was performed before and after the complex noise exposure using chinchilla subjects, and the difference in hearing threshold before and after the exposure determines the TTS incurred as a result of the complex noise exposure. TTS was collected at 3 points in time after the exposure, immediately after the exposure, 1 hour after and 2 hours and for six frequencies at 1, 2, 4, 8, 16, and 20 kHz, respectively. Permanent threshold shift (PTS) was also tracked 2 weeks after the exposure.

Figure 16 shows a sample of the ABR records before and after the noise exposure. The response to 512 stimulus presentations was averaged to generate the ABR waveform. The ABR stimulus consisted of tone burst 25 ms in length, with a ramp time of 2.5 msec, presented at 20/sec.

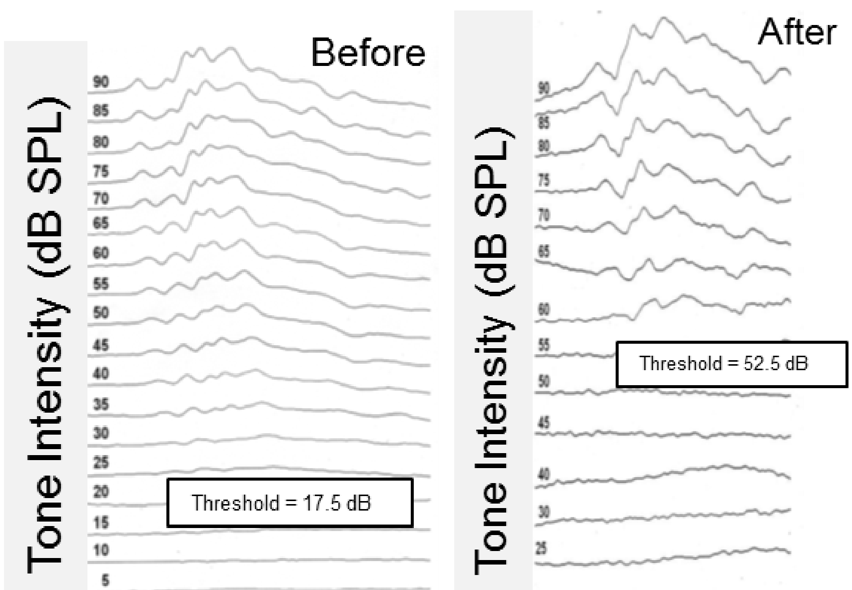

Figure 16. Sample ABR Records before and after blast exposure

1.6 Model Validation against Chinchilla Data

This section describes the procedures used to verify and to validate the chinchilla cochlear model, including the derivation of BM compliance from point stiffness data and the verification of the place-frequency map and basic properties of cochlear mechanics.

1.6.1 Derivation of BM compliance from point stiffness data

The location-dependent BM compliance, C_{BM} (x) was derived for the cochlear model using the point stiffness data collected as follows. First, the volume compliance (C_v) of the BM, defined as the ratio of the volume change to the differential pressure across the cochlear partition was calculated using the point stiffness (k_p) measured at the three locations along the cochlea. The beam model of the cochlear partition strip was used to derive C_v (Olson & Mountain, 1991). The present derivation accounts for the longitudinal coupling (λ) between individual BM partition strips. Next, the C_{BM} was calculated by multiplying C_v by the length (Δx) of the element of the model. C_{BM} was then fit to an exponential function of the longitudinal distance x for use in the cochlear model.

The resulting formula for C_{BM} is summarized in Eqs 1-2, where d represents the diameter of the probe used to measure the point stiffness and W_{BM}, the width of the BM.

$$C_v = \left({}^{1}/_{k_p(x)}\right) \cdot W_{BM}(x) \cdot \left(d + 2 \cdot \lambda(x)\right)^2 \cdot 2.0290 \ \ (m^4/N) \qquad (1)$$

$$C_{BM} = C_v \cdot \Delta x \ (m^5/\mathrm{N}) \qquad (2)$$

1.6.2 Verification of Place-Frequency Map

To verify that the cochlear filtering properties and place-frequency map are correctly represented in the electroacoustic cochlear model, the place-frequency map derived from the cochlear model response was compared to the experimental map. The model was simulated in passive mode (g_{OHC} = 0), and the frequency of the maximum BM displacement was compared to the passive map from (Eldredge, Miller, & Bohne, 1981; Greenwood, 1990). The location of the maximum displacement was determined for a range of frequency from 0.2 to 20 kHz.

1.6.3 BM Response Validation

The cochlear model response was validated by comparing the BM response to a click stimulus response from the experimental data from (Recio, Rich, Narayan, & Ruggero, 1998). In (Recio et al., 1998), the BM response to an acoustic click stimulus input from the ear canal of live chinchillas was measured simultaneously at the incus in the middle ear and on the BM at 3.5 mm from the base of the cochlea. The measured incus velocity was digitized and used as the input to the cochlear model, and the BM velocity response from the model was compared to the experimental data.

Figure 17 shows the digitized incus velocity (Figure 17a) and BM response (Figure 17b) to a 102 dB SPL click stimulus in live chinchilla measured 10 min post-mortem (Recio et al., 1998). The velocity of the closest 10 points to the 3.5 mm location obtained from the passive cochlear model simulation were averaged, and the resulting BM response was shifted by 5-10 dB as suggested by the data to obtained the corresponding active model response that was compared to the live data shown in Figure 17b.

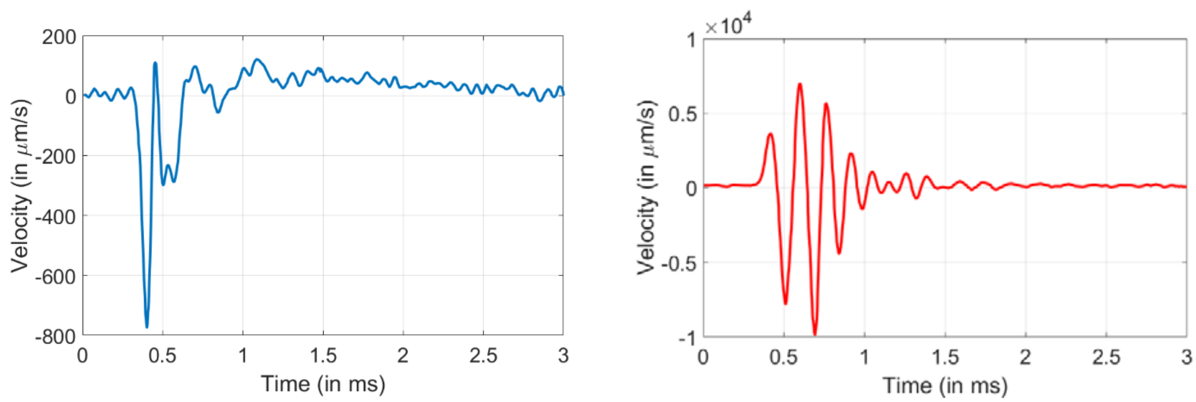

a) b)

Figure 17. Digitized incus and BM responses to click used for model validation (Recio et al. 1998). a) Incus velocity response b) BM velocity response

1.7 Development of Human Model

A cochlear model for human was developed using the generic electroacoustic model and cochlear tissue properties measured from postmortem human specimens. The electroacoustic cochlear model is useful for studying metabolic exhaustion within the cochlear resulting from complex noise exposure. The energy deficit caused by the unbalance between the high OHC energy demand and the available energy supply during the complex noise exposure can be calculated using the electroacoustic model to determine how the exposure dose accumulates to produce TTS in humans. Guided by the insights provided by the results of ME chinchilla model against a wide range of complex noise exposure tests, a full human model can be developed as data from human exposure to complex noise become available.

1.8 Results

1.8.1 Cochlear Stiffness Measurements

This section presents the results from the point stiffness experiment performed using chinchilla and post-mortem human specimen temporal bones. The results for the BM compliance required for calibration of the electroacoustic model that were derived from the point stiffness data are also described.

1.8.1.1 Chinchilla Cochlear Point Stiffness

The points stiffness data collected from BU are shown in Figure 18 and 19. The bar graph in Figure 18 show the summary of the point stiffness results. Figure 19 shows the data trend in the longitudinal variation for the pectinate and arcuate zones. As shown in Figure 19, the pectinate zone point stiffness decrease monotonically from base to apex that is representative of the stiffness gradient along the BM. Thus, the data from the pectinate zone of the BM were used to derived acoustic compliance of the BM per unit section (C_{BM}) of the electroacoustic cochlear model.

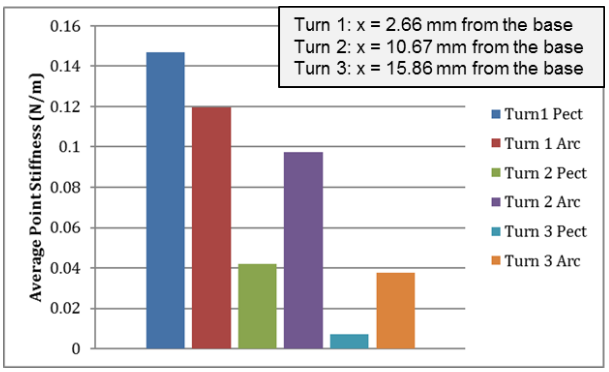

Figure 18. Summary of point stiffness results

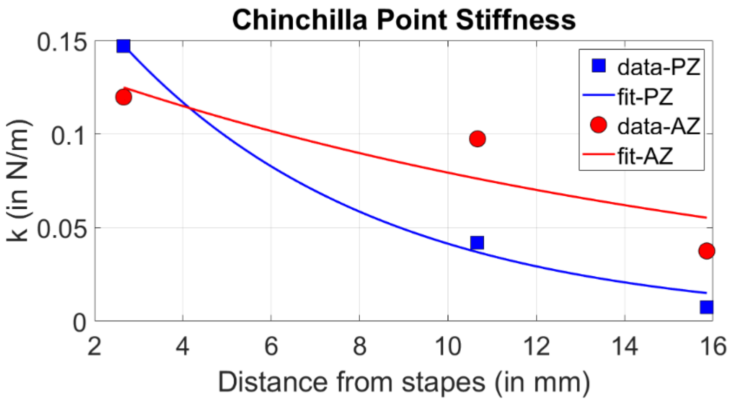

Figure 19. Comparison of longitudinal point stiffness (k) variation for AZ and PZ

The BM compliance derived using Eqs. 1-2 is given in Eq. 3. The parameters value used are d = 10 µm, $\lambda(x) = 8.5 + 1.8x$ µm (Naidu & Mountain, 2001), $W_{BM}(x)$ estimate from (Lim & Steele, 2002), and kp (x) is the BM stiffness data.

$$C_{BM}\,(x) = 10.0 \cdot exp(-29.62 + 3.16 \cdot x)\ (cm^5/dyne);\, x\ in\ cm \qquad (3)$$

1.8.1.2 Human Cochlear Point Stiffness

The results from the point stiffness measurements in the human temporal bones are summarized in Figure 20, showing the mean and standard deviation of the point stiffness values at the center of the BM for the three locations measured along the cochlea.

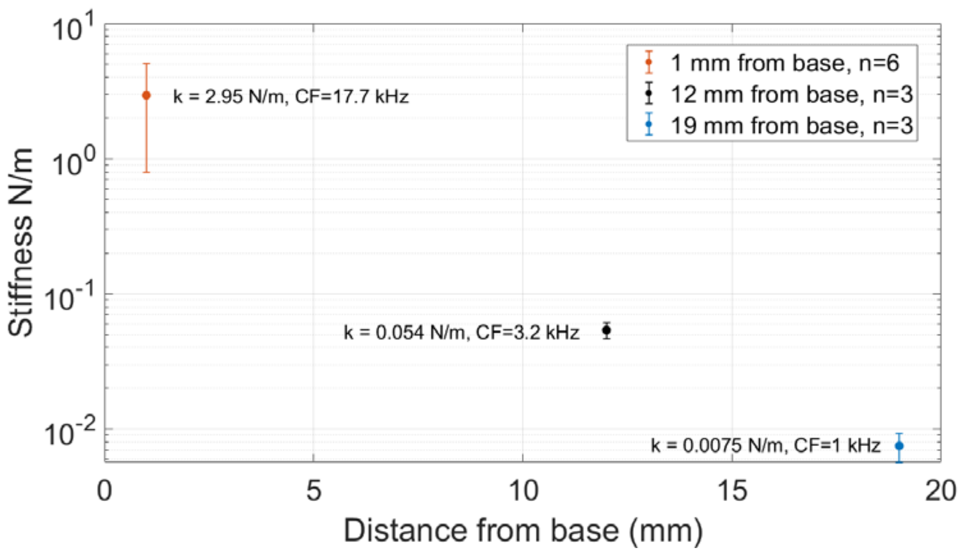

Figure 20. Summary of human stiffness data with standard error

The resulting BM compliance per unit length of the electroacoustic model is given in Eq. 4. The parameters used are d = 20 µm, $\lambda(x) = 0$ µm, $W_{BM}(x)$ from (Zwislocki, 2002), pp. 108, and $k_p(x)$ is the measured stiffness data.

$$C_{BM}\,(x) = 10.0 \cdot exp(-36.06 + 4.02 \cdot x)\ (cm^5/dyne);\, x\ in\ cm \qquad (4)$$

In Figure 21, the BM acoustic compliance per unit length derived using the new point stiffness data collected at MEEI is compared to the earlier estimate by Zwislocki (2002), who used the cadaver data collected by Von Bekesy (1960). The figure shows that the new acoustic compliance estimate differs noticeably from the previous estimate. The new BM compliance is smaller by 1 order of magnitude in the base and greater by 2 orders of magnitude at the apex than the previous estimate. Both estimates cross at ~1.4 cm from the base. The new estimate shows that the BM is more compliant in the base up to the 1.4 cm and stiffer beyond that location toward the apex. The new estimate shows a smaller stiffness gradient than the previous data. The effect of this longitudinal stiffness pattern change can be significant for the frequency map and BM response. The difference between the current and previous stiffness maps can perhaps be explained by the novel instrumentations available today compared to those used by Bekesy to perform the stiffness experiments. A high precision force probe calibration technique that uses atomic force microscopy (AFM) was used to calibrate the probe used for the new measurements.

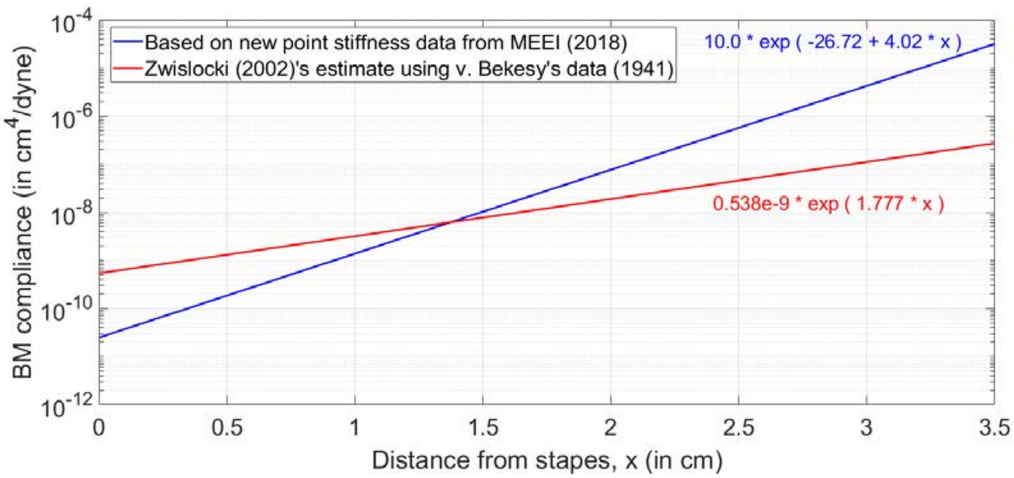

Figure 21. Comparison of human BM acoustic compliance per unit length

1.8.2 Model Validation against Chinchilla Data

1.8.2.1 Electroacoustic model parameters for Chinchilla

The electroacoustic model parameters for chinchilla are summarized in Table 2. The source of the parameters is provided in the last column of Table 2. Sources not shown are from modeling constraint or free parameters. N represents the total number of sections in the discretized model. The BM compliance was derived from the point stiffness data as described in earlier sections. The value of Q was chosen to match the BM displacement to experimental data by Recio et al. (1998).

Table 2. Electroacoustic model parameters for chinchilla

Name	Description	Value	Unit	Data source
N	Number of sections	400		-
L	Cochlear length	1.84	cm	(Bohne & Carr, 1979; Eldredge et al., 1981)
C_{BM}	BM compliance	$10.0 \cdot e^{(3.16.x-29.62)}$	cm^5/dyne	Point stiffness data from BU

CF	Frequency map	$163.5 \cdot (10^{\frac{2.1(L-x)}{L}} - 0.85)$	Hz	(Eldredge et al., 1981; Greenwood, 1990)
Q	BM quality factor	9.4		-
L_{BM}	BM inductance	$1/(C_{BM} \cdot (2\pi \cdot CF)^2)$	dyne·s²/cm⁵	-
R_{BM}	BM resistance	$\sqrt{L_{BM}/C_{BM}}/Q$	dyne·s/cm⁵	-
A_{OC}	Effective OC area	$A_{OC}(x)$	cm²	(Bohne & Carr, 1979)
A_{SV}	Effective SV area	$A_{SV}(x)$	cm²	(Dallos, 1970)
A_{ST}	Effective ST area	$A_{ST}(x) = 3A_{SV}$	cm²	(Dallos, 1970)
A_{FP}	Stapes area	2.0e-2	cm²	(Vrettakos, Dear, & Saunders, 1988)
R_{OHC}	OHC resistance	$10R_{BM}$	dyne·s/cm⁵	-
C_{OHC}	OHC compliance	$5C_{BM}$	cm⁵/dyne	(Mammano & Ashmore, 1993)
R_{RL}	RL resistance	$0.2\ R_{BM}$	dyne·s/cm⁵	-
L_{RL}	RL mass	$0.66L_{BM}$	dyne·s²/cm⁵	(Mammano & Ashmore, 1993)
C_{RL}	RL compliance	$5C_{BM}$	cm⁵/dyne	(Mammano & Ashmore, 1993)

1.8.2.2 Verification of Frequency-Place Map

The C_{BM} was incorporated into the cochlear model, and the model response was verified by comparing the place-frequency map produced by the model to the published literature map (Greenwood, 1990). The result is shown in Figure 22.

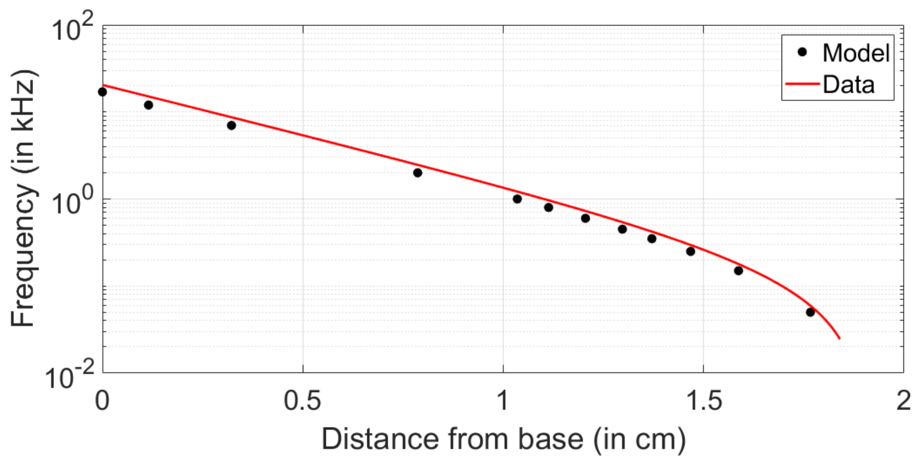

Figure 22. Verification of model's place-frequency Map

As shown in Figure 22, the characteristic frequency (CF) as determined by Greenwood (1990) (solid red line) and the location of maximal response obtained from the passive cochlear model (filled black circle), are in excellent agreement.

1.8.2.3 Basilar Membrane Response Validation

In Figure 23, the BM velocity from the model (blue line) is the average velocity from points close to the 3.5 mm location. The resulting average response was slightly shifted to align with the peak of the measured velocity for comparison. The measured BM velocity (red line) is the digitized data from (Recio et al., 1998).

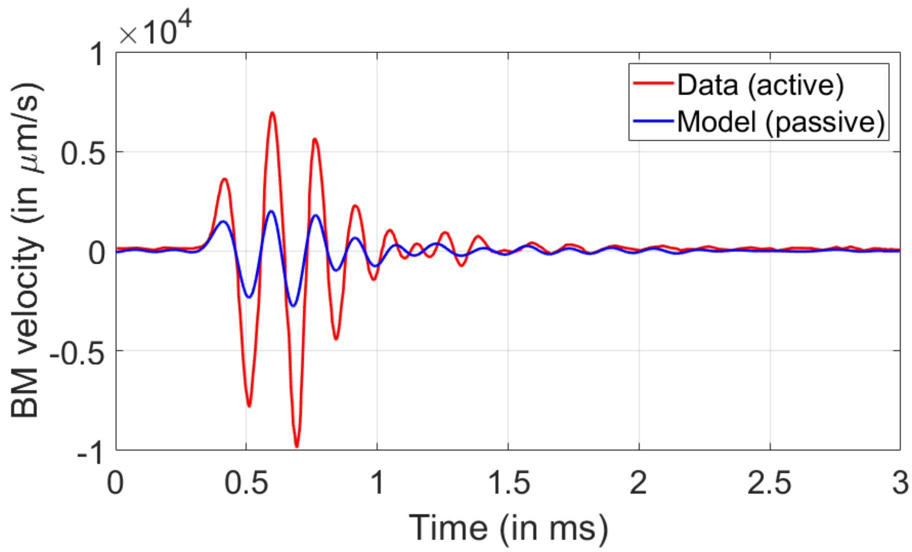

Figure 23. Comparison of BM response to click stimulus. Model response (*solid blue line*); Experimental data (*solid red line*)

The electroacoustic cochlear model closely replicates the BM response. The shift in the response is consistent with the incudo-stapedial-joint movement and time delay between active and passive BM responses. The response magnitude also reflects the BM velocity data. Data from (Recio et al., 1998) show that post-mortem velocity response is between 5.4 (green line) and 9.9 dB (light blue line) lower than that for live animal. As shown in Figure 24, the shifted passive response is similar to the experimental data. Therefore, the model and the data are in good agreement.

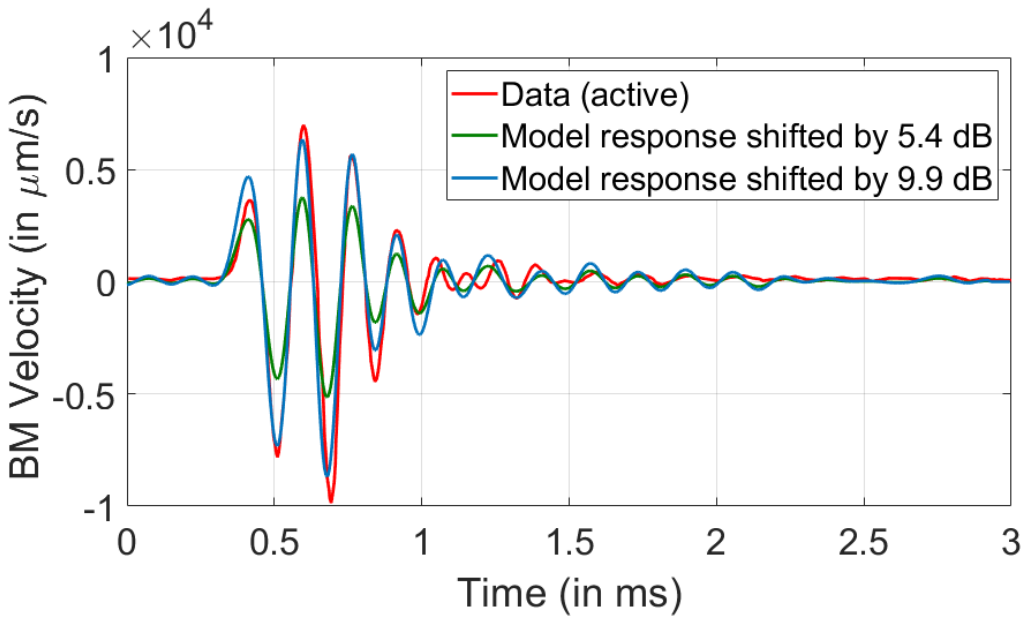

Figure 24. BM active response comparison

1.8.3 Chinchilla Complex Noise Exposure

1.8.3.1 Complex Noise Pressure Waveforms

A sample waveform for each of the TCs from test series 1-a and 2-a, and 1-b and 2-b performed without and with background noise, respectively is shown in this section. For Series 1-a and 2-a, the CNGS was not used, and the waveform is composed of the 10 individual blasts. For Series 1-a and 2-b, for which the CNGS was used, the individual blasts are superimposed with the continuous noise. The results for the reconstruction of the mixture of blast and continuous are also described.

A waveform sample is shown in Figure 25 for TC 1 from Series 1-a. TC 1 contains a sequence of 10 impulses with alternating intensity levels, L1, L2 at fixed IPI of 3 sec. Each spike is the individual actual impulse whose time features are not visible due to the long total exposure time required to show the complete sequence. The height of the spike indicates the peak pressure, and the separation between two consecutive spikes is the IPI. Figure 26 shows the zoomed-in traces for all 10 shots showing the L1 and L2 groups. The traces were time-shifted and superimposed for cross comparison. The two distinct peaks are clearly noticeable and the waveforms are consistent. Also, the time interval between the peaks is nearly constant. This result shows that the ARFST system is reliable and accurate. A selected waveform sample is shown in Figure 27 for TC 2 to 6.

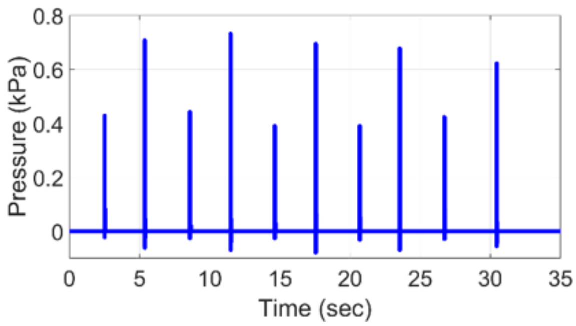

Figure 25. Waveform sample for TC 1 (sequence L1t1L2)

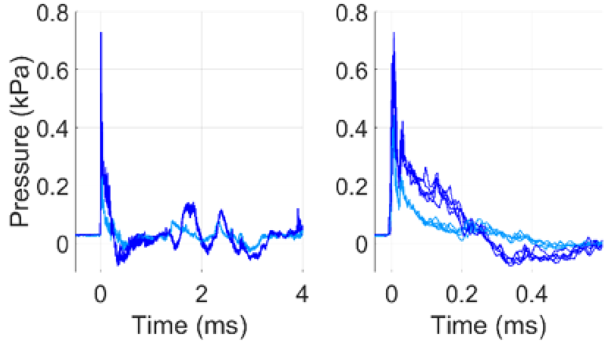

Figure 26. Zoomed-in traces for TC 1 (sequence L1t1L2)

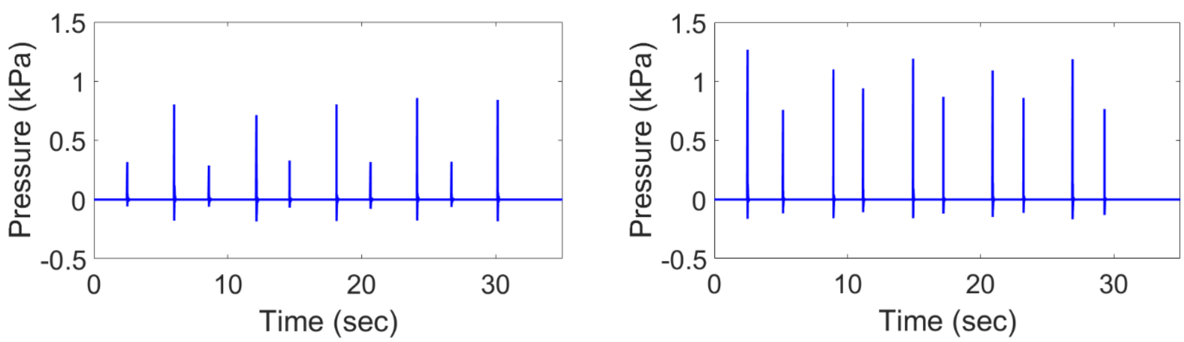

a) TC 2 **b) TC 3**

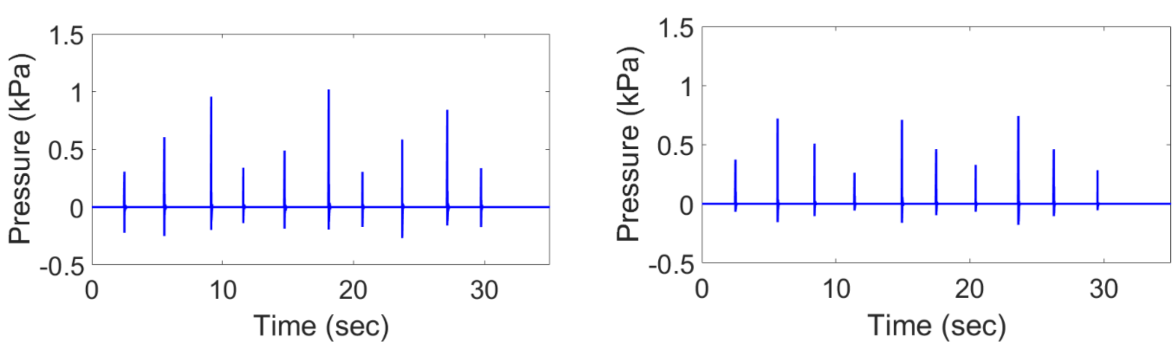

c) TC 4

d) TC 5

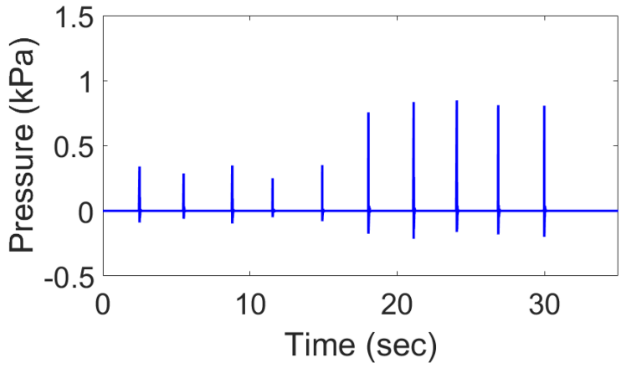

e) TC 6

Figure 27. Waveform sample for TC 2 through 6

A selected waveform sample from test Series 2-a is shown in Figure 28 for TC13 to TC18 of the ME test matrix (Table 1). As seen in Figure 28, the level and IPI are both varied for this test series according to the test matrix.

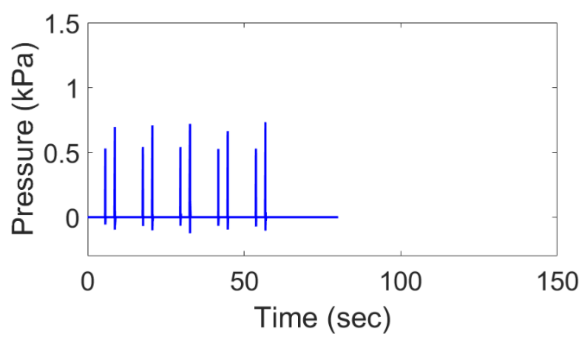

a) TC 13

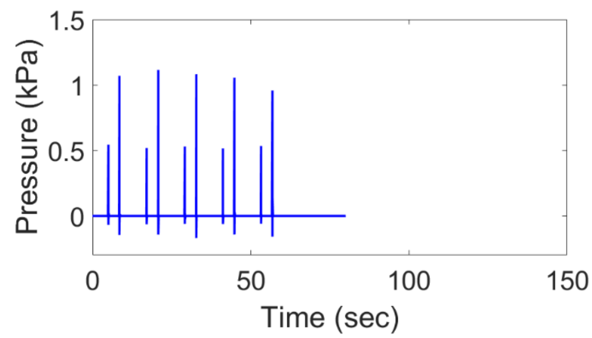

b) TC14

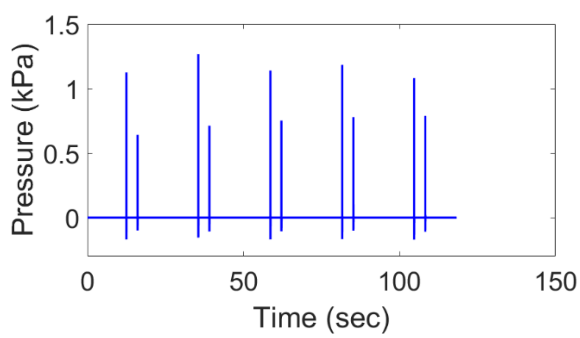

c) TC15

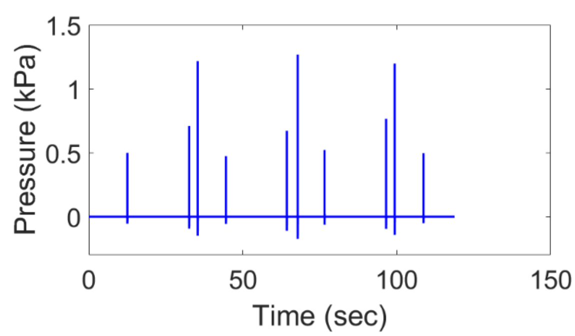

d) TC16

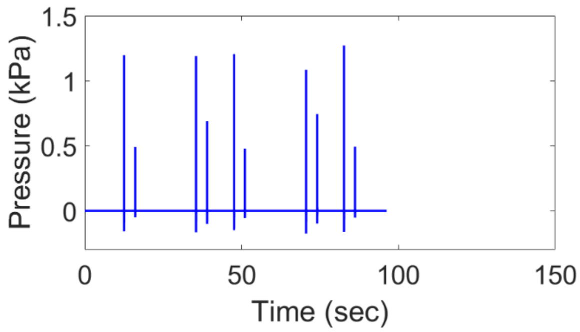

e) TC17

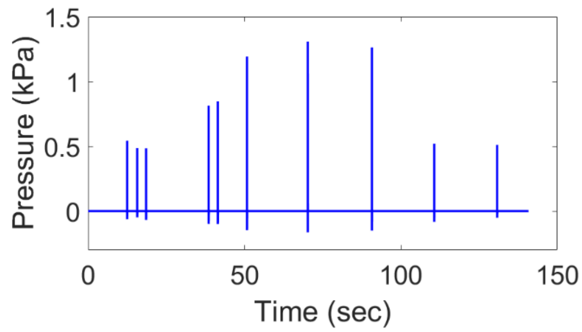

f) TC18

Figure 28. Blast waveform sample for Series 2-a for TCs 13 through 18

A selected waveform sample is shown for Series 1-b with background continuous white noise in Figure 29, which shows the pair of recordings representing the blast (Figure 29a) and the background noise (Figure 29b).

Figure 29a shows the recorded individual blasts as spikes with the background continuous white noise buried in the signal noise due to the low sensitivity of Microphone 1. On the other hand, Figure 29b shows the recorded background noise, but the individual blasts are clipped due to the range limitation for Microphone 2.

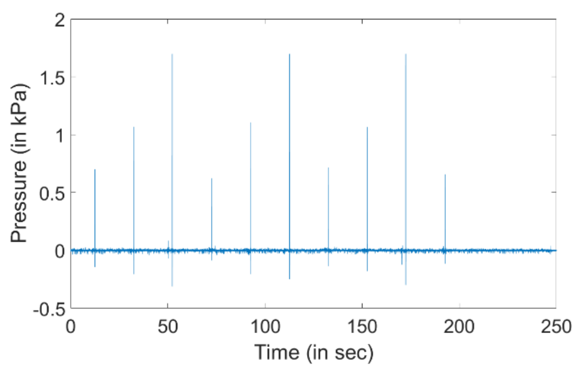

a) Blast

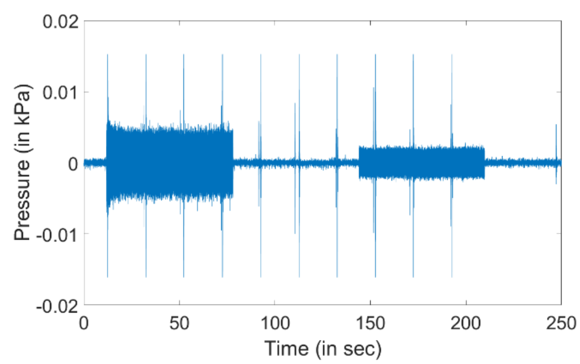

b) Background white noise

Figure 29. Sample waveform for Blast + background noise for TC10. a) Microphone 1 data (Blast recording); b) Microphone 2 data (Background noise recording)

The result for the reconstruction of the complex mixture of noise is shown for TC21 in Figure 30, which shows the pressure data from Microphone 1 and 2 and the resulting merged pressure time-trace data. Again, each spike represents the actual individual impulse whose detailed features are not visible due to the long time-scale required to show the complete sequence. The details of the background noise are also not clearly visible in the reconstructed pressure waveform due to the large scale required to show the blast peak levels. A sample of the reconstructed pressure waveforms from test Series 1-b and 2-b is shown in Figure 31 and 32, respectively. The variation of level and IPI is reflected in the individual pressure traces, comprised of closely spaced and widely spaced blasts with three intensity level combinations, riding on top of the moderate level continuous background noise (not clearly visible due to the long total duration shown).

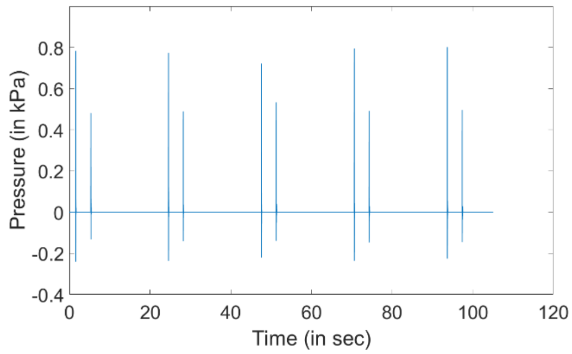

a) Blast

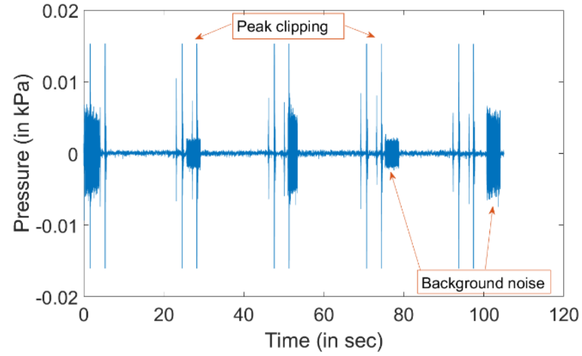

b) Background white noise

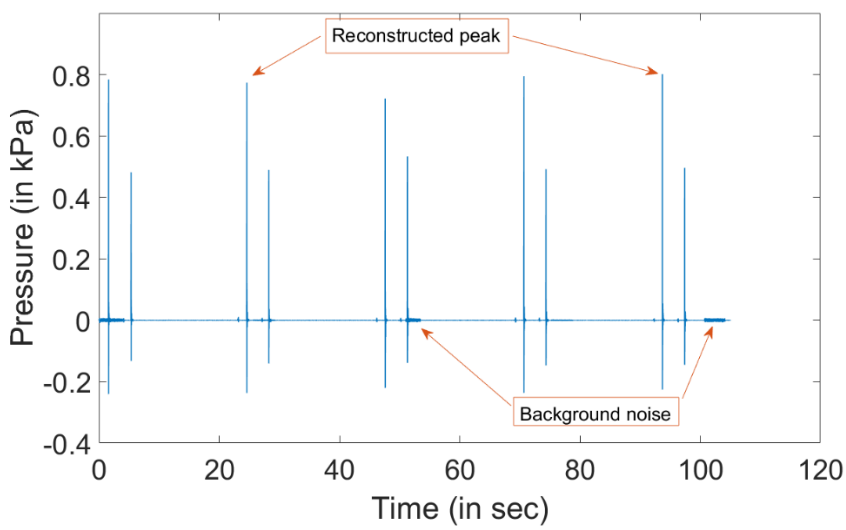

c) Merged data

Figure 30. Reconstructed waveform for TC21. a) Microphone 1 data (Blast recording); b) Microphone 2 data (Background noise recording); c) Merged data. Note the smaller scale for pressure in Figure 30b).

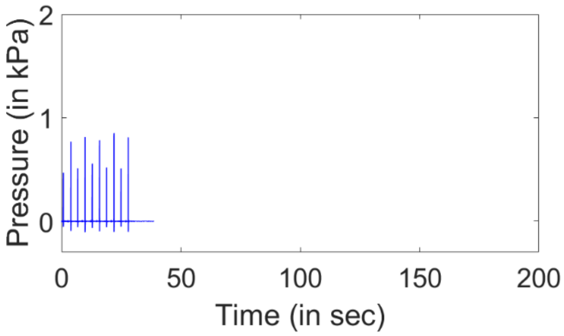

a) TC 7

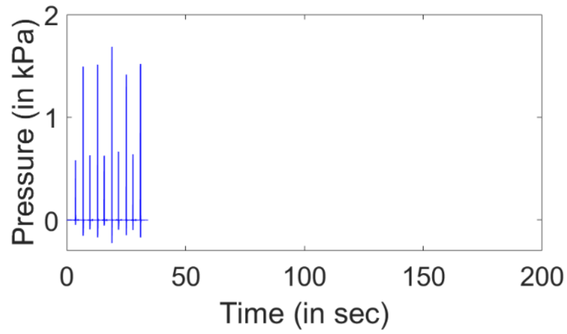

b) TC 8

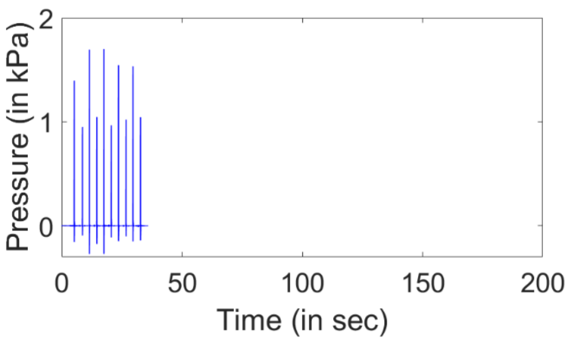

c) TC9

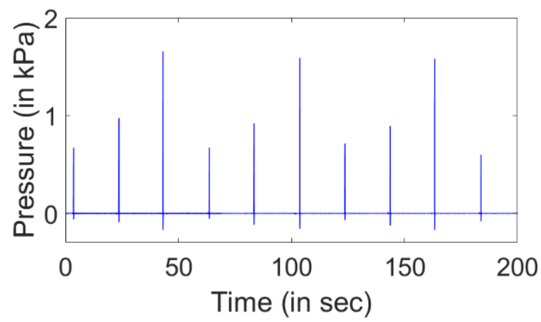

d) TC 10

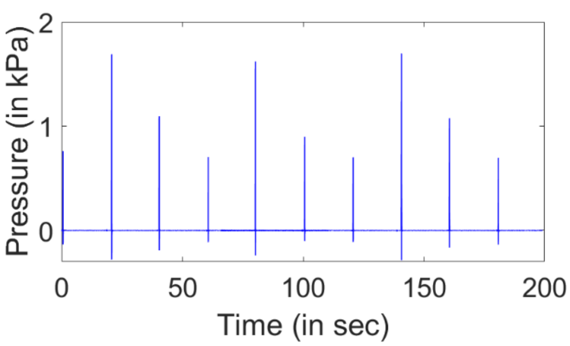

e) TC 11

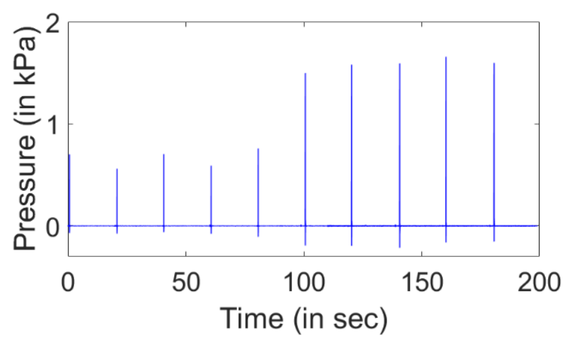

f) TC 12

Figure 31. Sample waveforms from Series 1-b with background white noise

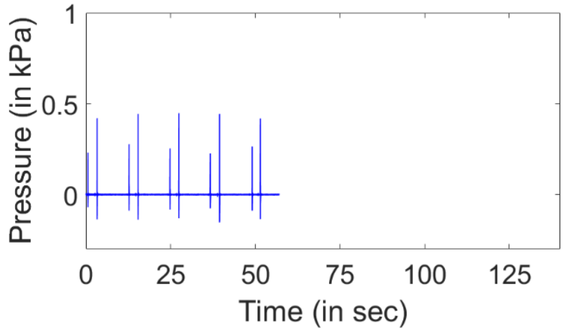

a) TC 19

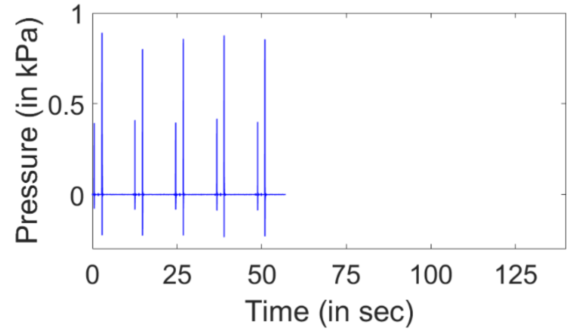

b) TC 20

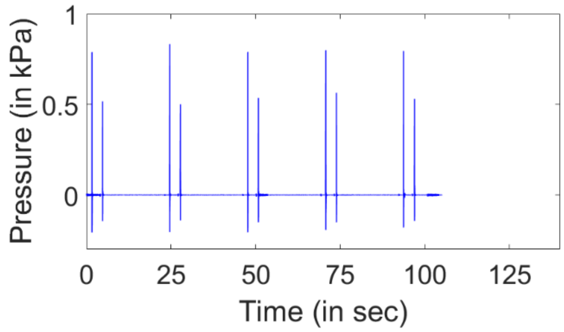

c) TC 21

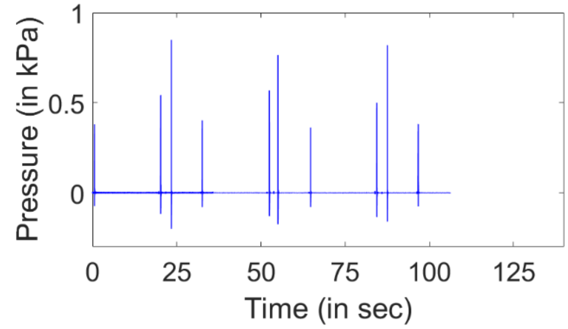

d) TC 22

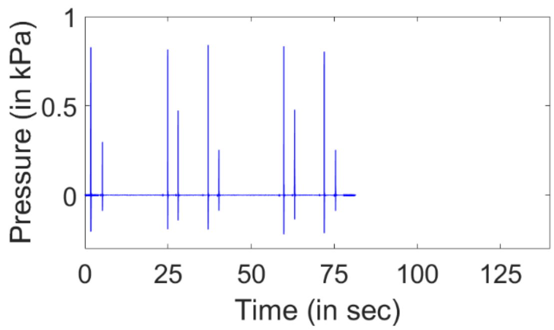

e) TC 23

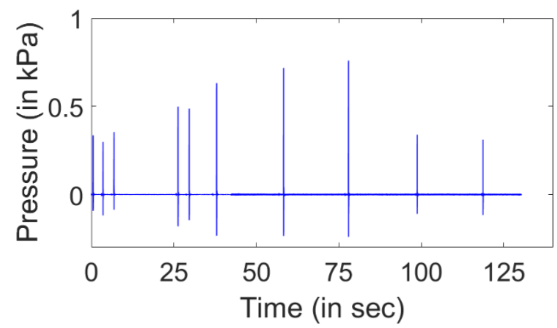

f) TC 24

Figure 32. Sample waveforms from Series 2-b with background white noise

1.8.3.2 TTS Data

In this section the results for the TTS data collected immediately post-exposure are summarized. The mean TTS obtained from the 5 samples are plotted as a function of frequency for all the test series of Table 1, and the TCs are compared to each other within each series using the standard t-test. The effects of the IPI and shot sequence are determined from the TTS outcomes.

1.8.3.2.1 *Mean TTS comparison*

Figure 33 shows the TTS mean as a function of frequency for all the TCs according to the test series of Table 1. Figure 33 shows that within each test series, the mean TTS incurred immediately post-exposure could span 30 dB across all frequency, with the exception perhaps for Series 2-a, which shows a wider range. The TTS ranges are 10-40, 30-50, 10-60, and 30-60 dB for Series 1-a, 1-b, 2-a, and 2-b, respectively. In Series 2-a, TC 13 produced the lowest TTS, while the other TCs are bundled with TTS ranging between 30 and 60 dB across frequency. For each TC and for all test series, the mean TTS does not vary by more than 20 dB across the frequency range.

The global effects of background noise can be determined by comparing the mean TTS from Figure 33a and b, on one hand and Figure 33c and d on the other. Comparing the TTS means as shown in Figure 33a and b shows there is a clear increase of about 20 dB in the lowest TTS value in Series 1-a compared to that in Series 1-b. Therefore, for regular IPI spacing (Series 1), the global effect of the background noise is to increase the mean TTS. The effect of background noise for TC 1, 2, and 3 is more clear in the bar graph of Figure 34 showing TTS_{124K} increases when background noise is added. Comparing the TTS means in Figure 33c and d, it can be observed that aside from TC 13, overall, the TTS mean from Series 2-a is similar to that from Series 2-b. Therefore, the irregular IPI (Series 2) appears to mitigate the effects of background noise.

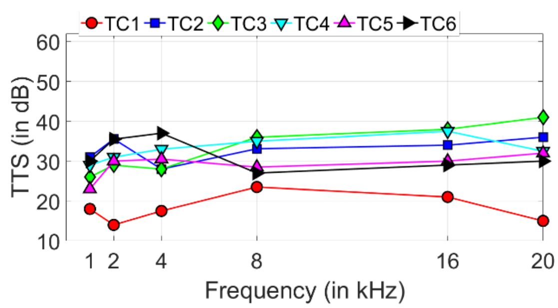

a) Series 1-a

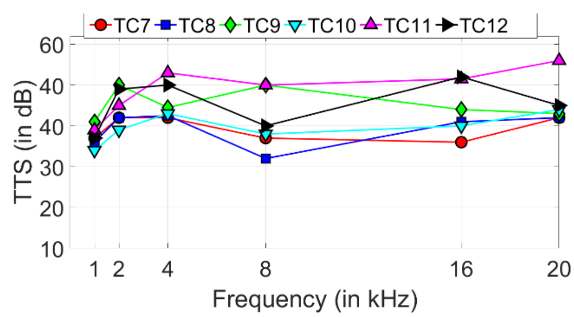

b) Series 1-b

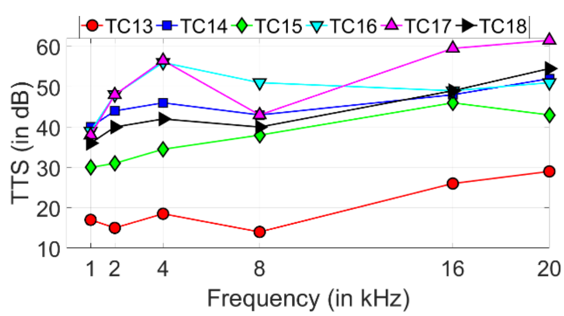

c) Series 2-a

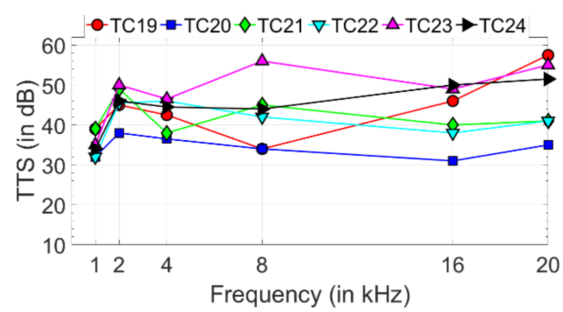

d) Series 2-b

Figure 33. Mean TTS incurred immediately post exposure as a function of frequency

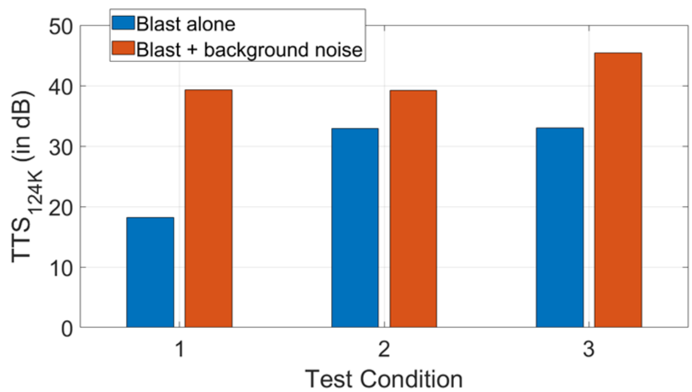

Figure 34. Effect of background on TTS_{124K} for TC 1, 2, and 3

Two-tail t-test performed within each test series by comparing test pairs showed mostly no significant difference between the TTS means for the majority of the TCs within each test series.

No TC pair from Series 1-a showed a significant difference for the TTS mean averaged across 1, 2, and 4 kHz (TTS_{124K}), and for all pairs in this series, $p>0.05$. When TTS was considered for individual frequencies, the difference in TTS mean was significant for TC 1 and 6 at 1 and 2 kHz, TC 1 and 2 at 2 kHz, and TC 1 and 3 at 20 kHz ($p<0.05$).

For Series 1-b, no pair combination showed any significant difference between the TTS_{124K} means. For the individual frequencies, when a significant difference existed, it was observed for the high frequencies. TC pairs 12 and 7, and 12 and 10 showed a significant difference at 16 kHz, while TC 9 and 11, showed a significant difference at 20 kHz.

For Series 2-a, TC 13 and all the other TCs, except TC 15 showed a significant difference in the mean TTS_{124K}. TC 15 and 16 also showed a significant difference in mean TTS_{124K}. When compared at the individual frequencies, 30 out of 90 pairs (1/3) compared showed a significant difference in TTS mean, with TC 13 showing a significant difference in TTS mean for all frequencies when compared to the other TCs. TC 14 and 15 shows a significant difference at 1 kHz, and TC 16 and 18 shows a significant difference at 4kHz.

For Series 2-b, the difference in TTS_{124K} was not significant for all TC pair combination. For the individual frequencies, TC pair 23 and 20 showed a significant difference for 8 and 20 kHz, and TC pair 23 and 19 showed a significant difference for 8 kHz.

1.8.3.2.2 *Effect of IPI and Shot Sequence on TTS*

The effects of IPI and shot sequence were assessed by comparing the TTS outcomes from the TCs. As described previously, TC pairs, (1, 13), (2, 14), (3, 15), and (4, 16) were designed such that only the IPI was changed for each pair of TCs. The total energy and shot sequence remained the same for each of these pairs. The TTS outcomes from the two TCs are compared to determine the effects of the IPI on the TTS incurred immediately post-exposure. The TTS means are compared by performing a significance test using standard two-tail t-test. The results are shown in Table 3.

As shown on the left in Table 3, 3 out of the 4 test-pairs (75%) indicate IPI has no significant effect on TTS ($p > 5\%$), and their associated power (pwr) values are also low (< 22%) suggesting there is weak power to reject the t-test results. Even for the last test-pair for condition 4 vs. 16 where the p-value of 3.33% suggests that IPI can affect TTS, the relatively high pwr value of 40.76% gives a high probability to reject the t-test result. As shown on the right, 22 out of 24 (92 %) pairs show no significant difference for the test pairs by frequency.

Table 3. Summary for 2-tail t-test results for effect of IPI on TTS

TTS averaged for 1, 2, and 4 kHz			
TC		p-value	Power (%)
1	13	0.952735	5.026241
2	14	0.145734	21.00568
3	15	0.60358	8.125691
4	16	0.033258	40.76127

TTS for individual frequencies				
Freq (kHz)	TC		p-value	Power (%)
1	1	13	0.847961	5.321969
1	2	14	0.115555	25.69862
1	3	15	0.408168	10.46374
1	4	16	0.272456	14.62083
2	1	13	0.889374	5.11695
2	2	14	0.272284	12.72993
2	3	15	0.830732	5.633684
2	4	16	0.035025	37.97747
4	1	13	0.908854	5.112562
4	2	14	0.131765	23.49675
4	3	15	0.606913	8.459337
4	4	16	0.006621	65.61023
8	1	13	0.197779	16.34725
8	2	14	0.209432	26.94952
8	3	15	0.823158	5.977949
8	4	16	0.074671	26.04824
16	1	13	0.419376	11.24626
16	2	14	0.108322	29.05522
16	3	15	0.510588	12.14844
16	4	16	0.316792	18.07966
20	1	13	0.060255	29.6893
20	2	14	0.097039	24.8363
20	3	15	0.855132	5.501318
20	4	16	0.127656	29.86979

Similarly, the potential effect of shot sequence was determined using the same procedure. The TTS data outcomes from TC pairs (2, 6) and (4, 5), which were designed by changing the shot sequence only, with all other noise feature remaining the same were compared using standard t-test. The t-test results are shown in Table 4.

The t-test results show that the effect of shot sequence is not significant. The two test-pairs in the upper corner in Table 4 clearly show the effect of shot sequence being insignificant on the TTS_{124K}

outcomes with p-values exceeding 5% and power values below 7%. Likewise, the effect of shot sequence is insignificant on the TTS outcomes by frequency, as shown on the right in Table 4.

Table 4. Summary for 2-tail t-test results for effect of shot sequence on TTS

TTS averaged for 1, 2, and 4 kHz			
TC		p-value	Power (%)
2	6	0.739858	5.77283
4	5	0.64071	6.2568

TTS for individual frequencies				
Freq (kHz)	TC		p-value	Power (%)
1	2	6	0.861928	5.243549
1	4	5	0.441887	8.394909
2	2	6	0.99571	5.000167
2	4	5	0.894632	5.109815
4	2	6	0.465601	9.496652
4	4	5	0.751138	5.773679
8	2	6	0.363668	13.19507
8	4	5	0.517648	8.360186
16	2	6	0.637887	7.964515
16	4	5	0.485101	10.45916
20	2	6	0.596565	7.69109
20	4	5	0.966913	5.017308

1.8.3.2.3 *Effect of Background noise on TTS*

To determine the effect of background noise, the TTS outcomes from a shot sequence that was given with the presence of the background continuous noise was compared to the TTS outcome without the background continuous noise. The outcomes from both the TTS_{124K} and TTS for the individual frequencies were compared, respectively for the shot sequences with background noise versus sequences without background noise. A significance test was performed using the student t-test.

The following TC pairs were compared: (1, 7), (2, 8), (3, 9), from Series 1-a and –b with constant IPI, and TC pairs (13, 19), (14, 20), (15, 21), (16, 22), (17, 23), and (18, 24) from Series 2-a and –b with varied IPI. As shown in Table 1, the first TC in each pair is the shot sequence without the background continuous noise and the second TC is with the background noise. The results of the 2-tail t-test are summarized in Table 5. The upper left corner of Table 5 shows the t-test results for TTS_{124K}. The lower left corner shows the results for TTS for individual frequencies for Series 1-a and -b. The comparison results for the individual frequencies for Series 2-a and –b with varied IPI are shown on the right. The test pairs that showed a significance difference are highlighted in light blue.

As shown in the upper left corner table, 3/9 TC pairs showed a significant difference for TTS_{124K}. TC pairs (1, 7), (3, 9), and (13, 19) showed a significant difference ($p<0.05$) with a high statistical power (power > 57%). As shown in the lower left corner table for TTS for the individual frequencies, Series 1-a and –b comparison resulted in 7/18 (38.9%) pairs showing a significant difference ($p<0.05$) with a high power (power > 58%). As shown in the right column, only 6/36 (16.7%) pairs showed a significant difference ($p<0.05$, power> 72%). Hence, the proportion of test pairs showing a significant difference in the TTS outcomes when background noise is added was twice as high for TC with constant IPI compared to TC with varied IPI.

The t-test results show that the background noise has some effects on the TTS that depend on frequency, IPI, and background noise intensity. As shown previously by comparing the global trend of the mean TTS, the t-tests results confirm that background noise tends to increase TTS. Constant and varied IPI influence the effect of background noise differently, with constant IPI being more sensitive to the background noise effect. As shown in Figure 34 and the t-test results for TTS_{124K} (Table 5, upper left), the effect of background noise was detectable when the background noise intensity was the highest. In fact, for TC pair (2, 8) involving the less intense background noise the t-test showed no significant difference between the test pair, while the difference in TTS was significant for test pairs (1,7), (3,9), and (13,19) involving the more intense background noise. Moreover, as shown by comparing the proportion of tests showing a significant difference in TTS outcomes, irregular IPI tend to mitigate the effects of the background noise.

Table 5. Summary for 2-tail t-test results for effect of background noise on TTS

TTS averaged for 1, 2, and 4 kHz			
TC		p-value	Power(%)
1	7	0.004762	92.05287
2	8	0.374874	13.4643
3	9	0.018676	57.83761
13	19	0.011573	99.73971
14	20	0.328097	27.94868
15	21	0.217329	19.283
16	22	0.173827	37.94603
17	23	0.340638	9.86662
18	24	0.700392	6.289952

TTS for individual frequencies, Series 1-a and -b				
Freq (kHz)	TC		p-value	Power (%)
1	1	7	0.012825	88.04027
1	2	8	0.543158	11.24626
1	3	9	0.029181	71.57998
2	1	7	0.006108	79.75721
2	2	8	0.502121	9.45852
2	3	9	0.009578	68.41694
4	1	7	0.015173	67.10264
4	2	8	0.251714	16.91246
4	3	9	0.067826	28.03111
8	1	7	0.17259	28.1257
8	2	8	0.936689	5.25828
8	3	9	0.054033	52.5192
16	1	7	0.024609	58.15874
16	2	8	0.491974	10.87561
16	3	9	0.441887	8.97695
20	1	7	0.013833	77.93051
20	2	8	0.587119	7.69109
20	3	9	0.759923	5.501318

TTS for individual frequencies, Series 2-a and -b				
Freq (kHz)	TC		p-value	Power (%)
1	13	19	0.003016	97.87925
1	14	20	0.12275	44.35053
1	15	21	0.115555	53.28687
1	16	22	0.286051	14.73185
1	17	23	0.535753	7.934488
1	18	24	0.696754	6.342601
2	13	19	0.002827	99.99335
2	14	20	0.460856	25.01959
2	15	21	0.078206	33.51737
2	16	22	0.641786	12.24477
2	17	23	0.6938	5.840902
2	18	24	0.273139	14.59832
4	13	19	0.095749	75.28789
4	14	20	0.411307	18.14796
4	15	21	0.785242	5.604375
4	16	22	0.047355	90.9748
4	17	23	0.14169	24.59074
4	18	24	0.76742	5.879522
8	13	19	0.026694	98.78862
8	14	20	0.329084	17.05934
8	15	21	0.565653	8.975956
8	16	22	0.238833	84.48342
8	17	23	0.073877	41.50935
8	18	24	0.738126	6.31803
16	13	19	0.110825	87.06849
16	14	20	0.115111	62.38711
16	15	21	0.658564	6.748098
16	16	22	0.344705	13.21291
16	17	23	0.017875	72.3204
16	18	24	0.886431	5.11695
20	13	19	0.003226	100
20	14	20	0.066307	87.23459
20	15	21	0.878285	5.23558
20	16	22	0.339661	13.70186
20	17	23	0.248303	18.46434
20	18	24	0.682552	7.154729

1.8.4 ME Model Computational Time

The computational time for the cochlear variable outcomes are reported in this section.

As described earlier, E_{OHC} and the OHC-ED are calculated by transferring the individual complex noise pressure trace into the ME cochlear model via the outer and middle ear TFs. The rate of work of stress on the OHC, W_{OHC} and the instantaneous energy supply, W_c are calculated, time integrated, and summed over the critical bands of the cochlea according to Eq. 10 to yield the energy deficit incurred.

The most time consuming stage for the cochlear analysis was the cochlear modes calculation which took 3 days of computation. As described earlier, the modes are only calculated once and used subsequently to calculate the response for an arbitrary pressure time trace. With the following parameter values for the longest trace, T_d = 200 seconds, with sampling frequency, f_s = 200 kHz, and a high frequency cut-off of 30 kHz, the number of modes required is N_m = 6,000,000. The parallelized computation method was implemented by subdividing N_m in 6 chunks of 1,000,000 modes, and each chunk was calculated using the MATLAB *parfor* loop command with 4 workers. A DELL Precision 5820 Tower computer with Intel® Xeon® CPU at 3.30 GHz was used. The process resulted in 3 days of computation to obtain all the cochlear modes.

The average time taken to calculate the cochlear response for an arbitrary pressure trace with duration, T_d < 200 seconds was ~10 min, with a total of ~20 hours for all 120 exposures from Table 1. Using the pre-calculated modal response, the time-dependent cochlear variables, E_{OHC} and OHC-ED were calculated for all 120 test cases via an automated batch run. The shortest duration exposure (T_d = 30 secs) took about 6 min while the longest (200 secs) took twice as long, ~13 min.

The average computational time of 10 minutes to calculate the OHC-ED incurred for the complex noise trace seems reasonable considering the inherently long time pressure trace required to represent the complex noise (200 sec). It is to be noted that the time required for the cochlear modes calculation is inconsequential for the day-to-day use of the model once packaged since the cochlear modes are pre-calculated as part of the model construction and do not required recalculation once the model has been packaged.

1.8.5 Dose-response Curve against TTS > 25 dB from Complex Noise

Using logistic regression calculations, the dose-response curve established against TTS_{124K}>25 dB based on the chinchilla blast exposure data using the OHC-ED as the injury correlate is presented in this section.

The dose-response curve against TTS_{124K} > 25 dB established based on the chinchilla complex noise exposure injury data is shown in Figure 35. The data points shown by the filled circles represent the mean failure rates based on 10-bin data grouping of all chinchilla data used. There is a good fit to the binned data, and the 95% confidence interval is tight (n = 120), considering the limited range of the data. Therefore, the logistic regression fit and the threshold prediction are well established.

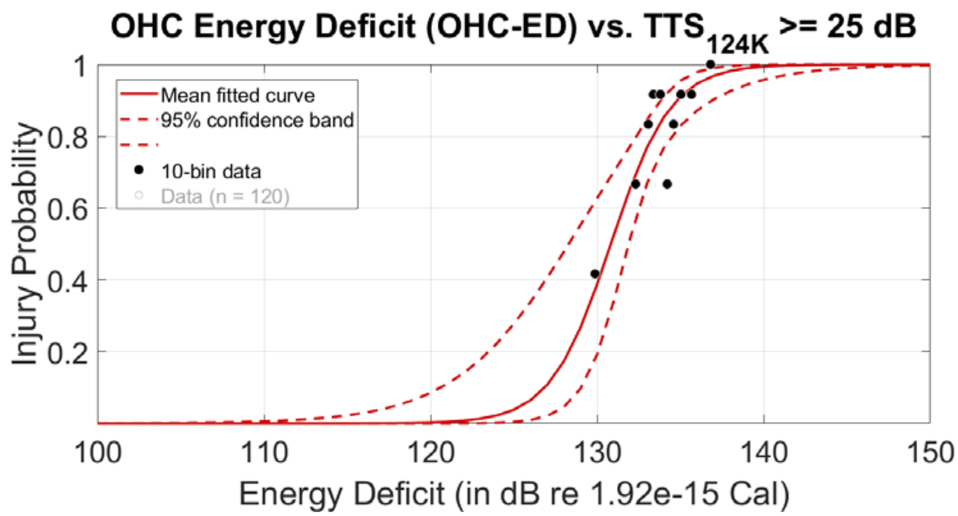

Figure 35. Dose-response curve against TTS_{124K} > 25 dB using OHC-ED

1.8.6 IPI contribution to OHC-ED

A biomechanical explanation for the insignificance of the IPI was sought by comparing the contribution of the IPI to the total OHC-ED. The IPI contributions for the TC pairs (1, 13), (2, 14), (3, 15), and (4, 16) were compared. The IPI contribution to OHC-ED is defined as the OHC-ED incurred during the IPI only, and is obtained by integrating the energy deficit formula (Eq. 12) over the IPI (silent interval).

Figure 36 shows the comparison result for the contribution of IPI to OHC-ED and the total OHC-ED. As shown in Figure 36, the IPI contribution to OHC-ED is four orders of magnitude smaller than the total OHC-ED. This result shows that contribution to the total OHC-ED is minimal, at least for the IPI in the range between 3 and 20 seconds, as considered in this study.

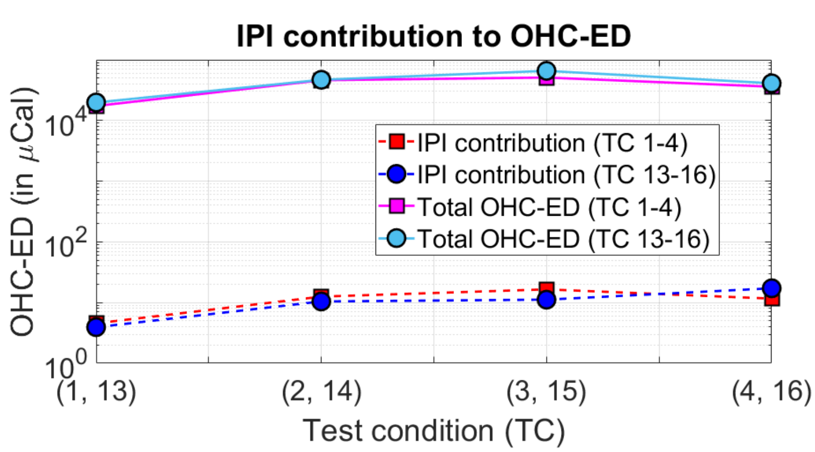

Figure 36. Effect of IPI on OHC-ED

A two-tail student t-test at the significance level of 5% was used to determine whether there is a significant difference between the IPI contribution for the elements of the TC pair, with the results shown in Table 6. As shown in Table 6, the p-values are greater than the 5% with a low power to reject the p-values, indicating that the IPI contributions are not significantly different. The TTS significance test shows no significant difference between the IPI contribution to OHC-ED for all the TC pairs compared, and suggests that the IPI does not have a significant effect on the total OHC-ED. The TTS significance test performed for these TC pairs also showed no significant difference between the TTS incurred. Therefore, the insignificance of the IPI contribution confirms that the TTS outcome is not affected by the IPI, at least for the IPI durations considered in this study.

Table 6. Significance test for IPI contribution to OHC-ED

TC		p-value (%)	Power (%)	Difference
1	13	79.63	6.39	Not Significant
2	14	58.26	13.25	Not Significant
3	15	6.31	29.87	Not Significant
4	16	43.2	49.08	Not Significant

Figure 37 shows a sample comparison along the cochlea of the mean IPI contribution for TC 2 and 4. As shown in Figure 37, the means of the IPI contribution to OHC-ED along the cochlea are similar. The IPI contribution varies between 0 and 2.5 µCal; it is frequency dependent and dominates at low frequency.

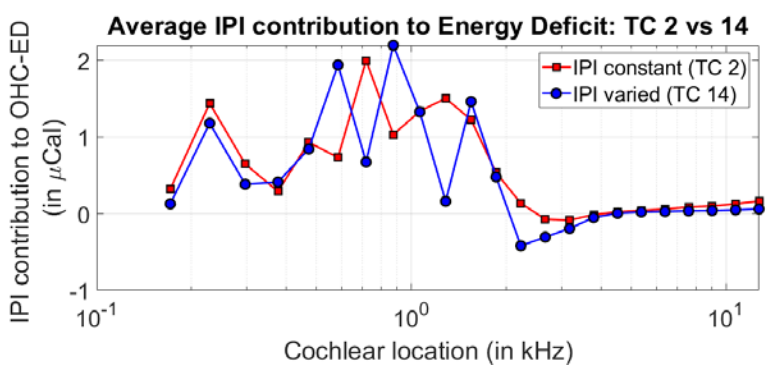

Figure 37. IPI contribution along the cochlea for selected TCs (TC 2 and 4)

1.8.7 Energy Demand vs. Supply

To evaluate the relative importance of energy demand and energy supply, they were both calculated and compared to each other for selected TCs. The result is shown in Figure 38.

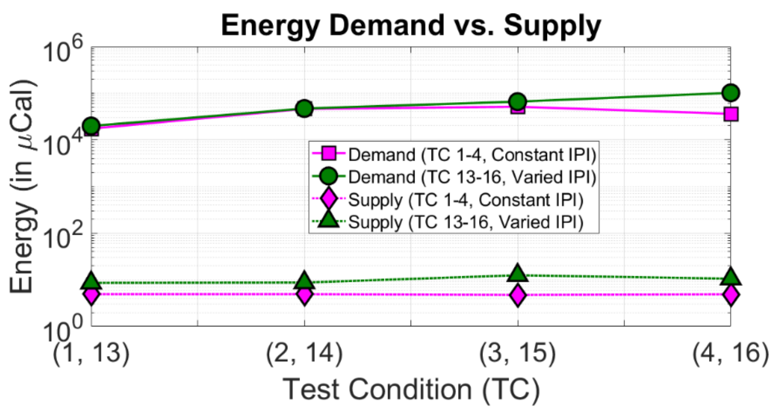

Figure 38. Comparison of energy demand and supply for selected TCs

As shown in Figure 38, the energy demand is always greater than the energy supply, regardless of whether the IPI is constant or varied. The difference between energy demand and supply is large, with the energy demand being four orders of magnitude greater than the energy supply. Therefore, the energy supply is practically negligible compared to the demand. Hence, the energy deficit is entirely determined by the energy demand.

The relative importance of the competing energies determined the OHC-ED, and the result can be summarized in Eq. 15, where the energy demand and supply terms can be readily identified from Eq. 12.

$$D = E_{Demand} - E_{Supply} \approx E_{Demand}; \quad E_{Supply} \ll E_{Demand} \qquad (15)$$

1.8.8 Effect of Background noise on OHC-ED

The effect of background noise on OHC-ED is shown in Figure 39 for TC 1, 2, and 3 which is analyzed in light of the results shown in Figure 34 for TTS_{124K}. As shown in Figure 34 and Figure 39, the TTS and OHC-ED clearly follow the same trend. Therefore, the OHC-ED model also captures the effect of background noise.

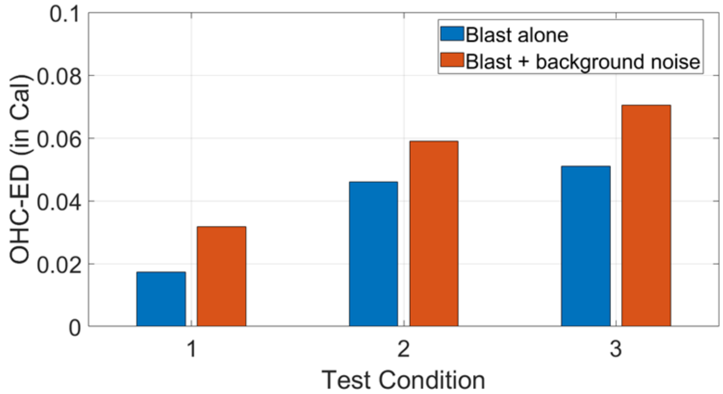

Figure 39. Effect of background noise on OHC-ED

1.8.9 Prediction of USAARL Chinchilla Data

The prediction capability of the energy deficit model was tested for very long IPI. The energy deficit model prediction is compared with the US Army Aeromedical Research Laboratory (USAARL) chinchilla PTS data. The PTS data are from chinchillas exposed to fast-acting valve impulses. The total exposure duration is between 10 and 1000 minutes.

As shown in Figure 40 (top panel), the USAARL data show when IPI is very long, injury decreased. This observation is explained by the model showing long IPI provides time for energy supply to increase resulting in lower energy deficit, hence lower injury. As shown in of Figure 40, the energy supply increased with IPI (lower panel), while the energy deficit decreased with IPI (mid-panel).

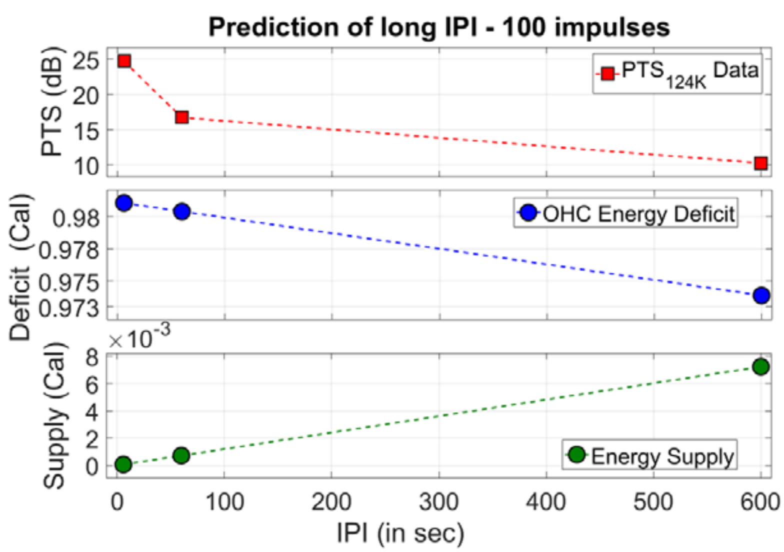

Figure 40. Model comparison with USAARL PTS data

1.9 Discussion

A ME model was developed that established a good correlation between the OHC-ED outcomes and the TTS data from complex noise exposure, explained the data collected, and provided many insights on the effect of complex noise exposure including the effect of IPI, shot sequence, and background noise. The dose-response curve was established with good fit and a tight confidence band with a reasonably narrow confidence band even though the data range is narrow with a small data sample size.

The ME model showed that the energy supply is low in general in response to the relatively high-level complex noise exposure, explaining the high injury rate observed during the noise exposure experiment as conducted. The energy supply was proportional to the IPI, hence the relatively short IPI also contributed to the low energy supply.

For the intensity levels used (145-154 dB), the OHC-ED model suggests that the effects of shot sequence and IPI on the order of 1 second on injury are not significant, but the effect of intense background noise is significant. The dominant effect on injury from the multiple shots was the intensity level.

The ME model is able to explain the effect of very long IPI on the reduction of auditory injury. When compared with the USAARL chinchilla data showing PTS decreases with IPI, the ME model showed that the long IPI provides time for the energy supply to increase, resulting in a lower energy deficit, and hence a lower injury.

Comparison of the results from the OHC-ED model against the previously developed ICE model showed that the OHC-ED metric is superior to the ICE metric for injury prediction for complex noise exposure involving multiple shots and background noise. There was a relatively poor correlation using ICE to predict the TTS data. This result shows that even though the ICE constitutes a good metric against mechanical damage from high-level impulse noise exposure, it cannot be used to predict metabolic damage from complex noise exposure. Both metrics are incorporated in the AHAAH-ICE model so that both mechanical and metabolic damage can be predicted. The chinchilla OHC-ED model provides a good foundation for understanding noise-induced auditory exhaustion in humans for which data are currently lacking.

For this project a specialized noise generation equipment was developed and unique experiments were performed. An ARFST was developed for multiple irregular shot sequence exposure testing. The ARFST constitutes a specialized test device that can be used for experiments involving repeated low to moderate intensity levels such as for the study of auditory injury and concussion from repeated blows. By selecting the appropriate Mylar size, the desired blast intensity can be obtained. The ARFST can fire 20 shots in 1 minute. Cochlear tissue properties data were collected for both chinchilla and human to build the cochlear model incorporating the energy deficit model. Tissue stiffness map for chinchilla cochlear was not available until now. The chinchilla cochlear tissue measurement experiment provided valuable data for the construction of the metabolic exhaustion model. The cadavers' cochlear stiffness data were collected using state-of-art novel measurement techniques, and thus provided very accurate measurement and new data.

1.9.1 Limitations

The validity of the dose-response curve against TTS > 25 dB established using the chinchilla blast exposure data is limited to IPI in the range from 3-20 sec and intensity level from 145-153 dB PPL. Combinations of level (L) and IPI in these ranges can be predicted using the dose-response curve. Up to 3 min long complex noise pressure trace including impulse train with IPI and L combinations as specified above and continuous noise with level between 90 and 100 dB can be run using the ME model to calculate OHC-ED. For longer duration trace, a hybrid method is used that calculates the individual impulses within the complex noise sequence and integrate the IPI contribution analytically to determine OHC-ED.

For the chinchilla blast exposure experiment, the test sample size and the narrow exposure range are potential limiting factors for the ME model developed. The sample size selection was mostly dictated by budget and ideally should be increased to 8 animals per test condition to achieve better statistical power. The narrow range of the dose and outcomes observed is directly related to the narrow range of impulse intensity level tested. The actual change of PPL range was less than 10 dB (145- 154 dB); likewise, the OHC-ED range was less than 10 dB (130-137 dB re 1.92e-15 Cal). However, the narrow exposure range used for the study was to a great extent by design since a key objective of the research was to study the effects of varying IPI and shot sequence on outcomes when the total exposure energy was more or less held constant. Nevertheless, a reasonable dose-response curve for 25-dB TTS was obtained with good statistical fit showing OHC-ED can serve as a good biomechanical metric that can provide physiological-based explanation of the observed outcomes. More tests should be performed at higher and lower exposure levels to see if similar trends are observed, including more variation of the total number of shots. Additional studies will strengthen the model-based dose-response model that can be related to the damage mechanism.

The middle ear nonlinearities, including the annular ligament and AR nonlinearities were not accounted for in calculating the OHC-ED outcomes since the chinchilla middle ear TF used to represent the middle ear transformation was obtained from low level exposures from pure tone experiments. Three main reasons led to the adoption of the data-driven TF implementation of the middle ear. Firstly, the AR model as implemented in the AHAAH-ICE model is inadequate for multiple shots because the AR does not account for the frequency and level dependency or the AR adaptation effect, which are all critical for multiple shots. Correcting the AR model requires a separate effort. Secondly, the AR for humans is still being investigated, with current data indicating that the AR is not prevalent among humans, and thus suggesting that if AR is to be implemented in damage risk criteria (DRC), a statistical distribution of the AR must be incorporated in the DRC to account for variation in the general population. Thirdly, the middle ear model could not match the chinchilla TF data using mere parametric optimization. The main reason is that chinchilla and human middle ear TFs are different. The chinchilla middle ear is rather tuned to the higher frequencies compared to that for human, while the accuracy of network models is intrinsically limited to 8 kHz. Improvement for chinchilla middle ear model is needed. The advantage of using the TF data is that the relevant high frequency components for chinchilla are readily captured. The disadvantage is the exclusion of annular ligament nonlinearity and the AR, which is likely to play a role when continuous noise is involved.

1.9.2 Knowledge Gaps

The following knowledge gaps still exist that need to be addressed by new research.

1. The role of AR on traumatic impulse noise effects is not well understood. Research is needed to quantify the response of acoustic reflex for the general population, and work is also needed to investigate how significant that is against impulse noise. The warned vs. unwarned predictions from the MIL-STD-174E AHAAH model has still not been validated. The unwarned response was implemented in the AHAAH-ICE model. However, even though the unwarned condition reflects the most realistic AR response compared to the warned condition, the single-curve AR elicitation model in AHAAH is too simplistic. The AR model needs to be fully developed to appropriately include the effects of frequency, level-dependent strength and latency, and saturation and adaptation mechanisms. Much progress has been made recently in the experimental front that will benefit modeling that can help bridge this knowledge gap (Flamme, Deiters, Tasko, & Ahroon, 2017; McGregor et al., 2018).

2. Moreover, the influence of the AR on the metabolic processes cannot be overlooked. The interplay between the two mechanisms in multiple impulses scenarios as controlled by the timing and the intensity of the impulses plays a significant role in determining the severity of the damage outcomes. Combinations of very short IPI in the AR regime and long IPI in the ME regime are likely for modern day military noise exposures. Therefore, the AR mechanism once adequately understood also needs to be implemented in the AHAAH-ICE model. The inclusion in the model of the neural pathways to injury as well as the feedback from the high brain centers that control

the auditory nerve damage will add a new dimension to the biomechanically-based auditory standard. This addition will augment the model capability and help predict the risk of sensory-related disabilities such as tinnitus, which remains a top military medical problem. However, although expansion of the biomechanical model is critical for determining the intrinsic damage mechanisms, the human data needed to validate the new features and construct the model are often lacking or very limited.

3. The lack of human data is well-known to the impulse noise study community and cannot be overstated. The Albuquerque Walk-up data, although limited, constitute the largest and best human dataset to date. It is unlikely that this experiment will be duplicated in the future. Therefore, the BOP Walk-up injury data will probably remain the only data available for the assessment of protected large weapon noise injury. Human complex noise exposure data are lacking. Small arm injury data are also lacking. The only comprehensive data available for rifle noise comes from the German and Belgian rifle data. Other datasets from rifle firing are available from the National Institute for Occupational Safety and Health (NIOSH) and other groups from within the noise community. However, the usefulness of these data is in general limited because they contain only the exposure pressure traces but not the matching injury data. A biomechanically-based model such as the AHAAH-ICE needs both the waveforms and the injury data for dose-response construction and validation. It would be beneficial if new exposure tests were performed at least for the protected rifle noise exposure to collect comprehensive data either during training exercises or as a separate study. Until new human experiments are designed, the use of animal models will be resorted to for the investigation of impulse noise injury mechanisms. Unfortunately, the use of animal models is not without issues of its own.

4. The scaling problem between animal and human constitutes a critical gap that needs to be closed to help relate animal findings to human. For ethical reasons, most in vivo mechanisms can only be explored by using an animal model. For impulse noise study, good animal models exist, and chinchilla is the preferred animal surrogate. However, translating the chinchilla results to human is not straightforward. For example, even though the chinchilla and human auditory systems have similar spectral and geometric characteristics, chinchillas have a lower injury threshold. Some controlled experiments should be performed to quantify the scaling relationships between chinchillas and humans.

1.10 Key Research Accomplishments

The key accomplishments for this project are summarized as follows:

- An ARFST was developed for multiple irregular shot sequence exposure testing.
- A complex noise measurement system was developed to simulate complex noise exposure.
- Cochlear tissue properties data were collected for both chinchilla and human.
- A dose-response curve has been established with good fit and a tight confidence band in the data range tested for the prediction of TTS injury from multiple irregular shots with background noise reflecting modern day noise exposures.
- The ME model showed that the energy supply is low in general in response to the relatively high-level complex noise exposure, explaining the high injury rate observed during the noise exposure experiment.
- For intensity level in the range as tested (145-154 dB PPL), the OHC-ED model suggests that the effect of the IPI on the order of 1 second on injury is not significant, but the effect of moderately high intensity background noise is significant. The dominant effect on injury from the multiple shots was the intensity level.
- The integrated cochlear energy (ICE) and OHC-ED metrics are incorporated in the AHAAH-ICE model for the prediction of both mechanical and metabolic damage.
- The chinchilla OHC-ED model provides a good foundation for understanding noise-induced auditory exhaustion in humans for which data are currently lacking.

1.11 Reportable Outcomes

- A dose-response curve has been established with good fit and a tight confidence band in the data range for the prediction of TTS injury from multiple irregular shots with background noise reflecting modern day noise exposures.
- The chinchilla OHC-ED model provides the foundation for understanding noise-induced auditory exhaustion in humans for which data are currently lacking.
- A paper entitled “Modeling metabolic exhaustion of the auditory system” based on work from this project was presented at the MHSRS meeting in Kissimmee, FL on August 19-22, 2019.

1.12 Conclusion

This work has provided a mathematical model for the prediction of complex noise-induced metabolic exhaustion within the cochlea. The complex, moderate noise exposures include impulses with unequal level and unequal IPI riding on top of moderate level continuous noise. The cellular components have been added to the cochlear model to capture the metabolic processes within the individual cells of the cochlea, the OHC in particular. The model thus provides a realistic biomechanical measure of noise-induced metabolic exhaustion within the OHC.

A dose-response curve has been established with good fit and a tight confidence band in the data range as tested for the prediction of TTS injury from multiple irregular shots with background noise reflecting modern day noise exposures. The ME model shows that the energy supply is low in general in response to the relatively high level complex noise exposure, explaining the high injury rate observed during the noise exposure experiment. The OHC-ED model effectively captures the effect of IPI and background noise. For sound exposure intensity level between 145-154 dB PPL, the OHC-ED model suggests that the effect of the IPI on the order of 1 second on injury is not significant, but the effect of intense background noise is significant. The dominant effect on injury from the multiple shots is the intensity level. The effect of background noise increases with intensity level of the background noise.

The integrated cochlear energy (ICE) and OHC-ED metrics are integrated in the AHAAH-ICE model for the prediction of both mechanical and metabolic damage. The chinchilla OHC-ED model provides the foundation for understanding noise-induced auditory exhaustion in humans for which data are currently lacking. A first step for the validation of the ME human model developed based on the chinchilla model is to compare the model prediction with the BOP walk up study data. However, the BOP walk data, just like the USAARL chinchilla data involved exposures with regular intensity level and constant IPI. Therefore, the BOP walk up data are insufficient for validation of the ME human model. A scientific study for human complex noise exposure is needed to collect data for validation of the ME human model.

1.13 List of Personnel

Employee
Zagadou, Brissi F
Ho, Hsinhsing
Calder, Stanley M
Chan, Philemon C
Adkins, Mark
Dickerson, Kyle T
Juhas, Brett
Randolph, Sandra D
Ryan, Allen F
UNIVERSITY OF CALIFORNIA SAN DIEGO
BOSTON UNIVERSITY
MASSACHUSETTS EYE AND EAR INFIRMARY

1.14 References

Bohne, B. A., & Carr, C. D. (1979). Location of structurally similar areas in chinchilla cochleas of different lengths. *J Acoust Soc Am, 66*(2), 411-414.

Chan, P. C., Ho, K., & Ryan, A. F. (2012). Auditory 4.0 Impulse Noise Injury Model (pp. 1-43). San Diego: L-3/Jaycor.

Dallos, P. (1970). Low-frequency auditory characteristics: Species dependence. *J Acoust Soc Am, 48*(2), 489-499.

Danielson, R., Henderson, D., Gratton, M. A., Bianchi, L., & Salvi, R. (1991). The importance of temporal pattern in traumatic impulse noise exposure. *JASA, 90*, 209-218.

Eldredge, D. H., Miller, J. D., & Bohne, B. A. (1981). A frequency-position map for the chinchilla cochlea. *J Acoust Soc Am, 69*(4), 1091-1095.

Flamme, Gregory A., Deiters, Kristy K., Tasko, Stephen M., & Ahroon, William A. (2017). Acoustic reflexes are common but not pervasive: evidence from the National Health and Nutrition Examination Survey, 1999–2012. *International Journal of Audiology, 56*(sup1), 52-62. doi: 10.1080/14992027.2016.1257164

Greenwood, D.D. (1990). A cochlear frequency-position function for several species--29 years later. *JASA, 87*(6), 592-605.

Hamernik, Roger P., Patterson, James H., & Salvi, Richard J. (1987). The effect of impulse intensity and the number of impulses on hearing and cochlear pathology in the chinchilla. *The Journal of the Acoustical Society of America, 81*(4), 1118-1129. doi: 10.1121/1.394632

Henderson, D., Subramaniam, M., Gratton, M. A., & Saunders, S. S. (1991). Impact noise: the importance of level, duration, and repetition rate. *J Acoust Soc Am, 89*(3), 1350-1357.

Hildesheimer, M., Henkin, Y., Muchnik, C., Anafi, R., Sahartov, E., & Rubinstein, M. (1991). Sedation effect on temporary threshold shift induced by acoustic overstimulation. *Hear Res, 51*(1), 161-166. doi: 0378-5955(91)90014-Z [pii]

Koka, K., Jones, H. G., Thornton, J. L., Lupo, J. E., & Tollin, D. J. (2011). Sound pressure transformations by the head and pinnae of the adult Chinchilla (Chinchilla lanigera). *Hear Res, 272*(1-2), 135-147. doi: 10.1016/j.heares.2010.10.007

Lim, K. M., & Steele, C. R. (2002). A three-dimensional nonlinear active cochlear model analyzed by the WKB-numeric method. *Hear Res, 170*(1-2), 190-205. doi: S0378595502004914 [pii]

Mammano, F., & Ashmore, J. F. (1993). Reverse transduction measured in the isolated cochlea by laser Michelson interferometry. *Nature, 365*(6449), 838-841. doi: 10.1038/365838a0

McGregor, K. D., Flamme, G. A., Tasko, S. M., Deiters, K. K., Ahroon, W. A., Themann, C. L., & Murphy, W. J. (2018). Acoustic reflexes are common but not pervasive: evidence using a diagnostic middle ear analyser. *Int J Audiol, 57*(sup1), S42-S50. doi: 10.1080/14992027.2017.1416189

Murphy, W. J., & Davis, R. R. (1998). The role of the chinchilla pinna and ear canal in electrophysiological measures of hearing thresholds. *J Acoust Soc Am, 103*(4), 1951-1956. doi: 10.1121/1.421376

Naidu, R. C., & Mountain, D. C. (2001). Longitudinal coupling in the basilar membrane. *J Assoc Res Otolaryngol, 2*(3), 257-267.

Nakajima, H. H., Dong, W., Olson, E. S., Merchant, S. N., Ravicz, M. E., & Rosowski, J. J. (2009). Differential intracochlear sound pressure measurements in normal human temporal bones. *J Assoc Res Otolaryngol, 10*(1), 23-36. doi: 10.1007/s10162-008-0150-y

Olson, E. S., & Mountain, D. C. (1991). In vivo measurement of basilar membrane stiffness. *J Acoust Soc Am, 89*(3), 1262-1275.

Recio, A., Rich, N. C., Narayan, S. S., & Ruggero, M. A. (1998). Basilar-membrane responses to clicks at the base of the chinchilla cochlea. *J Acoust Soc Am, 103*(4), 1972-1989.

Robles, L., Temchin, A. N., Fan, Y. H., & Ruggero, M. A. (2015). Stapes Vibration in the Chinchilla Middle Ear: Relation to Behavioral and Auditory-Nerve Thresholds. *J Assoc Res Otolaryngol, 16*(4), 447-457. doi: 10.1007/s10162-015-0524-x

Ruebhausen, M. R., Brozoski, T. J., & Bauer, C. A. (2012). A comparison of the effects of isoflurane and ketamine anesthesia on auditory brainstem response (ABR) thresholds in rats. *Hear Res, 287*(1-2), 25-29. doi: 10.1016/j.heares.2012.04.005

Von Bekesy, G. (1960). *Experiments in Hearing*. New York: McGraw-Hill.

Vrettakos, P. A., Dear, S. P., & Saunders, J. C. (1988). Middle ear structure in the chinchilla: a quantitative study. *Am J Otolaryngol, 9*(2), 58-67.

Wang, H. , A. Burgei, W., & Zhou, H. (2017). Interpreting Dose-Response Relation for Exposure to Multiple Sound Impulses in the Framework of Immunity. *Health, 9*, 1817-1842. doi: 10.4236/health.2017.913132

Ward, W. Dixon. (1962). Effect of Temporal Spacing on Temporary Threshold Shift from Impulses. *The Journal of the Acoustical Society of America, 34*(9A), 1230-1232. doi: 10.1121/1.1918309

Wightman, F. L., Flamme, G., Campanella, A.J., Luz, G., Rosentahal, T. , & Gallo, S. (2010). American Institute of Biological Sciences Peer Review of Injury Prevention and Reduction Research Task Area Impulse Noise Models: American Institute of Biological Sciences.

YOKELL, ZACHARY (2019). *Electromyographic Measurement of The Chinchilla Middle Ear Muscle Reflex Elicited by Acoustic or Blast Stimuli.* (Doctor of Philosophy), University of Oklahoma, Norman, Oklahoma.

Zagadou, Brissi, Chan, Philemon, Ho, Kevin, & Shelley, David. (2016). Impulse noise injury prediction based on the cochlear energy. *Hear Res, 342*, 23--38. doi: 10.1016/j.heares.2016.02.017

Zwislocki, J. Jozef. (2002). *Auditory sound transmission: An autbiographical perspective*. Mahwah, New Jersey: Lawrence Erlbaum Associates, Inc., Publishers

Part 2: Non-Lethal Research and Methodology Development – Accumulated Dose

2.1 Introduction

Sponsored by the Joint Non-Lethal Weapon Directorate (JNLWD), L3 ATI had developed the Auditory 4.5 model for assessment of risks of auditory injuries against impulse noise produced by multi-stimuli devices such as flashbangs (Chan, Ho, & Ryan, 2012). In addition to predicting the full range of temporary threshold shift (TTS) and permanent threshold shift (PTS), Auditory 4.5 predicts TTS recovery. Auditory 4.5 is an empirical model built from chinchilla data collected by the US Army Aeromedical Research Laboratory (USAARL) with validation against historical human rifle noise data. The TTS and PTS dose-response curves were developed using the A-weighted sound exposure level (SELA) as the dose metric. The dose accumulation algorithm in Auditory 4.5 was developed from data involving repeat blasts with each shot sequence made up of impulses with equal intensity (L) at equal inter-pulse interval (IPI). However, in theatre operation, exposures will likely involve irregular impulses with unequal L and IPI, and Auditory 4.5 has not been validated against such complex conditions.

Flashbangs produce multiple impulses at unequal L and unequal IPI within a short duration. The Non-Lethal Indirect Fire Munition (NL-IDFM) can deliver 14 payloads within 2 seconds producing irregular L and IPI which can be as short as 0.25 second. Novel non-lethal weapon systems will likely produce even more complex mixture of noise. However, no generalized dose accumulation algorithm is available to date for prediction of injury from such complex mixture of impulses for operational applications. Wang, A. Burgei, and Zhou (2017) recently developed a generalized dose-accumulation formula based on the dose-response relation and the dose-accumulation rule implemented in Auditory 4.5, but that has not been validated by data. In analyzing the data collected from the Auditory 4.5 effort, they also suggested that a stronger first shot could produce a larger protective effect for the subsequent shot but this hypothesis still needs to be validated.

Limited animal data in literature suggest complex combination of L and IPI can affect injury outcomes. The IPI can have a greater effect at low sound pressure levels (~125 dB) versus higher levels (~137dB) (Henderson et al., 1991). The mixing of IPI exacerbates injury in chinchillas (Danielson et al., 1991).

Literature review shows the response of the auditory system to complex noise exposure can be divided into two regimes: the metabolic exhaustion (ME) regime for IPI greater than 1 second and the acoustic reflex (AR) regime for IPI less than 0.25 second (Danielson et al., 1991; Hamernik, Patterson, & Salvi, 1987; Henderson et al., 1991; Ward, 1962). Most historical data were collected in the ME regime with IPI from seconds to minutes with equal L, while flashbangs are likely operating in the AR regime with very limited data available. The extension of historical knowledge to AR regime needs to be evaluated so that a generalized dose accumulation algorithm can be developed.

The objectives of this project are 1) to develop an empirical-based dose-accumulation algorithm in the ME regime for complex noise with unequal intensities and unequal IPI, where IPIs are on the order of seconds that can be incorporated in Auditory 4.5; 2) to explore the protective effects from acoustic reflex (AR) for exposure conditions representative of the NL-IDFM operations involving multiple shots with unequal level and IPI ranging from 0.1 to 1 second; and 3) to document findings for recommendation of full series of AR testing to extend the dose accumulation algorithm to the AR regime. This project leverages on the ME modeling project sponsored by the US Army Medical Research and Development Command (USAMRDC) presented in Part 1 of this report.

2.2 Method

2.2.1 Insight from USAARL and MRDC Data Analysis

Statistical significance tests were first performed using two existing chinchilla datasets to evaluate the effects of IPI and shot sequence on outcomes in the ME regime. The main dataset is the USAARL data from the historical blast overpressure project (BOP) with 903 subjects that had been used to develop the dose-response curves in Auditory 4.5. The other smaller dataset is that collected recently at the University of California San Diego (UCSD) for the USAMRDC-sponsored ME Modeling Project referred to here as the USAMRDC-UCSD data.

Table 7 shows a summary of the USAARL data relevant to flashbang conditions comprising 12 acoustic stimuli types (impulse-like exposures) that can be used for evaluating the effects of IPI on outcomes. In Table 7, keeping the original BOP designations, the Study in column 1 indicates the various impulse generation methods used, where each is further subdivided into various stimuli (Stim) representing various intensity levels as shown in Figure 41. Column 3 indicates the number of shots (Nshots) for each exposure sequence; column 4 shows the IPI (Interval) between shots; and the last column is the number of subjects (N) used for each test exposure sequence. For each Stim, Nshots were conducted at 1, 10 and 100 with IPI varying from 6, 60 to 600 s. It should be noted that for each exposure sequence in the BOP tests, both intensity level (L) and IPI were held constant, and they were changed only between exposure sequences. Therefore, the USAARL data can only be used for evaluating the effect of IPI on outcomes.

Table 8 summarizes the test conditions of the USAMRDC-UCSD tests that can also be used to evaluate the effects of IPI and exposure sequence on outcomes. A schematic representation of each 10-shot sequence for each of the 18 test conditions is shown in column 7 (Table 8), where each spike represents one individual impulse with the height proportional to its intensity. Three impulses with peak pressure levels at L1 = 140, L2 = 150, and L3 = 160 dB were used, and the IPI varied from t1 = 3, t2 = 9 to t3 = 20 s. In series 1-a, shot intensities were varied but IPI was kept at 3 s. In series 2-a, both shot intensity and IPI were varied. Supplementing the BOP tests, the UCSD tests included shot sequences that varied both L and IPI together.

Standard t-test analysis was performed to evaluate the effects of IPI on TTS and PTS incurred from exposures to the 10-shot sequences in the BOP test. Statistical power was also calculated to test if the significance test null hypothesis should be rejected. The accumulated A-weighted energy was designed to be the same for each test-pair.

Table 7. BOP chinchilla test summary

Study	Stim	Nshots	Interval (sec)	N	Study	Stim	Nshots	Interval (sec)	N
Conventional shock tube, nonreverberant	1	1		4	Fast-acting valve (3.5"), nonreverberant	7	1		5
		10	6	5			10	6	5
			60	5				60	5
			600	5				600	5
		100	6	5			100	6	5
			60	6				60	5
			600	5				600	5
	2	1		5		8	1		5
		10	6	5			10	6	5
			60	5				60	5
			600	5				600	5
		100	6	6			100	6	5
			60	6				60	5
			600	5				600	5
	3	1		6		9	1		5
		10	6	5			10	6	5
			60	6				60	5
			600	5				600	5
		100	6	5			100	6	5
			60	5				60	5
			600	5				600	5
Fast-acting valve (5"), nonreverberant	4	1		5	Spark gap, nonreverberant	10	1		5
		10	6	5			10	6	5
			60	5				60	5
			600	5				600	5
		100	6	5			100	6	4
			60	5				60	5
			600	5				600	5
	5	1		5		11	1		5
		10	6	5			10	6	5
			60	5				60	5
			600	5				600	5
		100	6	5			100	6	5
			60	5				60	5
			600	5				600	5
	6	1		5		12	1		5
		10	6	5			10	6	5
			60	5				60	5
			600	5				600	5
		100	6	5			100	6	5
			60	5				60	5
			600	5				600	5

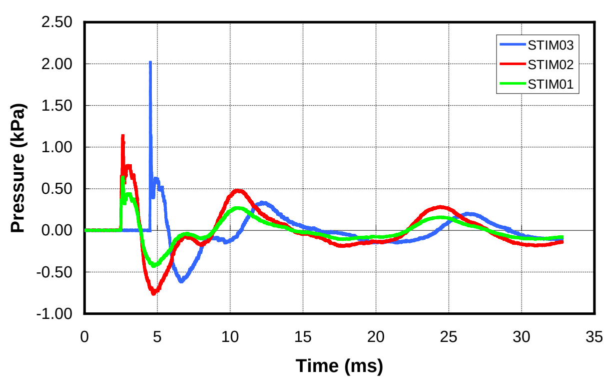

a) Shock Tube Non-reverberant

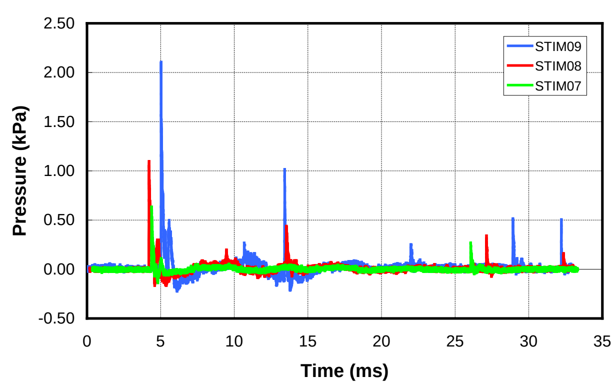

b) Fast-acting valve (3.5"), non-reverberant

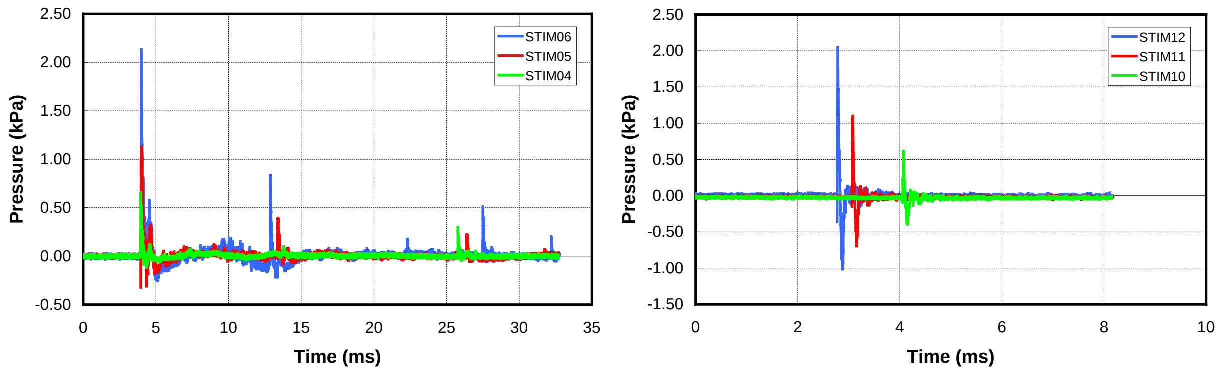

c) Fast-acting valve (5"), non-reverberant   d) Spark gap, non-reverberant

Figure 41. Sample BOP pressure traces

Table 8. USAMRDC-UCSD test Matrix for ME regime

Series	Test Condition	Peak Pressure Level (L)	N	IPI (t)	Number of Animal	Schematic Description of Multiple Shots	Total Impulses
1-a	1	L1, L2	10	t1	5		5L1+5L2
	2	L1, L3	10	t1	5		5L1+5L3
	3	L3, L2	10	t1	5		5L3+5L2
	4	L1, L2, L3	10	t1	5		4L1+3L2+3L3
	5	L1, L3, L2	10	t1	5		4L1+3L2+3L3
	6	L1, L3	10	t1	5		5L1+5L3
2-a	13	L1, L2	10	t1, t2	5		5L1+5L2
	14	L1, L3	10	t1, t2	5		5L1+5L3
	15	L3, L2	10	t1, t3	5		5L3+5L2
	16	L1, L2, L3	10	t3, t1, t2	5		4L1+3L2+3L3
	17	L3, L1, L2	10	t1, t3, t2	5		5L3+3L1+2L2
	18	L1, L2, L3	10	t1, t2, t3	5		5L1+2L2+3L3

Peak pressure level (L) L1, L2 and L3 = 140, 150 and 160 dB, respectively.
Interpulse interval (IPI) t1, t2 and t3 = 3, 9 and 20 seconds, respectively.

2.2.2 Development of Complex Noise Generation Equipment

Two complex noise generation systems were used for testing in the ME and AR regime, respectively. The Automated Rapid Fire Shock Tube (ARFST) system was first used and calibrated to produce multiple blasts with unequal intensity levels and unequal IPI in the ME regime. The ARFST system is shown again in Figure 42. The ARFST system is a pneumatically and electrically controlled device consisting of two separate shock tubes each synchronized with a large rotating disk that automatically cycles between shots to quickly replace the burst diaphragm between the compression chamber and the expansion section. The device uses two tubes that alternate shots to reduce the time interval between shots. An automated shock tube with a rotating wheel design has an inherent time delay due to the mechanics of the system. Having two symmetric systems built into this one machine cuts the delay time in half. Both tubes are made with a 4.5-inch long compression chamber and a 16-inch long expansion section. The system requires a high pressure helium line with pressure set at 100 psi. A compressed air source is also required to operate the pneumatic components. The pneumatic pressure required to maintain proper motion and chamber sealing during compression is 150 psi. The control, operation, and safety features of the ARFST are described in detail in Part I, with calibration details found in Appendix A.

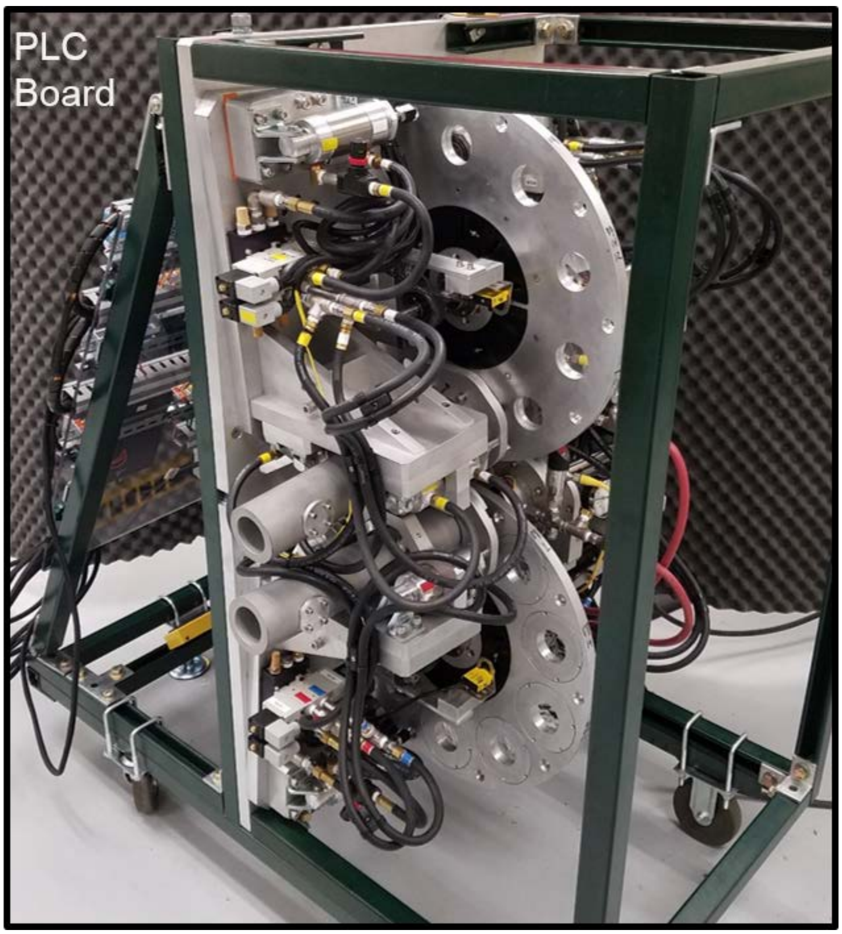

Figure 42. Automated Rapid Fire Shock Tube (ARFST) system for ME regime testing.

For the AR regime, noise generation equipment capable of producing a rapid firing sequence at intensity similar to flashbangs is needed. A three-paintball gun firing system was developed that can fire 3 guns alternately to generate shot sequences with IPI as short as 40 ms. The Spyder Fenix Electronic Paintball Gun Model was selected. Figure 43 shows the finalized three-paintball gun rapid fire system. A portable frame 30” (Height) x 30” (Width) x 60” (Length) was built to hold the guns. There are several advantages to this configuration. The frame is flexible, yet robust to withstand repeated impulses and requires a minimal amount of space. It also allows easily adjustable positioning of the individual paintball guns at different distances to the target. The system is controlled by a single programmable logic controller (PLC) unit. The details for the fabrication of the three-gun rapid firing system can be found in the monthly reports from June through December 2018.

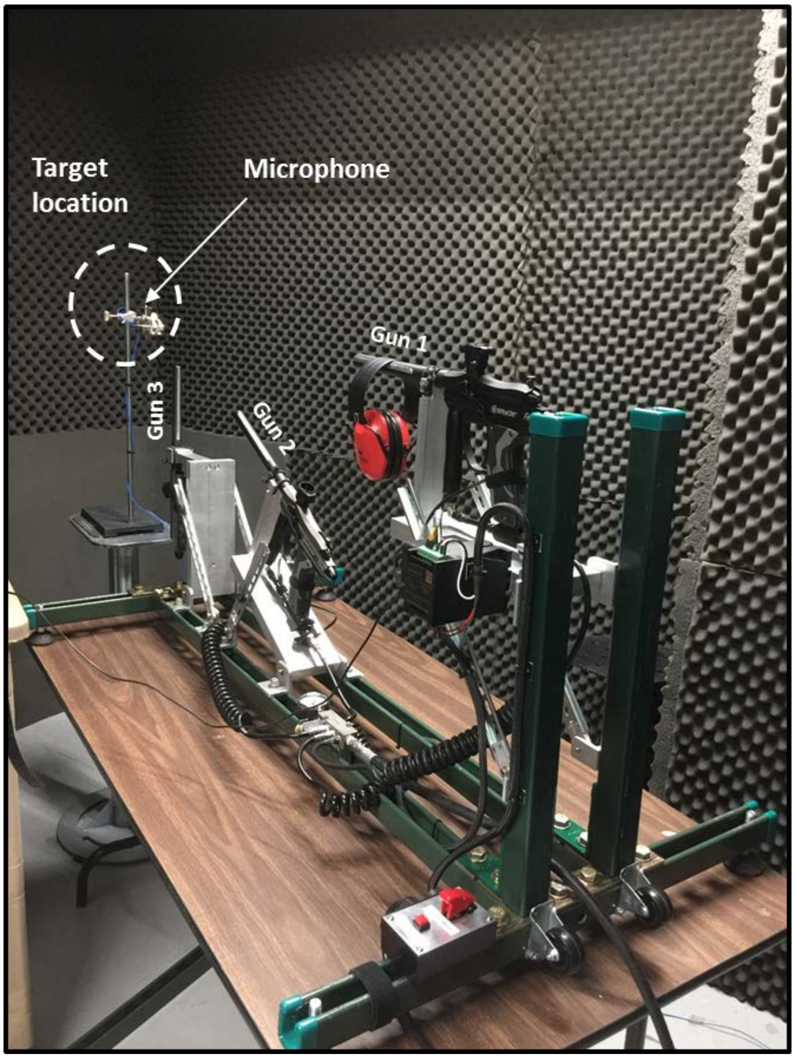

Figure 43. Paintball gun system for AR regime testing

2.2.3 Test Matrices for ME and AR regime

Table 9 shows the test matrix for the chinchilla tests performed for this JNLWD project (labeled as JNLWD-UCSD test matrix), combining ME and AR tests to fit within budget with guidance from some IDFM test data. The test matrix comprises a total of 10 TCs focusing on comparing the effects of sound source on outcomes in the ME regime and collecting explorative AR exposure data. In the table, the IPI, shot sequence, total impulse, target SELA, and the number of animals used are shown for each TC. The number of animals for each TC initially set at 8 was later adjusted to 6 due to budget limitation. Three TCs (TC 25, 26 and 31) for the ME regime with IPI = 3 sec used shock tube noise stimuli, as denoted by ST in Table 9. Seven TCs (TC 32, 33, 36, 37, 40, 41, and 42) used paintball gun noise stimuli, denoted by PG, with 3 TCs (37, 40, and 42) in the ME regime with IPI = 3 sec and 4 TCs (32, 33, 36, 41) in the AR regime with IPI = 50 ms. TC 25, 26, 32, and 33 will each only use two unequal shots (L1 and L3) to test the "immunity hypothesis" as suggested by Wang et al. (2017). TC 25 and 26 with IPI = 3 sec will be used to test the immunity hypothesis in the ME regime, while TC 32 and 33 will IPI = 50 ms will test the hypothesis in the AR regime. All the other TCs used 10 shots with equal intensity as indicated in the "total impulse" columns. In particular, TC 31 involves 10 equal shots (10L2) at regular IPI= 3 sec for benchmark comparison with the historical data that were used to develop Auditory 4.5. TC 37 is added for comparison with TC 31 and 36 to test the effect of sound source on outcomes, and TC 40 is similar to TC 37 but with a lower sound intensity (10L1 for TC 40 vs. 10L2 for TC 37). TC 41 and 42 are optional tests to see if the effects of AR on the difference in TTS between TC 36 and 37 can be repeated with stronger statistical significance to bolster the finding that the effects of AR is present. The total number of subjects tested is 57, excluding TC 41 and 42. The tests were designed to avoid eardrum rupture based on previous data guidance.

Table 9. JNLWD-UCSD Test Matrix for ME and AR regime

TC	IPI (t)	Schematic Description of Multiple Shots	Total Impulses	Target SELA	# of animal (n)
25	3 sec.	ST	L3+L1	113	8
26*	3 sec.	ST	L1+L3	113	8
32	50 msec.	PG	L3+L1	113	6
33	50 msec.	PG	L1+L3	113	6
36	50 msec.	PG	10L2	111	6
37	3 sec.	PG	10L2	111	7
40	3 sec.	PG	10L1	106	8
41	50 msec.	PG	10L3	113	6
42	3 sec.	PG	10L3	113	6
31**	3 sec.	ST	10L2	113	8

❖ Peak pressure level (L) L1, L2 and L3 = 140, 150 and 160 dB, respectively. ST = Shock Tube. PG = Paintball Guns

2.2.4 Experimental Procedures for Chinchilla Complex Noise Exposure

The procedure for the tests in the ME regime using the ARFST is the same as described in Part I, Section 5.2. The various equipment tests performed prior to chinchilla complex noise exposure using the three-paintball gun firing system are described, including the blast symmetry verification tests, paintball gun characterization tests, and gun placement verifications. The procedure for collecting the TTS and PTS data using the Auditory Brainstem Recording (ABR) is also described.

Prior to the initiation of the project at UCSD, an application to perform the proposed experiments was submitted to the UCSD Institutional Animal Care and Use Committee (IACUC) for approval. The Bureau of Medicine and Surgery (BUMED) Animal Use Approval and the UCSD IACUC-approved protocol was provided to JNLWD for approval. No experiment was initiated prior to JNLWD's approval.

2.2.4.1 Blast Symmetry Tests

Blast symmetry tests were performed to verify that the blast was symmetric at the left and right ear since both ears of the animals were used to collect the injury data. Sound pressure data were recorded using two microphones, each placed at the left and right ear location, respectively, without involving animals. The pressure traces, spectra, peak pressure level (PPL), and A-weighted sound exposure level (SELA) were analyzed. Five tests, labeled Test A, B, C, D and E were performed with a constant IPI of 3 second. Test A was a replicate of TC 25 with the L3-L1, 2-shot sequence. Test B replicated TC 31 with 10 shots at L1. Test C and D were single-shot tests at level L1 and L2, respectively. Test E comprised 3 levels starting with L1 followed by L2 and L3. The pressure traces were stored on a Synergy data acquisition system and processed later to calculate the PPL and SELA values.

As shown in Table 10, the left and right microphone data were similar overall, showing the exposure was symmetric between the left and right ear. As shown in Table 10, the PPL mean and standard deviation (SD) differences between left and right data were similar, and the mean differences were even smaller between the left and right SELA values.

Table 10. Blast Symmetry Tests: PPL and SELA (in dB) from left and right microphones

	Test A (TC 25)		Test B (TC 31)		Test C		Test D		Test E	
	Right	**Left**	**Right**	**Left**	**Right**	**Left**	**Right**	**Left**	**Right**	**Left**
Mean PPL	149.06	150.95	148.57	150.37	145.71	148.13	149.06	150.15	149.22	151.08
SD	4.41	5.42	0.39	0.47	-	-	-	-	2.89	2.92
Mean SELA	109.29	112.39	109.45	109.51	105.67	105.56	109.08	108.95	109.50	109.46
SD	6.04	3.85	0.33	0.76	-	-	-	-	3.37	3.28

- SD value is not reported for single shot (n=1).

2.2.4.2 Paintball Gun Characterization Tests

The paintball gun characterization tests consisted of measuring the pressure waveforms as a function of distance and angle from the muzzle to establish PPL and SELA contour maps for each paintball gun. The data were used for optimizing the PPL and SELA combinations from the 3 guns to develop the AR matrix. As shown in Figure 44 for the sound pressure characterization test setup, r is the horizontal distance from the muzzle to the target and θ is the angle from the muzzle with zero-degree being in the plane of symmetry. The inset shows the zoomed-in picture of the microphone and pressure gauge used to record the sound pressure. The values for r are 40, 30, 20, 5, and 2 inches, respectively, and θ is varied in increment of 10^o from 0 to 40^o as shown at the bottom right of the Figure 44. The pressure traces are collected on a Synergy data acquisition system for later processing.

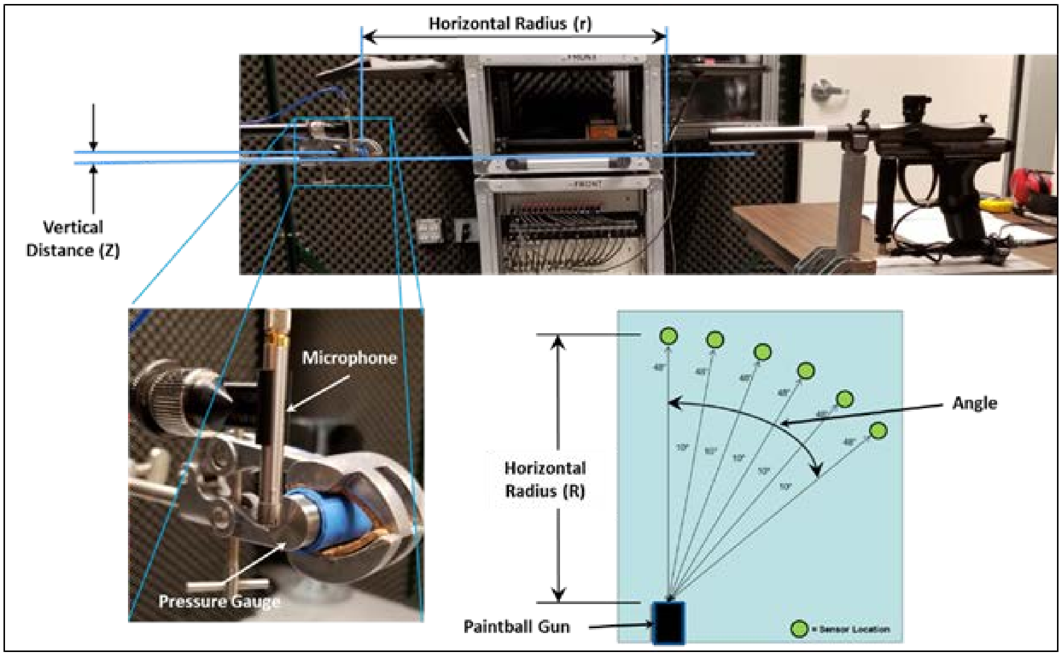

Figure 44. Sound pressure characterization test setup schematic

Using the pressure waveforms collected at several distances and angles from the muzzle, PPL and SELA contour maps were established for each paintball gun. The contour maps for PPL and SELA can be summarized by the following fitted formulae:

$$PPL_{\theta}(r) = \beta_{\theta} + \alpha_{\theta} * \ln(r)$$

$$SELA_{\theta}(r) = \lambda_{\theta} + \sigma_{\theta} * \ln(r),$$

where the fit coefficients, α, β, σ, and λ are angle-dependent.

Table 11 summarizes the angle-dependent fit coefficients for PPL and SELA vs. distance for all 3 guns tested. Overall, the coefficients are similar for all 3 guns for a fixed θ. The coefficients are fairly uniform for PPL and SELA for $\theta > 10^{o}$, above which the blast wind effects are avoided. The wind blast effect from the shock expansion appear as a low frequency dip in the waveforms. In general, this dip due to wind effects is to be avoided if possible for blast testing in the laboratory using shock tubes since they do not represent field conditions. Based on the sound pressure characterization results for the three guns, gun position at $\theta = 20^{o}$, r = 10" appears to be ideal for producing the highest PPL and SELA values without blast wind effects. At $\theta = 20^{o}$, r = 10", the maximum PPL estimate is 155 dB, and the maximum SELA estimate without blast wind is 110.7 dB.

Table 11. Fit coefficients for PPL and SELA versus distance for all 3 guns tested

	Gun-1				Gun-2				Gun-3			
Angle	PPL (in dB)		SELA (in dB)		PPL (in dB)		SELA (in dB)		PPL (in dB)		SELA (in dB)	
(θ in °)	β	α	λ	σ	β	α	λ	σ	β	α	λ	σ
0	178.8278	-9.6048	155.8197	-15.3629	178.9368	-9.2119	154.2116	-14.4904	180.3557	-9.2906	154.6099	-13.6109
10	175.96	-8.9215	145.3143	-13.8661	176.6045	-8.7272	148.0182	-13.4352	177.9008	-8.9988	131.8649	-8.2809
20	174.7085	-8.6238	138.9932	-12.2637	176.149	-8.6903	140.6853	-12.0613	176.4393	-8.5632	139.7149	-11.5596
30	172.7172	-8.1549	129.9117	-9.531	174.1757	-8.2142	133.5122	-10.1442	176.3024	-8.5523	134.2509	-9.9447
40	169.9251	-7.8072	124.5405	-7.9489	174.3505	-8.8136	127.6615	-8.6216	173.5984	-7.8549	127.9641	-8.1445

2.2.4.3 Gun placement verifications

The 3 paintball gun positions were first determined using the sound pressure characterization map to determine TC settings to match those used for the ME testing followed by the gun position verification tests for the TCs of the test matrix. To determine the paintball gun positions, the PPL for each gun position was determined given the target SELA value produced by the shock tube blast, and the PPL determined were compared to the target PPL produced by the shock tube to see if the difference was acceptable. The paintball gun placement verifications were first performed at the L3 ATI lab before transporting to the UCSD lab, and they were verified again at UCSD before performing animal testing. Test set up adjustment was performed as needed to account for differences in laboratory environment and to match the target SELA. The verified positions of the paintball guns for each TC were used to perform the animal tests and are summarized in Table 12. Values of distance and angle not reported for a given gun means the gun was not fired for that TC.

Table 12. Gun Placement in three-paintball gun fire system

TC	Gun-1		Gun-2		Gun-3	
	r (in inch)	θ (in °)	r (in inch)	θ (in °)	r (in inch)	θ (in °)
32	18.76	20	-	-	8.28	20
33	18.76	20	-	-	8.28	20
36	10.69	20	10.69	20	-	-
37	10.69	20	10.69	20	-	-
40	10.69	20	10.69	20	-	-

2.2.4.4 Noise Exposure Experiment Set Up

The set up for the chinchilla noise exposure experiment at UCSD is shown in Figure 45. The animal is placed in a holder with two microphones positioned near its left and right ear to record the pressure waveforms at each ear's entrance. The three guns are positioned such that the distance, r from the muzzle to the ear and the angle, θ between the centerline of fire and the ear are as defined in Table 12. The animal is anesthetized with rodent cocktail (ketamine, xylazine, acepromazine), which has not been shown to reduce sensitivity to noise-induced hearing loss (Hildesheimer et al., 1991). Electromagnetic fields of unknown sources were detected in the UCSD laboratory during calibration tests that caused the paintball guns to trigger at random. As shown in Figure 45, the problem was resolved by using aluminum foils to shield the solenoid for each of the three guns against electromagnetic interference.

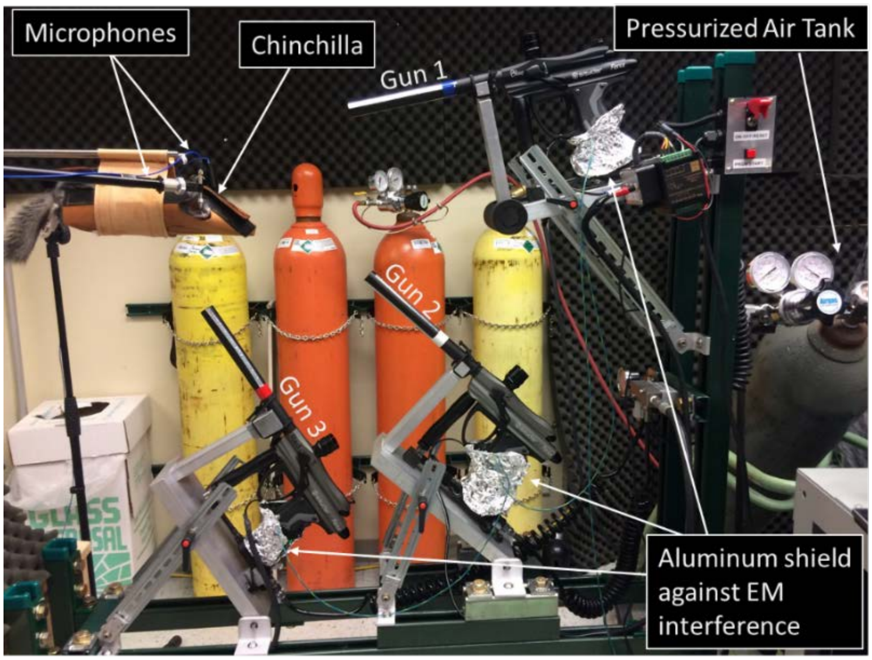

Figure 45. UCSD Chinchilla Noise Exposure Experiment Set Up using the 3-Paintball Gun System

2.2.4.5 ABR Measurement

Standard ABR testing was used to record hearing level (HL) in chinchillas before and after exposure to complex noise. For recording, the active electrode was placed ventral to the ear canal, the reference electrode was placed on the vertex, and the ground electrode was placed on the leg. The signal was filtered at 0.5-3 kHz and gated to the acoustic stimulus. The response to 512 stimulus presentations was averaged to generate the ABR waveform. At high stimulus intensities, if the waveform was visually obvious, the test could be halted and the waveform recorded at proportional amplitude to increase the speed of data collection.

The ABR stimulus consisted of tone bursts 25 msec in length, with a ramp time of 2.5 msec, presented at 20/sec. Thresholds were tested using a descending stimulus method, beginning at 90 dB SPL and descending in 5 dB steps until the waveform had clearly diminished into the background of the recording, after which one additional step was taken. Threshold was assigned as halfway between the lowest intensity at which a waveform could be distinguished and the next lower intensity.

The TTS and PTS were determined by the difference between the HL measured pre-exposure and post-exposure. For each animal, both ears were recorded with TTS recorded first for the right ear at 1, 2, and 4 kHz, followed by the left ear about 30 minutes later. The ABR measurements were at 3 time points, "immediately (when accessible)", 1, and 2 hours post-blast, converting to gas anesthesia as necessary. Each animal was also followed up afterwards for 2 weeks to track PTS.

2.2.5 Tympanometry Tests

Limited tympanometry tests were conducted at UCSD using 3 animals that verified the presence of AR under anesthesia. AR data were collected with and without anesthesia using 3 animals. Tympanometry data were collected under the supervision of a student audiologist. Three chinchillas were used that were identified by their animal ID, 928, 929, and 930, respectively. For each animal, the acoustic reflex threshold (ART) (in dB) and middle ear admittance change (in mmho) were measured for 3 stimulus frequencies (1, 2, and 4 kHz) whenever possible for right and left ears, with anesthesia (Sleep) and without anesthesia (Awake) anesthesia, respectively. The effect of anesthesia was determined by comparing the outcomes with and without anesthesia.

2.2.6 Data Processing and Analysis

2.2.6.1 SELA

Based on the results from the analysis of the USAARL and USAMRDC data (presented later in the results section), the IPI effects are first ignored, and the formula from Wang, A. Burgei, and Zhou (2017), shown in Eq.1, is adopted to calculate the combined SELA values for irregular impulses. The SELA for the individual shots ($SELA_i$) are calculated using the pressure waveforms and summed according to Eq. 1 to obtain the combined dose $SELA_{comb}$:

$$SELA_{comb} = \lambda \cdot log_{10}\left(\sum_i 10^{\frac{SELA_i}{\lambda}}\right), \quad \text{i = 1 to N} \qquad (1)$$

where N is the number of shots and $\lambda = 3.44$, based on previous work for the human walk up tests with rifle data validation.

2.2.6.2 TTS

The TTS data collected were analyzed by comparing the TTS trends post-exposure for the left and right ears for each TC. For each individual test sample and for all TCs, the average TTS for 1, 2, and 4 kHz (TTS_{124K}) is calculated and used for all analysis. The TTS_{124K} mean and standard deviation are plotted as a function of the average time of measurement. Additionally, the TTS_{124K} at the first measurement time point post-exposure for the left and right ear are compared.

2.2.6.3 Data Organization

The injury data in terms of TTS and PTS and the associated pressure waveforms were paired using a unique identification code for each individual subject. For each of the 57 animal tested, the individual TTS and PTS measured at 1, 2, and 4 kHz, for the left and right ears, and for the three time points are organized in an Excel file. Each subject is identified by a unique 5-digit number, with the first 2 digits representing the TC number, and the last 3 digits are the original subject ID used during testing at UCSD which will match the animal to the pressure waveform. For the finalized data, this 5-digit identification code is used and will be matched to any wave file sample delivered to JNLWD. In a separate Excel file, the SELA for the individual shots, the combined SELA, the TTS_{124K}, and the PTS_{124K} were collected with the 5-digit identification code linking the data between the two files. These two files contain the data are used to validate the dose-accumulation algorithm developed as described in the subsequent sections. The Excel files are delivered to JNLWD alongside with this report.

2.2.7 Immunity Test in ME and AR regimes

The immunity hypothesis was tested in the ME and AR regime by comparing the TTS outcomes between TC 25 and 26, and TC 32 and 33, respectively using the 2-tail t-test at significance level of 5%. The average TTS values for each test pair were compared using data from both ears together, hence effectively doubling the sample size, but also using data from the right and left ear separately. A p-value > 5% indicates the difference between the TTS outcomes is not significant and shows that the shot sequence is not important. The statistical power for rejecting the null hypoethesis of the test is also calculated.

2.2.8 Development of Accumulated Dose Algorithm

The approach is to use the USAARL data to develop the dose-response curves for comparison with the MRDC-UCSD and JNLWD-UCSD data as a closed-book test. Based on the results from the USAARL and USAMRDC data analysis as shown later in the results section, the effect of shot sequence was assumed negligible, and the effect of IPI was modeled to see if the IPI effect can improve data fit. The SELA is used as the dose metric adopting the Wang et al. (2017) formula to calculate the combined SELA for irregular shots. To account for the incident angle difference between the USAARL and the current UCSD tests, 3 dB was subtracted from the SELA obtained for the UCSD tests to convert the dose from gazing to normal incidence.

2.2.8.1 Accumulated Dose Formula Optimization

The Wang et al. (2017) formula is adopted and extended to include the potential effect of IPI by adding an α-term, which represents a correction of Δi to SELA for the ith impulse:

$$SELA_{comb} = \lambda \cdot log_{10}\left(\sum_i 10^{\frac{SELA_i - \Delta_i}{\lambda}}\right), \quad \Delta i = \alpha \cdot log_{10}\left(\frac{IPI_i}{IPI_0}\right), \qquad (2)$$

where i = 1 to N (number of shots).

In Eq. 2, Δi increases with IPI based on the findings from analysis of the USAARL data and confirmed by the ME model. The reference IPI_0 is chosen to be 1 sec, and λ is fixed at 3.44 based on the previous human walk up test analysis.

The formula in Eq. 2 is optimized against the USAARL data to find the value of α that minimizes the error (ε) between predicted and observed TTS. The error, ε is defined in Eq. 3:

$$\varepsilon(\alpha) = \sqrt{\sum_j \left(Y_j - Y_{pj}\right)^2} \Big/ \sqrt{\sum_j Y_j^{\,2}}\,, \ \text{Y}_\text{j}\text{: TTS data; Y}_\text{pj}\text{: predicted TTS} \qquad (3)$$

Logistic regression fit to a subset of the USAARL data with impulse-like waveforms and IPI ≤ 20 sec is used to obtain the dose-response curve for TTS vs SELA for which ε is evaluated to find the optimal value for α. Sensitivity of the results to inclusion of the 1-shot data is assessed.

To obtain the dose-response curve for TTS vs SELA, ordered logistic regression analysis was performed to determine the fit for different thresholds of TTS/PTS. The 50th percentile points for TTS vs SELA were used to evaluate ε. The procedure is illustrated in Figure 46. As shown in Figure 46, the dose-response curve for TTS vs SELA for the ith-percentile is determined by collecting the SELA values at the intersection of the ith-percentile line and logistic regression curves (50th percentile line shown as dashed line).

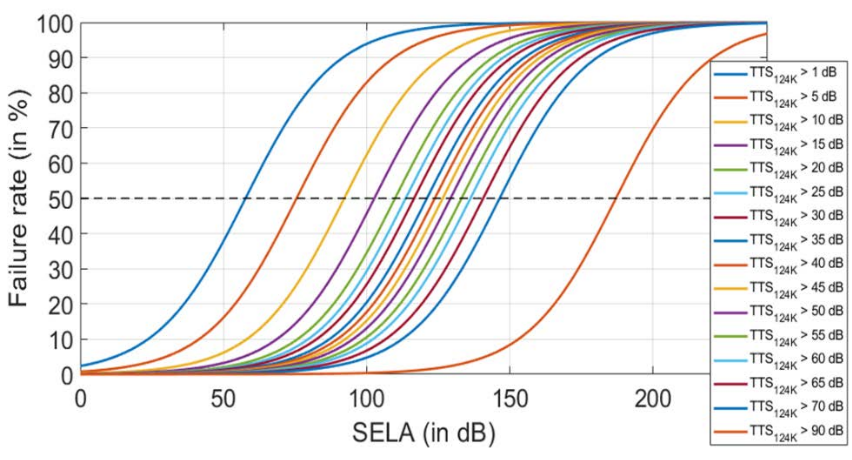

Figure 46. Ordered logistic regression analysis (Shown for TTS)

2.2.8.2 Accumulated Dose Model Options

Three models were developed and compared based on subsets of the USAARL data. Model A was developed using all the available USAARL data. Model B was developed using a subset including IPI ≤ 20 sec, the 1-shot cases, and excluding the broadband noise (BBN) that are not representative of flashbangs. Model C is the same as Model B, but excluding the 1-shot cases. The models were compared against each other for their ability to predict the UCSD data against TTS and PTS for the following 3 thresholds as recommended by the Institute for Defense Analyses (IDA).

1. TTS≥ 25 dB
2. PTS ≥ 25 dB
3. PTS ≥ 45 dB

The failure rates from the UCSD data were calculated by binning the data following standard procedure for comparison with the dose-response curve that would be generated by the maximum likelihood analysis. The TTS/PTS for all subjects were first converted to 0 or 1 against the specified threshold: a value of 0 is assigned if TTS/PTS is less than the threshold of injury (no injury) and 1 if TTS/PTS is greater or equal to the threshold (injury occurred). The binning procedure consists of sorting the individual subject data in increasing order of SELA values, dividing the sorted data in 5 quintiles, and calculating the mean for both SELA and TTS or PTS within each quintile. The resulting binned data points are plotted against the dose-response curve generated for each model for comparison of the predicted and observed failure rates.

To compare the predicted values to the observed values for the binned data, the following approach was adopted. A linear regression for the observed vs predicted values for the binned data points is obtained whenever possible, and the slope, Y-intercept, and r^2 are compared between the three models. The model comparison criterion is: the closer the slope is to 1, the Y-intercept to 0, and the r^2 to 1, the better is the general predictive power of the model. The predictor error, defined as the distance between the observed and predicted values, can also be evaluated.

The models were also compared based on their ability to predict the TTS and PTS for all available impulse-like data from the USAARL and UCSD datasets. The average TTS for each test condition is used for comparison with the model prediction. The SELA values corresponding to the 50th percentile line from the ordered logistic regression analysis are plotted against the average TTS and PTS, respectively, and the predicted and observed TTS are compared using the prediction error defined in Eq. 3. The prediction and fitting errors are calculated for each model for TTS and PTS, respectively. The prediction error is calculated using all impulse-like waveforms, and the fitting error is calculated using the data group that the model was built on.

2.3 Results

2.3.1 Effect of IPI and Shot Sequence from USAARL and MRDC Data Analysis

Table 13 summarizes the results for the USAARL dataset showing that the effect of IPI is insignificant on the TTS outcomes. As shown for each test-pair, the p-value for the null hypothesis is calculated, with p>5% taken as the indication for no statistical significance between the outcomes. In addition, the statistical power to reject (pwr), which represents the probability of rejecting the null hypothesis given that the alternate hypothesis is true, is also indicated for each test-pair. For all the test-pairs except that for Stim 3 with IPI at 1 min vs. 10 min (highlighted in red), all p-values exceed 5% suggesting that IPI has insignificant effect on TTS outcomes. This observation is further strengthened by observing that most pwr values are below 15% while a few exceed 30%. For the three test-pairs exposed to Stim 5 (highlighted in yellow), the pwr values exceed 70% suggesting the null hypothesis that IPI has insignificant effect on TTS should be rejected even though their p-values exceed 5%. It should also be mentioned that, for the test-pair for Stim 3 for IPI at 1 min vs. 10 min, the pwr value is relatively high at 51.93% suggesting that there is high probability to reject the p-value (at 4.96%) that suggests IPI can affect TTS for this pair.

Table 13. TTS significance t-test – USAARL 10 shots

IPI		6 sec. vs. 1 min.	6 sec. vs. 10 min.	1 min. vs. 10 min.
Exposure Time		1 min. vs. 10 min.	1 min. vs. 100 min.	10 min. vs. 100 min.
Shock Tube	Stim 1	p = 32.31%, pwr = 13.77% No significant difference	p = 13.85%, pwr = 24.77% No significant difference	p = 56.36%, pwr = 7.94% No significant difference
	Stim 2	p = 30.52%, pwr = 19.30% No significant difference	p = 52.38%, pwr = 14.99% No significant difference	p = 90.64%, pwr = 5.23% No significant difference
	Stim 3	p = 50.24%, pwr = 9.55% No significant difference	p = 17.57%, pwr =25.29% No significant difference	p = 4.96%, pwr = 51.93% Significant difference
Fast Valve (5")	Stim 4	p = 31.63%, pwr = 38.46% No significant difference	p = 77.35%, pwr = 6.39% No significant difference	p = 27.87%, pwr = 14.23% No significant difference
	Stim 5	p = 11.81%, pwr = 71.54% No significant difference	p = 33.40%, pwr = 97.93% No significant difference	p = 14.70%, pwr = 87.42% No significant difference
	Stim 6	p = 24.71%, pwr = 15.8% No significant difference	p = 12.17%, pwr = 19.26% No significant difference	p = 76.03%, pwr = 5.46% No significant difference
Fast Valve (3.5")	Stim 7	p = 25.57%, pwr = 27.18% No significant difference	p = 57.76%, pwr = 12.10% No significant difference	p = 70.70%, pwr = 6.84% No significant difference
	Stim 8	p = 57.77%, pwr = 7.74% No significant difference	p = 69.64%, pwr = 6.46% No significant difference	p = 87.85%, pwr = 5.25% No significant difference
	Stim 9	p = 23.09%, pwr = 24.63% No significant difference	p = 92.67%, pwr = 5.51% No significant difference	p = 52.81%, pwr = 23.09% No significant difference
Spark gap	Stim 10	p = 93.69%, pwr = 5.20% No significant difference	p = 58.51%, pwr = 13.25% No significant difference	p = 73.33%, pwr = 6.01% No significant difference
	Stim 11	p = 56.73%, pwr = 8.81% No significant difference	p = 97.44%, pwr = 5.01% No significant difference	p = 53.01%, pwr = 7.60% No significant difference
	Stim 12	p = 45.25%, pwr = 12.81% No significant difference	p = 66.67%, pwr = 7.13% No significant difference	p = 73.43%, pwr = 6.00% No significant difference

Table 14 shows the results in similar manner obtained for PTS from the USAARL dataset, corroborating the observed trend that the effect of IPI is weak on the outcomes. As shown for most test-pairs, the p-values exceed the 5% threshold. Only two test-pairs (highlighted in red) for IPI at 6 sec vs 10 min (Stim 7) and 1 min vs. 10 min (Stim 5) show p-values below 5% but both pwr values exceed 80% suggesting the t-test results should be rejected. In addition, for the test-pair for Stim 10 (highlighted in yellow) for IPI at 6 sec vs. 10 min, the pwr value is high at 89.46% for rejecting the p-value result. It is clear that the overall results in Table 14 suggests a strong finding that the effect of IPI is weak on PTS outcomes.

Table 14. PTS significance t-test – USAARL 10 shots

IPI		6 sec. vs. 1 min.	6 sec. vs. 10 min.	1 min. vs. 10 min.
Exposure Time		1 min. vs. 10 min.	1 min. vs. 100 min.	10 min. vs. 100 min.
Shock Tube	Stim 1	p = 24.20%, pwr = 18.94% No significant difference	p = 89.60%, pwr = 5.12% No significant difference	p = 13.65%, pwr = 24.56% No significant difference
	Stim 2	p = 37.45%, pwr = 19.25% No significant difference	p = 17.94%, pwr = 22.83% No significant difference	p = 7.23%, pwr = 31.42% No significant difference
	Stim 3	p = 21.84%, pwr = 15.80% No significant difference	p = 36.33%, pwr =11.40% No significant difference	p = 77.34%, pwr = 5.96% No significant difference
Fast Valve (5")	Stim 4	p = 47.44%, pwr = 9.57% No significant difference	p = 68.14%, pwr = 6.34% No significant difference	p = 23.27%, pwr = 19.09% No significant difference
	Stim 5	p = 32.84%, pwr = 11.58% No significant difference	p = 6.44%, pwr = 33.65% No significant difference	p = 0.18%, pwr = 98.04% Significant difference
	Stim 6	p = 81.32%, pwr = 5.59% No significant difference	p = 45.52%, pwr = 9.94% No significant difference	p = 34.45%, pwr = 12.61% No significant difference
Fast Valve (3.5")	Stim 7	p = 37.297%, pwr = 18.63% No significant difference	p = 3.40%, pwr = 82.25% Significant difference	p = 20.44%, pwr = 23.37% No significant difference
	Stim 8	p = 96.65%, pwr = 5.02% No significant difference	p = 25.65%, pwr = 17.38% No significant difference	p = 29.78%, pwr = 13.64% No significant difference
	Stim 9	p = 37.87%, pwr = 10.12% No significant difference	p = 94.83%, pwr = 5.04% No significant difference	p = 34.81%, pwr = 27.33% No significant difference
Spark gap	Stim 10	p = 65.08%, pwr = 23.90% No significant difference	p = 47.85%, pwr = 89.46% No significant difference	p = 70.19%, pwr = 7.73% No significant difference
	Stim 11	p = 46.80%, pwr = 39.98% No significant difference	p = 34.55%, pwr = 15.53% No significant difference	p = 27.63%, pwr = 11.98% No significant difference
	Stim 12	p = 49.68%, pwr = 10.10% No significant difference	p = 80.21%, pwr = 5.59% No significant difference	p = 64.78%, pwr = 6.83% No significant difference

In like manner, Table 15 and 16 show the t-test results for the MRDC-UCSD TTS data (test matrix in Table 2) suggesting that the effects of IPI and shot sequence are weak on the outcomes. Table 15 shows 3 out of the 4 test-pairs indicate IPI has no significant effect on TTS ($p > 5\%$), and their associated pwr values are also low (< 22%) suggesting there is weak power to reject the t-test results. Even for the last test-pair for condition 4 vs. 16 where the p-value of 3.33% suggests that IPI can affect TTS, the relatively high pwr value of 40.76% gives a high probability to reject the t-test result. Furthermore, the two test-pairs in Table 16 show the effect of shot sequence being insignificant on the TTS outcomes with p-values exceeding 5% and pwr values below 7%.

Table 17 shows the t-test results for MRDC-UCSD TTS data suggesting that the combined variation of the shot sequence and IPI can have a significant effect on TTS. However, only 2 TC pairs with combined variation of shot sequence and IPI are available (TC 5 and 16, and TC 4 and TC 6 and 14). Comparison of TC 5 and 16 shows there is a significant difference in the TTS, with $p = 5\%$ and pwr = 99.75%. On the other hand, TC 4 and 16 comparison shows there is no significant effect on TTS with $p > 5\%$ and pwr = 26.59%.

Table 15. TTS significance test: Effect of IPI (MRDC-USCD data)

	TTS			
	T-test between Condition 1 and 13	T-test between Condition 2 and 14	T-test between Condition 3 and 15	T-test between Condition 4 and 16
P(T<=t) two-tail	95.27%	14.57%	63.50%	3.33%
Power	5.03%	21.01%	7.55%	40.76%
Results	No significant difference	No significant difference	No significant difference	Significant difference

Table 16. TTS significance test: Effect of shots sequence (MRDC-UCSD data)

	TTS	
	T-test between Condition 4 and 5	T-test between Condition 2 and 6
P(T<=t) two-tail	64.07%	73.99%
Power	6.26%	5.77%
Results	No significant difference	No significant difference

Table 17. TTS Significance test: Effect of combined variation of shot sequence and IPI

	TTS	
	TC 5 vs 16	TC 6 vs 14
P(T≤t) two-tail t-test	5%	13.85%
Power	99.75%	26.59%
Results	Significant difference	No significant difference

Key Findings from USAARL and UCSD Data Analysis

The findings from the USAARL and MRDC data analysis can be summarized as follows with study limitations identified.

IPI variation with same shot sequence has statistically insignificant effect on outcomes. There is strong evidence from USAARL data for equal impulses that IPI effects on TTS and PTS are not statistically significant: 35 out of 36 pairs of TCs showed the effect of IPI on TTS is not significant, and 33 out 36 showed the effect of IPI on PTS is not significant.

Combined variation of shot sequence and IPI can have significant effects on outcomes and needs further study. Only 1 out of 2 pairs from MRMC-UCSD data shows no effect: P-value ~5% with pwr = 99.75% for 1 pair, and p = 13.85% with pwr = 26.59% for the other pair. Data is very much lacking for combined variation of short sequence and IPI. No conclusive assessment can be made to eliminate the effect of combined variation of IPI and shot sequence on outcomes. More tests in this category needs to be performed for model development.

2.3.2 Chinchilla Complex Noise Exposure Test Results

The tests matrix for the JNLWD-UCSD tests is reproduced in Table 18 with the addition of 3 columns for the actual SELA, the corresponding TTS mean, and PTS mean measured, respectively from the complex exposure. The outcomes for the 57 animals tested will be delivered to JNLWD according to the IDA recommended delivery format as described in the method section. For completeness, the MRDC-UCSD ME test matrix is also reproduced in Table 19 with additional columns for the SELA and TTS outcomes.

The following observations can be made from Table 18 based on the Mean TTS and actual SELA values. For the same actual SELA value of 114 dB, TC 25 and 26 produce the identical Mean TTS of 14 dB. TC 32 and 33 with actual SELA of 113 dB produce Mean TTS that differs by 4.2 dB from each other. Similarly, TC 36 and 37 with actual SELA of 109 dB produce TTS that differs by 5.9 dB. TC 31 using shock tube exposure produces a relatively high TTS of 41.7 dB for an actual SELA value of 113 dB. Statistical t-test results will determine whether the Mean TTS differences observed for the test pairs are significant.

Overall, the Mean TTS values for the JNLWD-UCSD tests are lower than those for the MRDC-UCSD tests, and the trend appears to be consistent with the differences in the actual SELA values obtained and number of shots delivered. For example, TC 25 and 26 from JNLWD-UCSD tests (Table 18) and TC 4 and 5 from MRDC-UCSD tests (Table 19) have the same SELA of 114 dB, but the Mean TTS for TC 4 and 5 is about twice as high than that for TC 25 and 26. The higher TTS value for TC 4 and 5 appears to be attributed to their higher number of shots, that is, 10 shots vs 2 shots only for TC 25 and 26. Similarly, TC 37 from the JNLWD-UCSD tests can be compared with TC 1 and 13 from the MRDC-UCSD tests since IPI=3 sec for these TCs. The actual SELA values are not significantly different (109 vs 110 dB), and so are the Mean TTS (15.2 vs 16.5-16.8 dB). TC 31 with actual SELA value of 113 dB produces Mean TTS of 41.7 dB, which is a few dB on the high side but not completely out of statistical variance when compared to TCs from the MRDC-UCSD tests with similar SELA values (e.g., 114 dB).

Table 18. JNLWD-UCSD Test Results Summary

TC	IPI (t)	Schematic Description of Multiple Shots	Total Impulses	Target SELA	Actual SELA	# of animal tested (n)	Mean TTS (dB)
25	3 sec.	ST	L3+L1	113	114	8 of 8	14.1
26*	3 sec.	ST	L1+L3	113	114	8 of 8	14.4
32	50 msec.	PG	L3+L1	113	113	6 of 6	13.9
33	50 msec.	PG	L1+L3	113	113	6 of 6	18.1
36	50 msec.	PG	10L2	111	109	6 of 6	9.3
37	3 sec.	PG	10L2	111	109	7 of 7	15.2
40	3 sec.	PG	10L1	106	105	8 of 8	4.3
41	50 msec.	PG	10L3	113	111+	0 of 6	
42	3 sec.	PG	10L3	113	111+	0 of 6	
31**	3 sec.	ST	10L2	113	113	8 of 8	41.7

❖ Peak pressure level (L) L1, L2 and L3 = 140, 150 and 160 dB, respectively. ST = Shock Tube. PG = Paintball Guns

* Missing TTS data for 4 kHz for 1 animal. ** One animal expired during gas anesthesia after data were recorded. + Estimate based on current UCSD tests.

Table 19. MRDC-UCSD ME Test Results Summary

Test Condition	Peak Pressure Level (L)	IPI (t)	Schematic Description of Multiple Shots	Total Impulses	SELA		$TTS_{average\ 1,2,4\ kHz}$	
					Mean	SD	Mean	SD
1	L1, L2	t1		5L1+5L2	110.16	0.75	16.5	9.8
2	L1, L3	t1		5L1+5L3	115.06	0.68	31.5	14.3
3	L3, L2	t1		5L3+5L2	114.53	0.44	28.0	11.5
4	L1, L2, L3	t1		4L1+3L2+3L3	114.22	0.70	31.0	13.4
5	L1, L3, L2	t1		4L1+3L2+3L3	114.12	0.41	27.8	5.7
6	L1, L3	t1		5L1+5L3	115.33	0.37	34.2	9.6
13	L1, L2	t1, t2		5L1+5L2	110.57	0.29	16.8	7.3
14	L1, L3	t1, t2		5L1+5L3	115.07	0.12	43.3	7.9
15	L3, L2	t1, t3		5L3+5L2	116.76	0.47	31.8	13.0
16	L1, L2, L3	t3, t1, t2		4L1+3L2+3L3	114.89	0.25	47.7	5.5
17	L3, L1, L2	t1, t3, t2		5L3+3L1+2L2	115.67	0.30	47.5	8.0
18	L1, L2, L3	t1, t2, t3		5L1+2L2+3L3	114.89	0.41	39.3	9.1

2.3.3 Immunity Hypothesis Test and Exploratory AR Effect

2.3.3.1 Immunity Test in the ME Regime

The immunity hypothesis test results are summarized in Table 20 and 21 when both the left and right ear data are combined together (n= 16), and in Table 22 and 23 when left and right ear data are considered separately (n = 8). Table 20 and 22 show the mean and standard deviation (SD) for the three time points of measurement for each TC, and Table 21 and 23 show the t-test results for each test pair, respectively.

As shown in Table 20, the TTS Mean and SD for TC 25 and 26 are similar for all 3 time points of measurement. Overall, the difference between the TTS Mean values are less than 2 dB. The TTS Mean values are practically identical for the first time point. The t-test results shown in Table 21 confirm the difference in the TTS outcomes between TC 25 and 26 is not significant for all 3 time points of measurements (p>38% with power<11%), corroborating the previous finding that the effect of shot sequence is not important.

Table 20. TTS mean and SD for TC 25 and 26 (all ears, n = 16)

Time point	TC 25		TC 26	
	Mean	SD	Mean	SD
1	14.0625	7.4714	14.3750	5.1595
2	13.7500	9.7515	12.2917	5.2308
3	13.4375	7.6308	11.4583	4.6098

Table 21. Immunity hypothesis test: TC 25 and 26 (all ears, n = 16)

Time point	P-value (%)	Power (%)	Difference
1	89.15	5.15	Not Significant
2	60.20	6.94	Not Significant
3	38.16	10.95	Not Significant

The result is the same when the left and right ears are considered separately. As shown in Table 22, the TTS Mean and SD for each ear are similar for all 3 time points. The t-test results in Table 23 show that considering the left and right ear separately does not change the findings that the difference in the TTS outcomes between TC 25 and 26 is not significant, p> 47% with power<10%.

Table 22. TTS mean and SD for TC 25 and 26 (individual ear, n = 8)

	TC 25				TC 26			
	Right Ear		Left Ear		Right Ear		Left Ear	
Time point	Mean	SD	Mean	SD	Mean	SD	Mean	SD
1	14.6875	8.6824	13.4375	6.5834	13.3333	5.3266	15.4167	5.1177
2	14.2708	12.4995	13.2292	6.8492	11.8750	5.8546	12.7083	4.8947
3	14.0625	9.0571	12.8125	6.4694	11.0417	4.8947	11.8750	4.6022

Table 23. Immunity hypothesis tests: TC 25 vs 26 (individual ear, n=8)

	Right Ear			Left Ear		
Time point	P-value(%)	Power (%)	Difference	P-value (%)	Power (%)	Difference
1	71.25	5.98	NS	51.29	8.68	NS
2	63.11	6.49	NS	86.36	5.23	NS
3	42.05	9.54	NS	74.33	5.84	NS

NS: Not Significant; S: Significant

2.3.3.2 Immunity Test in the AR Regime

Paintball gun tests show potential AR effects on outcomes. As shown in Table 24 when data from all ears are analyzed together, the Mean TTS values differ by at least 4 dB between TC 32 and 33 for all time points of measurement. The t-test results shown in Table 25 show that the differences observed in the TTS outcomes between TC 32 and TC 33 are significant for the 2nd and 3rd time points of measurement, but not for the 1st time point. Even so, the relatively low p-value of 11.89% compared to the significance level of 5% for the 1st time point seems to indicate there is some potential effect of the AR.

The results obtained when the left and right ears are considered separately show that the AR effect is stronger for the left ear. As shown in Table 26, the TTS Mean is at least 7 dB higher for TC 33 compared to TC 32 for the left ear for all time points of measurement. For the right ear, the difference in the TTS Mean between TC 32 and 33 is about 3 dB. As shown in Table 27, although the t-test results for the left ear show the difference in TTS Mean between TC 32 and 33 is significant only for the 2nd time point of measurement, the p-values for the 1st and 3rd time points are very close to the significance level of 5%. For the right ear, the difference in TTS outcome between TC 32 and 33 is not significant for all time points of measurement.

Table 24. TTS mean and SD for TC 32 and 33 (all ears, n = 12)

Time point	TC 32		TC 33	
	Mean	SD	Mean	SD
1	13.8889	4.5965	18.0555	7.6156
2	10.1389	5.1473	16.8055	7.8643
3	8.3333	3.3710	13.6806	8.0282

Table 25. Immunity hypothesis test: TC 32 and 33 (all ears, n = 12)

Time point	P-value (%)	Power (%)	Difference
1	11.89	56.47	Not Significant
2	2.23	85.80	Significant
3	4.48	96.00	Significant

Table 26. TTS mean and SD for TC 32 and 33 (left and right ear, n = 6)

	TC 32				TC 33			
	Right Ear		Left Ear		Right Ear		Left Ear	
Time point	Mean	SD	Mean	SD	Mean	SD	Mean	SD
1	15.2778	5.0735	12.5000	4.0139	16.3889	7.0448	19.7222	8.4437
2	12.7778	5.0461	7.5000	4.0139	16.6667	7.5462	16.9444	8.8924
3	9.7222	3.0123	6.9444	3.3610	12.7778	7.9524	14.5833	8.7520

Table 27. Immunity hypothesis tests: TC 32 vs 33 (individual ear, n=6)

	Right Ear			Left Ear		
Time point	P-value(%)	Power (%)	Difference	P-value (%)	Power (%)	Difference
1	76.03	6.37	NS	8.77	80.16	NS
2	31.87	22.71	NS	3.92	95.55	S
3	39.94	35.56	NS	7.39	94.26	NS

NS: Not Significant; S: Significant

2.3.3.3 AR Effect from Repeat Shots

Table 28 shows the results for the t-test comparison for TC 36 and 37 when the left and right ear data are analyzed together (n=12). As shown in the table, p>5% for all measurement time points, with power <60%, showing the difference in TTS outcomes between TC 36 and 37 is not significant. The potential effect of AR seems to be more apparent for the first time point with p =

12.37%, which is closer to 5% compared to the value for the other time points. The mean TTS comparison for the 1st time point suggests AR may have played a role for TC 36 to have lower TTS than TC 37 (9.3 vs 15.2 dB, as shown in Table 17).

When the data from left and right ears are analyzed separately, the results remain the same. As shown in Table 29, p>32% for right ear, and p> 27% for the left ear. The difference in TTS outcomes between TC 32 and 33 is not significant for all measurement time points when the ears are considered separately.

Table 28. Statistical Comparison of TTS_{124K} for TC 36 and 37 (All ears, n = 12)

Time point	P-value(%)	Power (%)	Difference
1	12.37	58.17	Not Significant
2	53.95	-	Not Significant
3	41.17	-	Not Significant

Table 29. Statistical Comparison for TC 36 and 37 (individual ear, n = 6)

	Right Ear			Left Ear		
Time point	P-value(%)	Power (%)	Difference	P-value (%)	Power (%)	Difference
1	32.16	22.91	NS	27.75	36.07	NS
2	54.66	8.87	NS	83.70	-	NS
3	62.92	-	NS	54.06	-	NS

NS: Not Significant; S: Significant

2.3.3.4 Effect of Noise Type

To determine the effect of noise type, shock tube and paintball exposures with similar conditions are compared. More precisely, the TTS outcomes between TC 31 and TC 37 are compared. Table 30 and 31 show the results for the t-test performed when the left and right ears are analyzed together and separately, respectively.

Based on the TTS mean comparison between TC 31 and 37 shown in Table 18, the TTS incurred from TC 31 is almost 3 times as higher as that from TC 37. We note that the actual SELA for TC 31 is 4 dB larger than that for TC 37. As shown in Table 30 and 31, the t-test results show that the difference in the TTS Mean between TC 31 and 37 is significant, whether data from the left and right ears are analyzed together or separately. However, the difference in the TTS outcomes is probably due to the large difference in the actual SELA delivered. No clear conclusion can be drawn from this comparison regarding the effects of noise type on outcomes.

Table 30. Statistical Comparison for TC 31 and 37 (All ears, n = 12)

Time point	P-value(%)	Power (%)	Difference
1	<5%	99.99	Significant
2	<5%	-	Significant
3	<5%	-	Significant

Table 31. Statistical Comparison for TC 31 and 37 (Individual ear, n = 6)

	Right Ear			Left Ear		
Time point	P-value(%)	Power (%)	Difference	P-value (%)	Power (%)	Difference
1	<5%	99.13	S	<5%	99.92	S
2	<5%	99.99	S	<5%	-	S
3	<5%	-	S	<5%	-	S

NS: Not Significant; S: Significant

2.3.4 Tympanometry Tests: Effect of Anesthesia on AR

Tympanometry measurements show ARTs were readily detected in the anesthetized animals. For two unanesthetized animals, due to the movement of animals despite being held by two technicians, thresholds were much more difficult to obtain. However, once finally obtained they were similar to those from the anesthetized animals, suggesting that anesthesia had no significant effect on the acoustic reflex. Recent literature data also confirm the presence of AR in chinchillas under anesthesia (YOKELL, 2019). The tympanometry test results are summarized from Figure 47 to 52 for ART and admittance change.

Figure 47 and 48 show the results for Animal 928 for ART and admittance change, respectively. As shown in Figure 47a, ART data for the right ear were obtained for 1 and 2 kHz, but not for 4kHz. For the left ear, ART could not be collected for 2 and 4 kHz, but was obtained for 1kHz when the animal was under anesthesia (Figure 47b). ART could not be measured due to lack of optimal seal of the ear and animal behavior when the animal was awake. In general, when ART was collected for both conditions, Sleep and Awake, the ART magnitudes were similar, showing AR is still present under anesthesia. As shown in Figure 48, admittance change was detectable whenever ART was measured. Note that admittance is an absolute value while ART is in dB; this makes the admittance change differences between Awake and Sleep somewhat more pronounced.

Figure 50 and 51 show the results for Animal 929 for ART and admittance change, respectively. For this animal, ART was measured for all 3 stimulus frequencies, but could not be measured under anesthesia for 4 kHz for the left ear due to lack of good seal of the ear. For this animal also, when ART was detected, an admittance change was also measured. Data for ART and admittance change show AR is still present under anesthesia.

Figure 51 and 52 show the results for Animal 930 for ART and admittance change, respectively. The AR tests using this animal was the most successful of all tests. ART and admittance change were obtained for all 3 stimulus frequencies for both Awake and Sleep conditions. As shown in Figure 51, ART with and without anesthesia are similar for all stimulus frequencies tested, suggesting anesthesia has little effect on AR. Also, whenever ART was detected, an admittance change was also measured. Overall, the data show AR is still present under anesthesia for all stimulus frequencies tested.

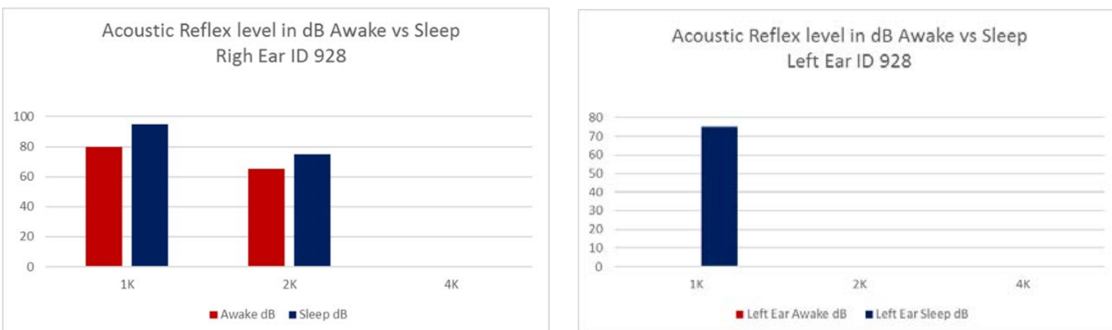

a) Right Ear b) Left Ear

Figure 47. Effect of anesthesia on ART, Animal ID 928

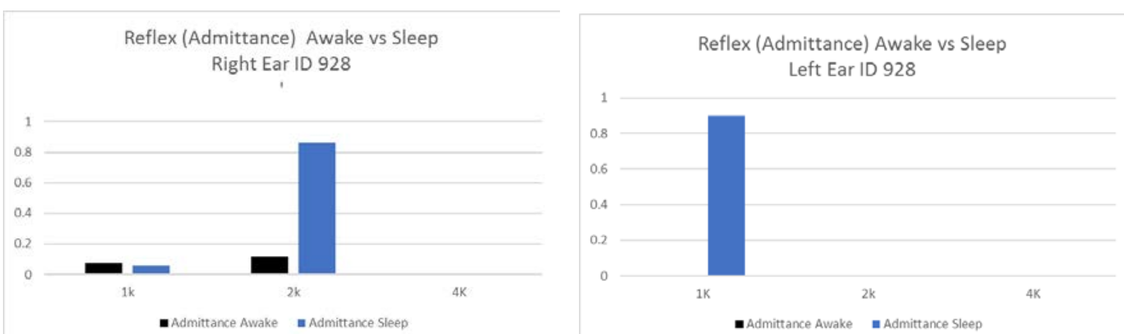

a) Right Ear b) Left Ear

Figure 48. Effect of anesthesia on admittance, Animal ID 928

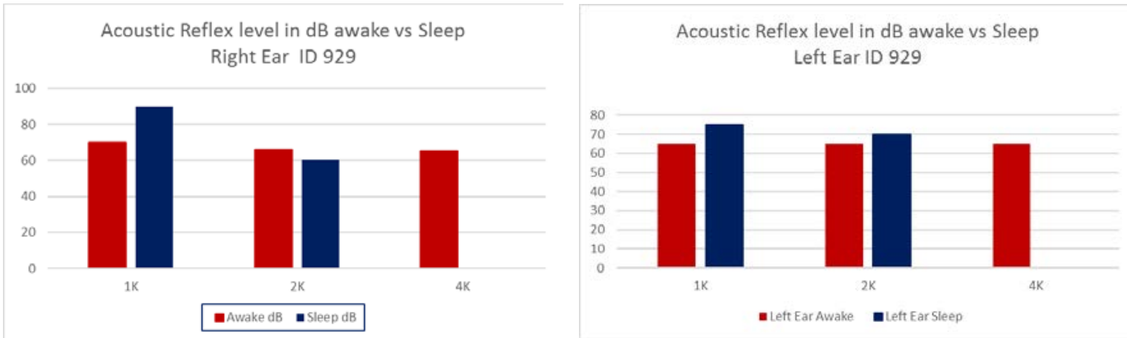

a) Right Ear b) Left Ear

Figure 49. Effect of anesthesia on ART, Animal ID 929

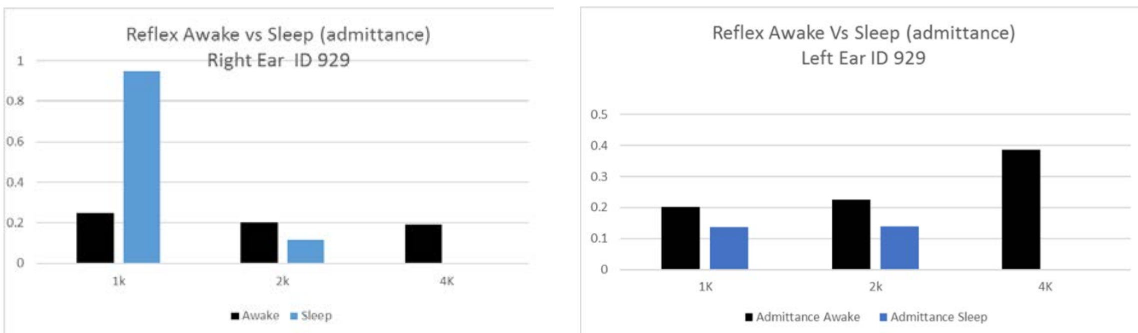

a) Right Ear b) Left Ear

Figure 50. Effect of anesthesia on admittance, Animal ID 929

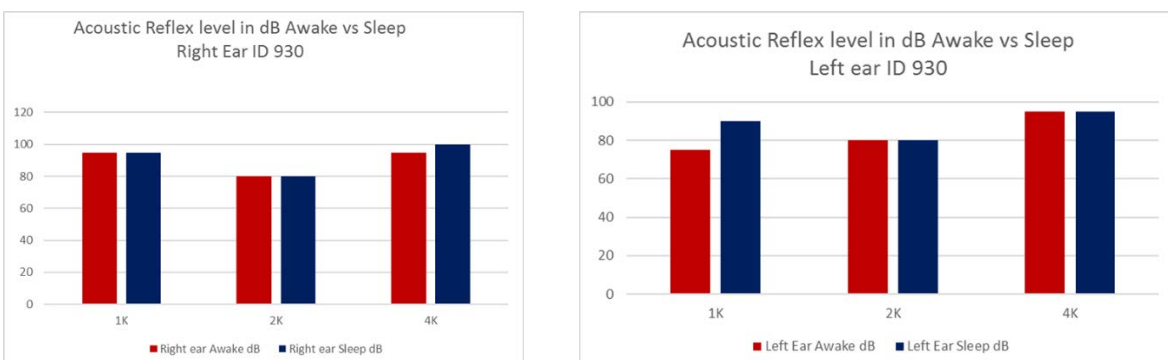

a) Right Ear b) Left Ear

Figure 51. Effect of anesthesia on ART, Animal ID 930

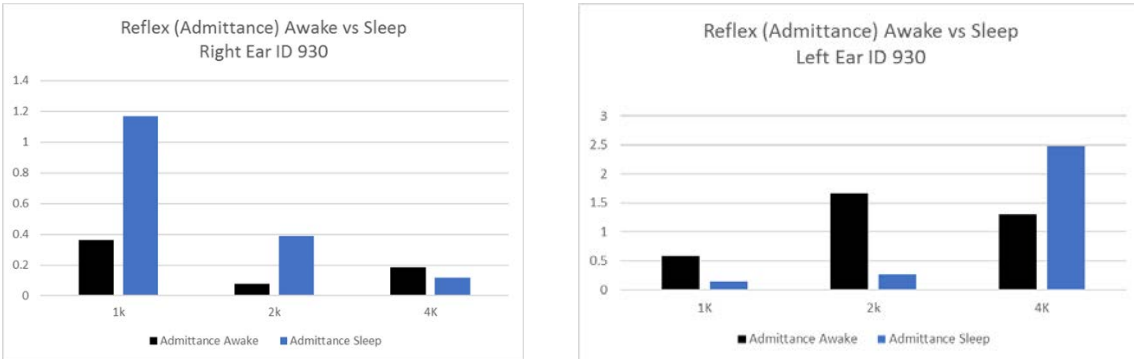

a) Right Ear b) Left Ear

Figure 52. Effect of anesthesia on admittance, Animal ID 930

2.3.5 Accumulated Dose Formula Optimization: α-Term Effect and N-Sensitivity

Figure 53 and 54 show the results for the accumulated dose formula optimization for $N \geq 1$ and $N > 1$, respectively. The optimization results confirm the effect of IPI is weak (α~0). As shown in Figure 53, the error between the predicted and observed value increases with α. The optimal α-value is equal to 0 when the 1-shot cases are included. As shown in Figure 54, ε is practically constant (ε~28.45-28.75 %) for α varying between 0 and 1 when the N=1 case is excluded. The maximum SELA correction for individual shots is 1.3 dB for IPI≤20 sec, for α=1.

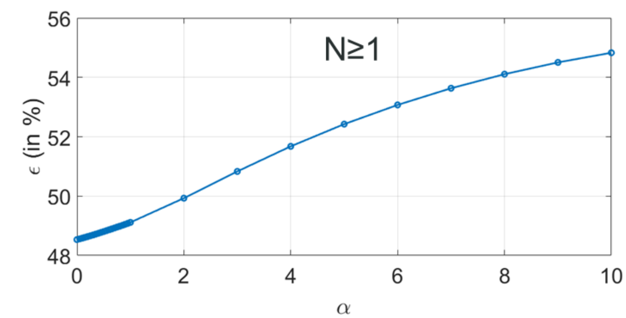

Figure 53. α-Term Effect for N ≥ 1

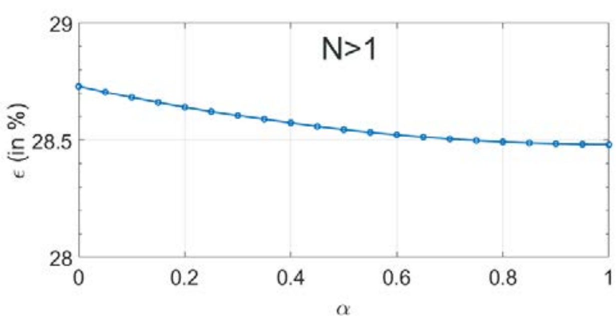

Figure 54. α-Term Effect for N >1

It should be mentioned that the purpose of this optimization exercise is to see if there is “second order” correction to the SELA-based dose-response model and the results do not yield a meaningful correction factor. It is recognized the optimization can come right out of the application of maximum likelihood through logistic regression but that is expected to give α=0 as suggested by the previous statistical analysis of the USAARL. This explicit computational exercise was carried out to see if more insights can be obtained and the results suggest that there is a limitation to the use of SELA as the dose metric for differentiating the effects of complex blast exposure on the outcomes based on empirical correlation. Likely a more biomechanically-based dose metric is needed, such as OHC-ED illustrated in Part 1.

2.3.6 Accumulated Dose Model Options

2.3.6.1 Model Comparison Based on Injury Risk Prediction

The results for model comparison of the dose-response curves against specified thresholds are presented. The results for TTS≥ 25 dB, PTS ≥25 dB, and PTS ≥ 45 dB are presented in turn. For each of the injury criteria, the raw TTS/PTS data from the UCSD tests are plotted vs SELA for visualization, and the dose-response curves for the 3 model options are also plotted together for comparison with the binned UCSD data. The linear regression fits for the observed vs predicted injuries whenever possible are plotted together for comparison, and a table summarizing the findings is provided.

2.3.6.1.1 *TTS ≥ 25 dB*

As shown in Figure 55, TTS data for 117 chinchillas tested at UCSD are plotted against SELA. The TTS incurred range from 0 to 60 dB, while the SELA is between 100 and 120 dB. This shows the SELA range is narrow compared to the TTS range. The plot also shows that about one half of the TTS is greater than 25 dB.

Figure 56 shows the dose-response curves for Model A, B and C for prediction of failure rate for TTS ≥ 25 dB together with the 23-point bins from the UCSD test data. Recall that Model A uses all the available USAARL data, Model B uses a subset including IPI ≤ 20 sec and the 1-shot cases but excluding the broadband noise tests, and Model C is the same as Model B but excluding the 1-shot cases. As shown in Figure 56, the slope for Model C is the steepest, followed by Model A, and Model B. The data comparison suggests Model C has the best prediction of the failure rates, and this is confirmed by the linear regression fit in Figure 57 with the fit statistics and error comparison shown in Table 32.

As shown in Figure 57, the slope for Model C is the closest to the perfect prediction slope, while the y-intercepts for all 3 models are similar. Overall, the values in Table 32 are similar, with all model predictions far from yielding a perfect prediction. However, the difference in the values can be used to separate the models to select the best model for predicting the UCSD data. Based on the values in Table 32, no single model satisfies at least two linear fit criteria in terms of the Y-intercept, slope, and r^2. Model A yields the smallest Y-intercept value, and Model B the largest r^2, and Model C the largest slope. However, the prediction error is the lowest for model C. Hence, model C satisfies 2 of 4 comparison criteria. Therefore, Model C yields the best prediction against TTS ≥ 25 dB.

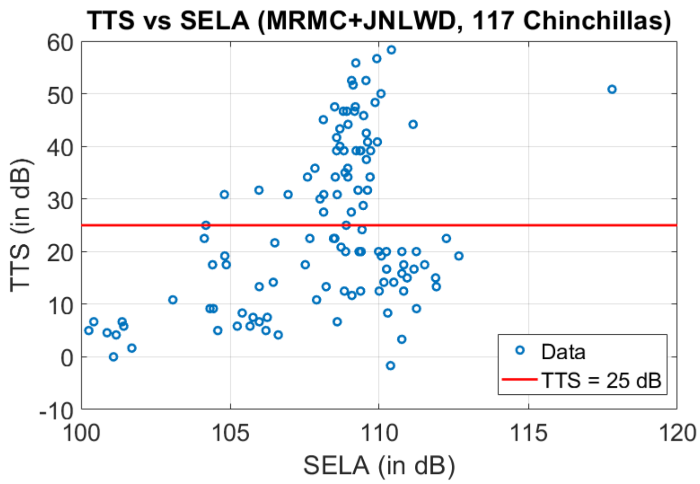

Figure 55. TTS vs SELA (UCSD data) showing TTS = 25 dB threshold

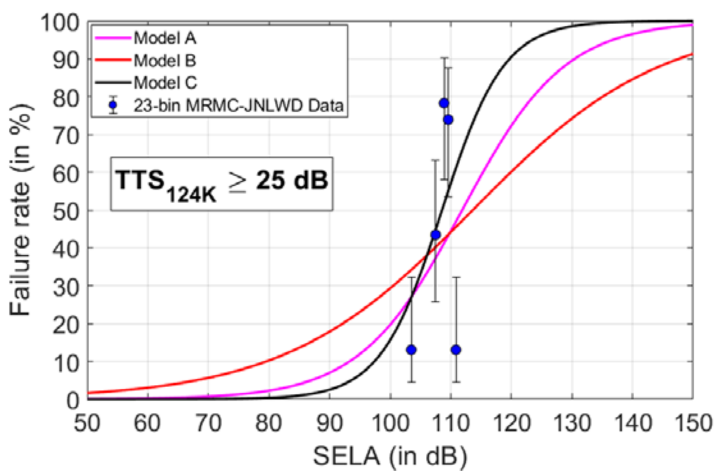

Figure 56. Dose-response curve comparison with binned UCSD data for TTS124K ≥ 25 dB

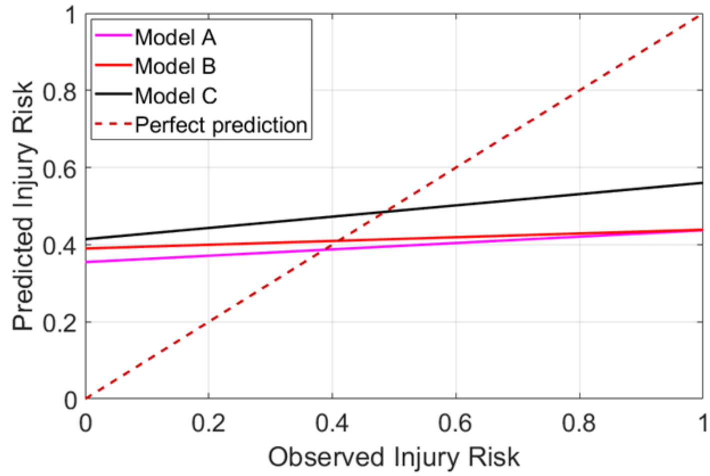

Figure 57. Comparison of observed and predicted Injury Risk

Table 32. Summary of model comparison data for TTS ≥ 25 dB

	Model A	**Model B**	**Model C**
Y-intercept	0.3549	0.3901	0.4140
Slope	0.0825	0.0487	0.1463
r^2	0.1167	0.1250	0.1240
Prediction error (ε in %)	51.7124	51.9047	50.8252

2.3.6.1.2 *PTS ≥ 25 dB*

Figure 58 shows the plot for 96 chinchilla PTS data points available out of 117 chinchillas tested. There were eleven noise exposures from which the PTS data were not collected because the animals expired during maintenance under gas anesthesia and they are labeled as missing data. Figure 58 shows the PTS values range from about -15 to 40 dB. More importantly, the data show only 1 data point satisfying PTS ≥ 25 dB. The implication is that the binning of the data will result in mostly 0 failure rate.

Figure 59 shows the dose-response curves for Model A, B and C for prediction of failure rate against PTS≥ 25 dB and the 19-point bins from the UCSD data. Similar to the case for TTS ≥ 25 dB, Figure 59 shows that for PTS ≥ 25 dB the slope for Model C is the steepest, followed by Model A and Model B. Failure rate appears to be better predicted by Model A or C as confirmed by the linear regression fit in Figure 60 with fit statistics and error comparison shown in Table 33.

As shown in Figure 60, the linear fits for Model A and C are closer to the perfect prediction line than Model B. As observed from the values in Table 33, Model B gives the worst prediction against the UCSD data. Model A and C satisfy 2 of the 4 criteria, including the prediction error. Note the prediction error is given in absolute rather than relative value because most of the binned data are zero for PTS ≥ 25 dB. Model A yields the smallest Y-intercept and prediction error, and Model C gives the steepest slope and largest r^2 value. Therefore, Model A or C predicts the data better against PTS ≥ 25 dB.

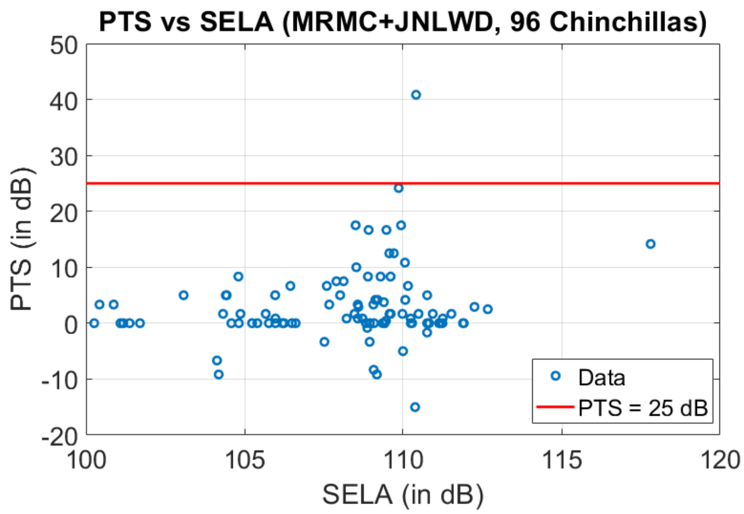

Figure 58. PTS vs SELA (UCSD data) showing PTS = 25 dB threshold

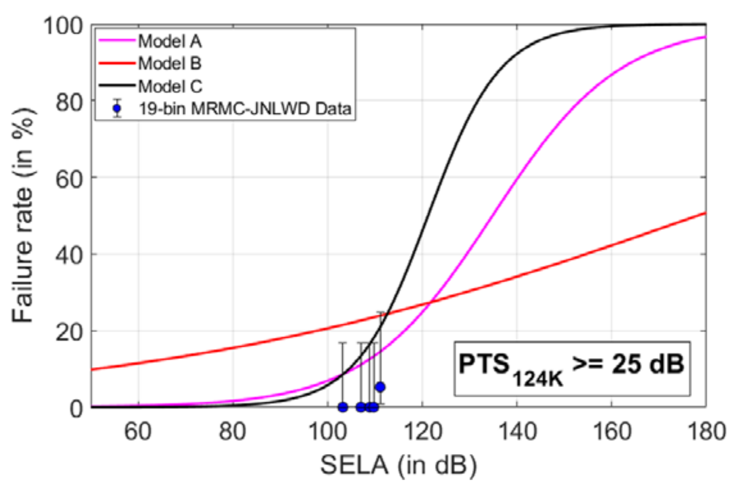

Figure 59. Dose-response curve comparison with binned UCSD data for PTS_{124K} ≥ 25 dB

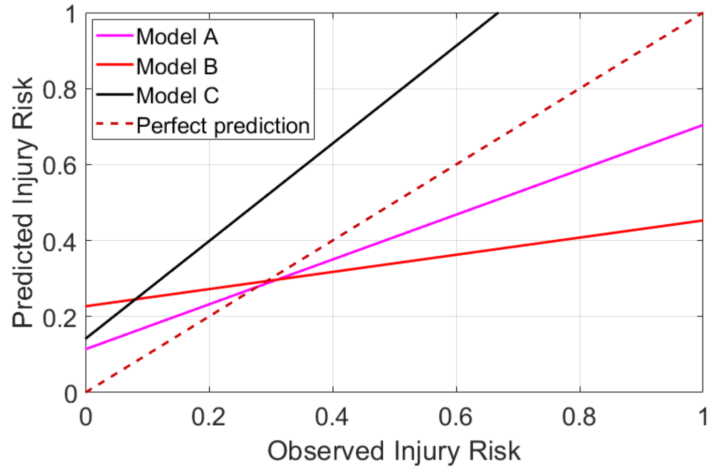

Figure 60. Comparison of observed and predicted Injury Risk for $PTS_{124K} \geq 25$ dB

Table 33. Model comparison data for PTS ≥ 25 dB

	Model A	Model B	Model C
Y-intercept	0.1140	0.2270	0.1414
Slope	0.5901	0.2259	1.2845
r^2	0.3752	0.3316	0.4087
Prediction error	0.2486	0.4909	0.3311

2.3.6.1.3 *PTS ≥ 45 dB*

Figure 61 shows the UCSD PTS data compared against the PTS ≥45 dB threshold. The data points are from 96 chinchillas out of 117 tested. The PTS values range from about -15 to 40 dB. As shown in Figure 61, there are no data points that satisfy PTS ≥ 45 dB. This means that the binning of the data will result in 0 failure rate.

Figure 62 shows the data comparison of the dose-response curves for Model A, B and C against PTS ≥ 45 dB together with the 19-point bins from the UCSD data. As for the previous two cases, Figure 62 shows that for PTS ≥ 45 dB the slope for Model C is the steepest, followed by Model A, and Model B. The results show Model A or C predicts the failure rate better than Model B for the binned data. This is confirmed by the error comparison shown in Table 34. Note that for PTS ≥ 45 dB, the linear regression fit could not be obtained since all observed values are zero. The prediction error alone is thus used for selection of the best model. Based on this criterion, Model C is the best model against PTS ≥ 45 dB for predicting the UCSD data.

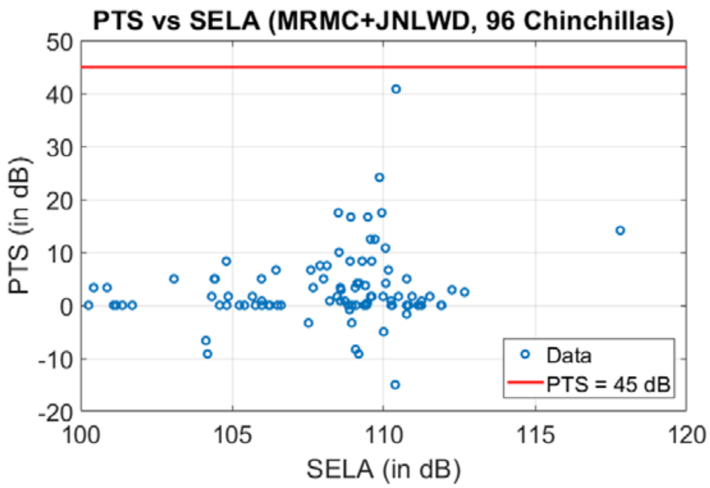

Figure 61. PTS vs SELA (UCSD data) showing PTS = 45 dB threshold

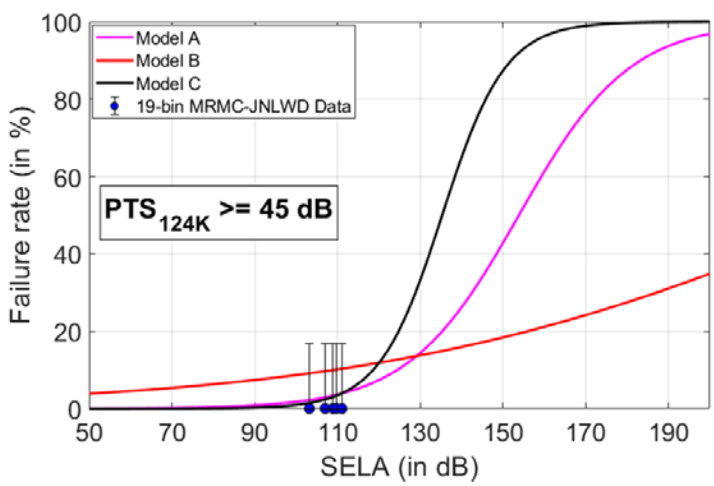

Figure 62. Dose-response curve comparison with binned UCSD data for PTS124K ≥ 45 dB

Table 34. Model comparison data for PTS ≥ 45 dB

	Model A	Model B	Model C
Prediction error	0.0727	0.2202	0.0659

2.3.6.2 Model Comparison Based on TTS/PTS Prediction

The overall model comparison against TTS and PTS data are shown in Figure 63 and 64, respectively. The solid data points represent the average value for each TC for all available impulse-like exposures (no BBN) for both the USAARL and UCSD data. Color coding is used to identify the different test groups. For the USAARL data, orange data points represent TCs with multiple shots (N>1), and the yellow data points represent the 1-shot cases (N=1). For the MRDC-UCSD data, the blue data points represent TCs with constant IPI within the shot sequence, and the cyan data points represent TCs with varied IPI. The JNLWD-UCSD data points are shown in green.

Figure 63 shows the TTS vs SELA plot for Model A, B, and C. As shown in the figure, the curve for Model A lies between those for Model B and C for SELA > 110 dB but vice-versa for SELA < 110 dB. Overall, the three models appear to predict the data reasonably well for SELA < 115 dB for TTS.

Figure 64 shows the range is narrower for the observed PTS compared to TTS. In particular, the PTS vs SELA curve for Model B is almost flat; Model B shows PTS is practically constant across the SELA range with values between about 14 and 16 dB.

The model error comparison is shown in Table 35. As shown in the table, based on the prediction error, Model A gives a better prediction against TTS, while Model C predicts PTS better. Based on the fitting error, Model C yields the best fit to the data against both TTS and PTS.

The pros and cons for each model are summarized in Table 36. Model A gives the best TTS prediction overall and fair PTS prediction against single-shots. However, Model A gives the worst PTS prediction overall compared to the other two models. Model B gives the best TTS prediction against single-shots, but underestimates TTS against multiple shots. Model C gives the best PTS prediction overall, and a good TTS and PTS prediction against multiple shots. Model C is conservative against single shots for both TTS and PTS, but it is rare that only one shot is fired in operation. Based on these results, two model options can be adopted: the first option (Option 1) is to use two model: Model A and C. The other option (Option 2) is to use one model: Model C. The final decision will depend on the consideration of the boundaries for risks of significant injuries (RSI) against operational envelopes. For PTS predictions against RSI, Model C is recommended.

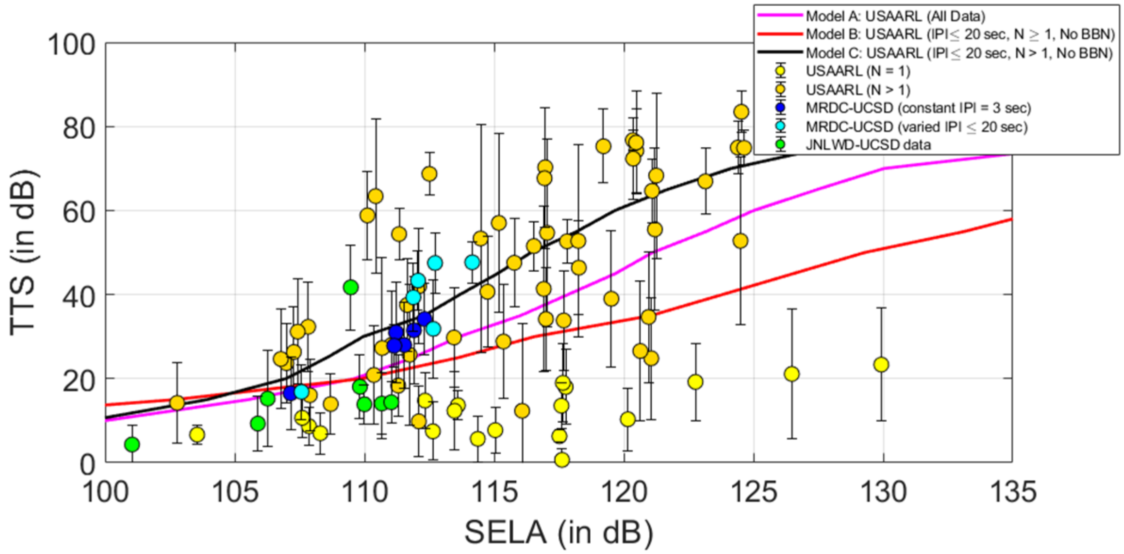

Figure 63. TTS vs SELA

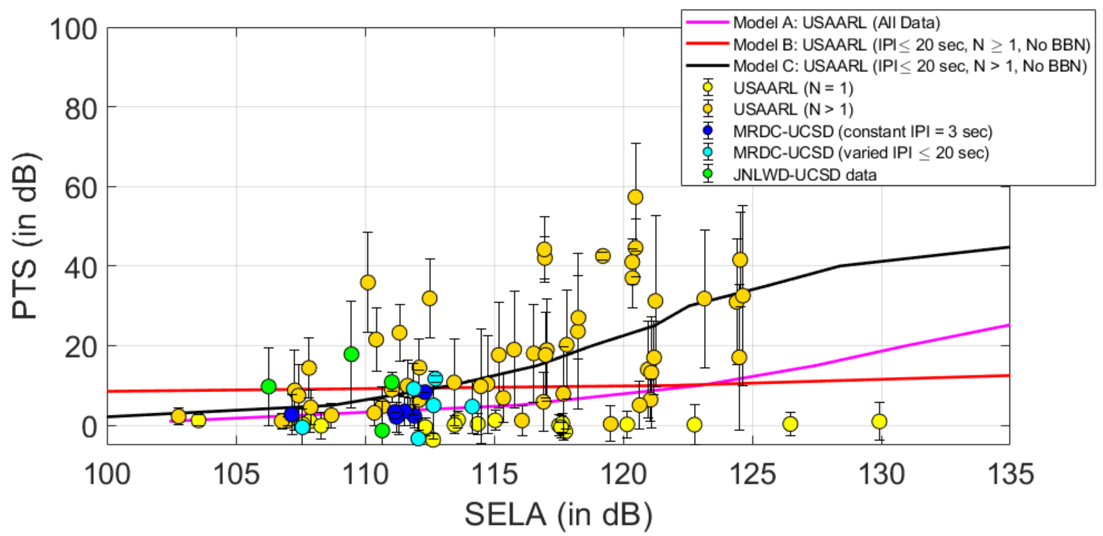

Figure 64. PTS vs SELA

Table 35. Model Error Comparison

Error Type	Injury Type	Model A	Model B	Model C
Prediction Error (ε in %)	TTS	47.3	51.2	51.7
	PTS	80.0	76.0	73.2
Fitting Error (ε in %)	TTS	38.3	52.3	32.3
	PTS	75.3	85.5	54.7

Table 36. Model Pros and Cons

Model	Pros	Cons
A	• Best TTS prediction overall • Good PTS prediction against single-shot	• Worst PTS prediction overall
B	• Best TTS prediction against single shot	• Underestimate TTS against multiple shots
C	• Best PTS prediction overall • Good TTS and PTS prediction against multiple shots	• Overly conservative against single shot for TTS and PTS

2.4 Discussion

Three models have been developed for accumulated dose in the ME regime. The results suggest Model C is the most adequate for typical flashbangs for both TTS and PTS predictions. Model C gives the best prediction against TTS > 25 dB and PTS > 45 dB. For PTS>25 dB, Model C or A can be used. Based on the results from model comparison against TTS and PTS, two model options are plausible: the first option (Option 1) is to use two models: Model A and C. The other option (Option 2) is to use one model, Model C. Risk curves from the three models are available for both TTS and PTS for further RSI analysis against operational needs.

The findings showing three empirical model options are most likely due to the limitation of the use of A-weighted energy as the dose metric. SELA is borrowed from occupational health research limiting daily exposures to continuous noise. The data comparison for the model-based approach presented in Part 1 shows the use of OHC-ED as the dose metric is able to differentiate the dose-risk correlation better than the use of SELA. Certainly, the new data collected are still limited and kept to a narrow SELA range by default in order to identify the effects of complex exposure on outcomes, and many test pairs are needed for statistical analysis. The in-depth analysis of the USAARL data shows the effect of IPI is negligible but the tests did not include any variation of IPI even within a shot sequence with equal impulses, not to mention the combined variation of IPI, intensity and sequence, and the need for that study is real since theater operations produce very complex exposures. Furthermore, a model-based approach to develop a true "internal" dose for injury correlation should be pursued for future study.

Novel devices will likely operate within the AR regime and data and research are still very much limited for extending the dose-response curves to the AR regime. The exploratory data collected from the current project suggests there are potential AR effects on the outcomes. Again, a model-based approach is likely needed for research in the AR regime. Recent research from human studies will provide beneficial data for model development. Injury data are still needed using animal testing. More controlled studies should be performed to improve the scaling from chinchillas to humans.

Appendix A: Calibration of the Noise Generation Systems

A.1 Calibration of the ARFST System

A.1.1 Impulse waveform comparison based on diaphragm thickness

All of the various diaphragm thicknesses were used in the ARFST system and the waveforms were recorded at the optimal distance from the shock tube exit (4 ft radial distance at a 15° centerline offset). This location was determined by the various characterization studies described later. Figure 65 shows the waveform comparison for the various thicknesses of the Mylar diaphragms. As expected, thicker diaphragms produce larger impulses and pressure peak grows with diaphragm thickness.

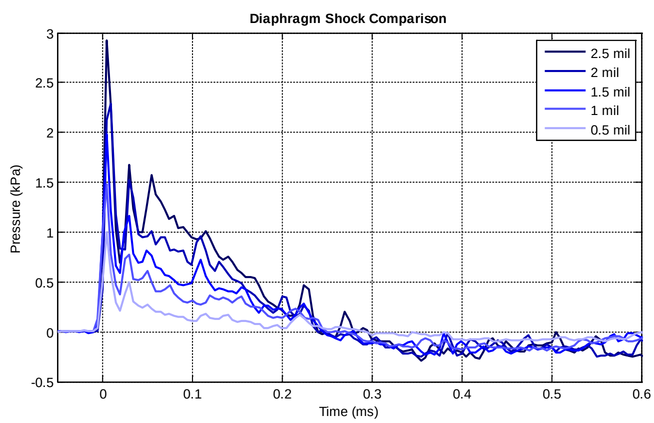

Figure 65. Shock wave comparison for the various thicknesses of Mylar diaphragms tested.

A.1.2 Testing of typical shot sequencing and timing based on test matrix

The ARFST is capable of rapidly firing high pressure shock waves in a very controlled and repeatable sequence. Controlling the exact timing between shots is an important aspect of the proposed testing matrix and the accuracy of the shock tube timing algorithms and control system were thoroughly tested. The current test matrix calls for a maximum of 10 shots in one sequence of testing. The PLC controller was programmed to successfully handle this amount of shots but we are near the memory limits of the hardware. The ARFTS is capable of holding a total of 20 diaphragms between the two separate wheels, and it is possible to do all 20 shots sequentially if desired but a soft reset of the system is required between the 10th and 11th shot. This soft reset will take the user approximately five seconds to complete.

With the current requirement of 10 shots, the ARFTS was thoroughly tested to ensure that the machine is capable of handling all of variability in the proposed test matrix. A sample test sequence with a variety of shot intensities (different diaphragm thicknesses) and also variable timing intervals between shots is shown in Figure 66. Testing was done with the microphone at a 4 ft radial distance and a 15° offset from the shock tube centerline. Plotting all of the shots on a long time history scale makes it difficult to analyze each pressure pulse individually but allows for a better visualization regarding the timing and magnitude of each shot. A numerical breakdown of this test sequence is shown in Table 38. Test matrix for ARFST calibration, where it is clear that the true timing delays match very well with the desired values.

Table 37. Test matrix for ARFST calibration

Shot #	Diaphragm Mil	Microphone Location		Desired Time Delay (sec)	True Time Delay (sec)	Microphone Peak dB
		Radial Distance	Angle			
1	2.5	48"	15°	9	8.91	163.3
2	1	48"	15°	9	9.00	157.5
3	2	48"	15°	3	3.09	161.2
4	1	48"	15°	3	2.95	158.2
5	1.5	48"	15°	20	20.11	159.9
6	2.5	48"	15°	20	20.01	163.3
7	1	48"	15°	20	19.93	157.4
8	1.5	48"	15°	3	3.25	160.7
9	0.5	48"	15°	3	2.89	154.0
10	1	48"	15°	-	-	157.9

Time intervals are accurately maintained despite the varying levels of shot intensities tested. Figure 66 shows the pressure time records of a 20-shot sequence by repeating the test matrix shown in Table 38.

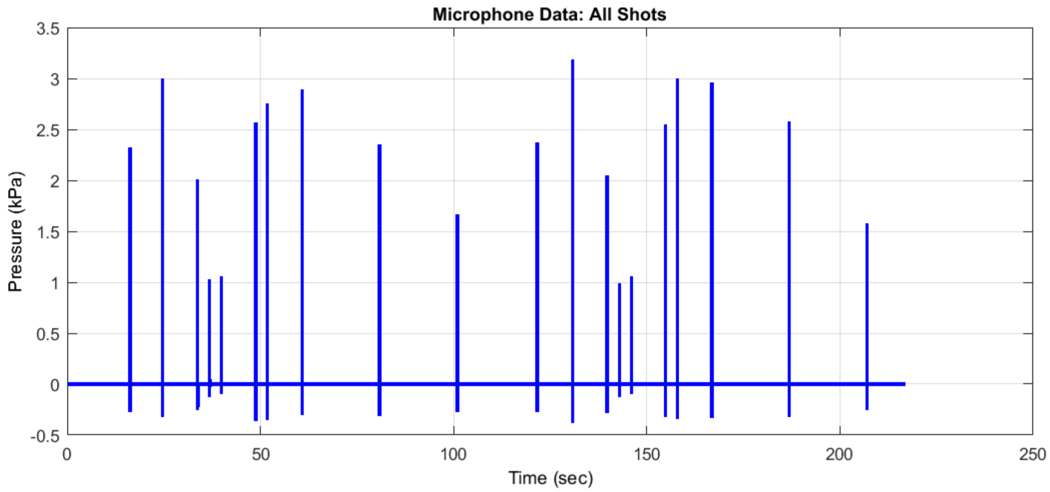

Figure 66. Twenty sequentially shots performed by the ARFTS at varying intensities and time intervals.

A.1.3 Spatial characterization study

Three characterization studies were performed that evaluated the effects of shock wave reflection, peak variations with angle from the centerline, and spherical spreading of the wave front. The characterization study helps determine the optimal acoustic conditions for animal exposure for metabolic exhaustion study.

The ground reflection effects were evaluated as shown in Figure 67. With a bare floor, the ground reflections are clearly captured in the acoustic data recorded (Figure 67a).

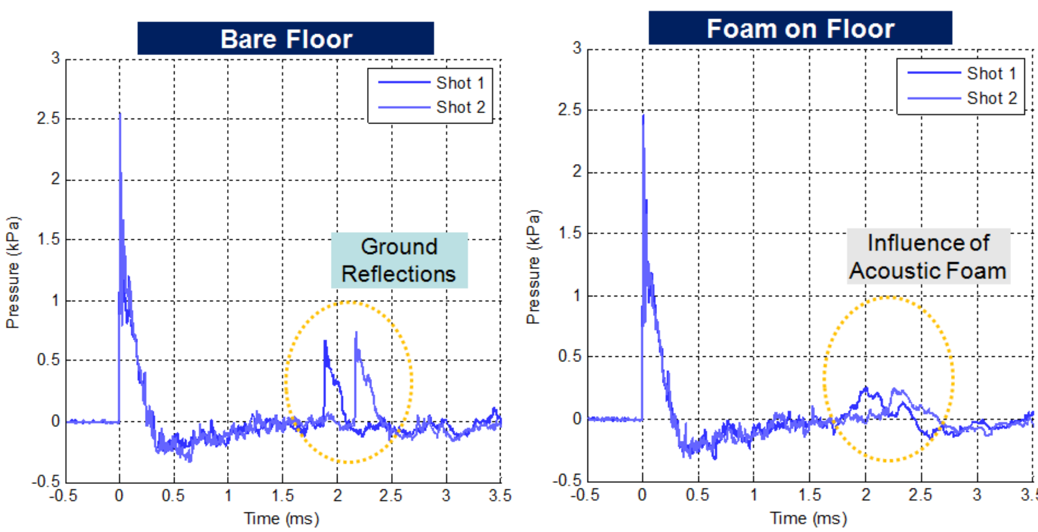

a) b)

Figure 67. Attenuation of ground reflection using foam. a) Bare floor b) Foam on floor

In Figure 67a there were two shots given, shot 1 was from the bottom tube and shot 2 was from the top tube. The time vector for each shot was shifted to time-align both traces for comparison. The effect of the height difference between the shot sources is observed in the time delay between the ground reflections from shot 1 and shot 2. When testing at the same conditions shown in Figure 5a, a layer of acoustic foam layered on the floor under the shock tube does an excellent job in reducing the secondary blast wave (Figure 67b). During testing with animal subjects, acoustic foam must be placed on the floor of the laboratory to mitigate the effects of this ground reflection. There is still a slight rise in pressure from the reflection but the peak is drastically reduced. More modifications can also be made in the experimental setup to further reduce this reflection effect.

To study angle-dependent effects on the pressure peak, the microphone and pressure sensor were held at a constant radial distance while the angle with the shock tube centerline was gradually increased in 10 degree increments. The tests consisted of two shots with two mil diaphragms at five second intervals. The sensors were mounted to rigid fixtures at a height of 29 inches, which is the average height of the two shock tubes and thus ensures symmetric shock data. The peak pressure of each shot was averaged between the microphone and the pressure sensors as shown in Figure 68. It was observed that the peak pressure slightly decreased as the angle from the centerline increases. For a 50 degree rotation, a change of 2.1 dB is considered a relatively minimal increase based on the proposed testing levels and their increments.

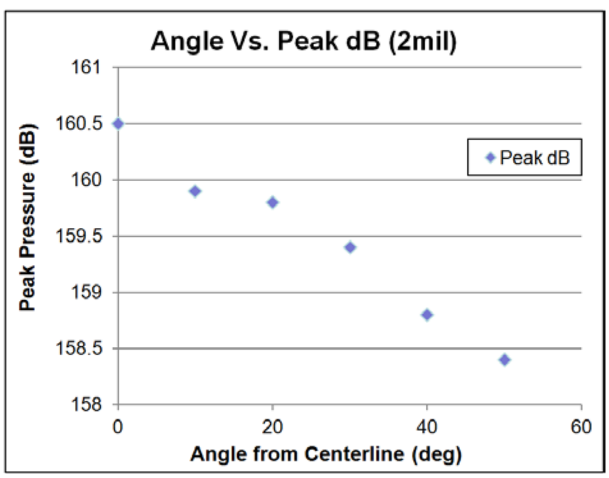

Figure 6

Figure 68. Relationship between the peak pressure and the shock tube centerline angle

To characterize variation of peak pressure with radial distance, the radial distance between the shock tube and sensors was gradually increased from 2 feet to 20 feet. For this test series, data was collected using 2 PCB microphones rigidly mounted at a height of 29 inches. Once again two shots were done for each test and the data was averaged to calculate the peak pressure relationship (Figure 69). The attenuation of pressure with distance has a very smooth and predictable logarithmic trend. The pressure peak variation with log of radial distance is linear with a slope of -10.13. This slope is much larger than -1 for spherical spreading. This data was collected using 0.5 mil diaphragms.

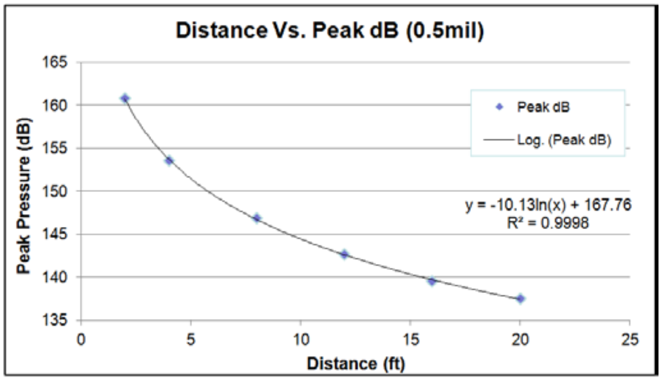

Figure 69. Relationship between microphone distance and peak pressure

The results from this characterization study suggest that 1) acoustic insulation must be used to reduce ground reflection; 2) angular deviations from the animal initial position will not have significant effect on the exposure dose; 3) radial effects on peak pressure can be significant in the near field (near the exit) since the peak pressure in dB varies as ~$\ln(1/r^{10})$. However, this effect will be minimal far from the exit. Based on the data collected, the animal placement during testing can be between 5 to 20 feet from the shock tube exit and at 10 degree from centerline. The exact radial distance was determined by the ability to produce a meaningful amount of auditory threshold shift in the animal as predicted from literature and previous experimental data.

A.1.4 Mapping of Microphone position at UCSD

To verify the initial calibration of the PPL versus microphone location performed at the L3 laboratory using the ARFST, a new calibration test series was performed at the UCSD laboratory. The calibration is necessary to map the PPL to microphone location in order to determine the optimal animal placements for blast exposure at the various required levels.

The floor mapping of the UCSD laboratory for microphone positioning is shown in Figure 70. Figure 70 shows the ARFST in the back with the double shock tube outlets aimed towards the front at the animal position. Two microphones are positioned near the animal head location, one close to the ear and the other in the free field, at the corresponding head location (without the animal). The animal is represented here by the empty holder. The locations tested are determined from the blue marks on the floor, which delineate the angles from the centerline of the ARFST and the radial distances from the shock tube outlet. Figure 70 is used for illustration purpose only to show the marked positons on the floor. During the actual tests, the floor and walls were covered with foams to attenuate the effects of reflection off the bare surfaces.

The PPLs were measured for two angles and four distances. The angles were 10^{o} and 20^{o} from the centerline, and the radial (standoff) distances were 4, 6, and 8 feet from the shock tube outlet. The measured PPLs for each position are shown in Table 39 for the three diaphragm thicknesses used in the ARFST. The diaphragm thicknesses were 0.5, 1.0, and 2.0 mil.

As shown in Table 39 the PPLs range spans from 146 to 160 dB for all positions and diaphragm thickness tested. As previously noted, angle variation has minimal effect on the PPL, with less than 1 dB PPL variation per 10^{o} angle deviation. For a fixed radial distance, the diaphragms provide between 3 to 5 dB gain.

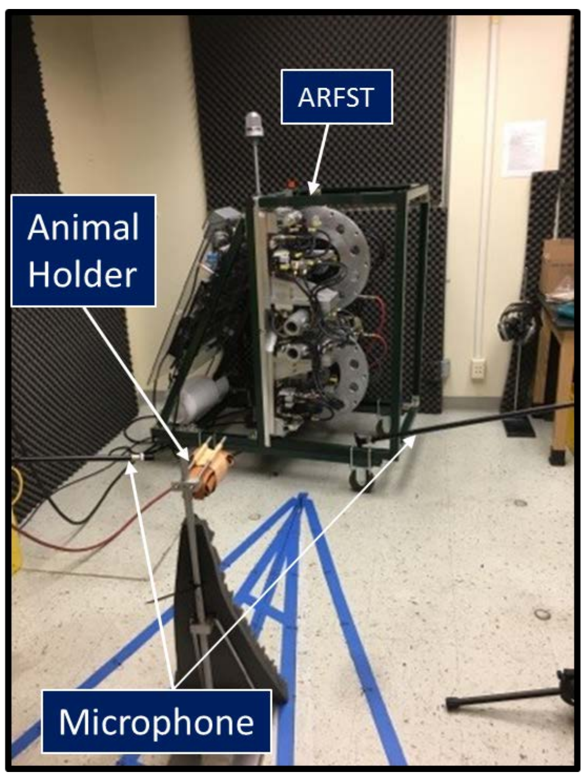

Figure 70. Illustration of UCSD lab floor mapping of PPL to microphone location

Table 38. PPL (in dB) versus microphone location (UCSD lab data)

Radial Distance (in ft.)	Angle (in ^{o})	Diaphragm thickness (in mil)		
		2.0	1.0	0.5
4	10	159.88	156.93	152.82
	20	160.58	157.02	153.26
6	10	156.04	152.85	149.33
	20	156.39	152.55	149.08
8	10	153.41	150.21	146.48
	20	153.21	149.80	145.92

Figure 71 shows the data comparison of the PPL calibrations performed at UCSD and L3 for an angle of 10^{o}, selected based on results from the spatial characterization study. The UCSD laboratory results for the three radial distances tested are plotted together with those from the full tests performed in the L3 laboratory.

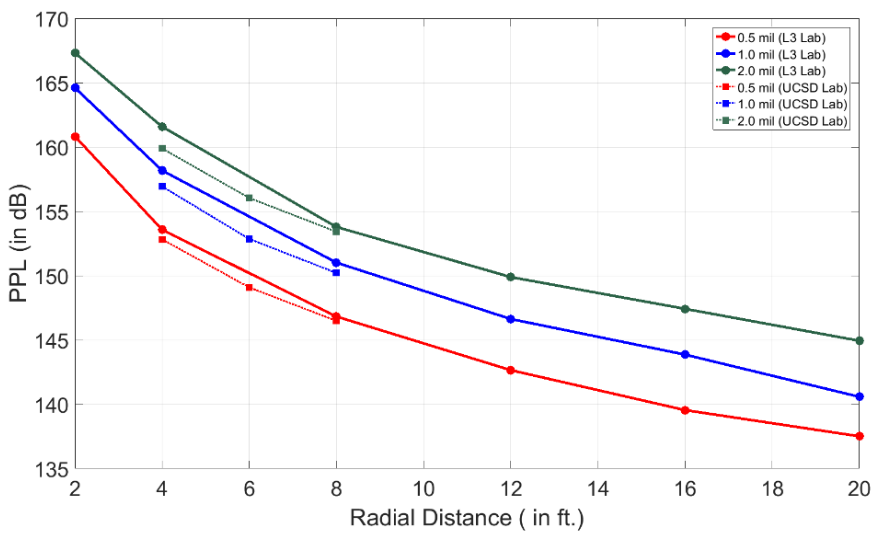

Figure 71. Comparison of PPL vs. standoff distance at 10^{o} from ARFST centerline

The results show that both calibration results agree with each other to within 2 dB across the three radial distances tested. At 8 ft. the USCD lab PPLs of ~146, 150, and 153 dB, for the 0.5, 1.0, and 2.0 mil diaphragm thicknesses, respectively are within 1 dB of those from the L3 lab. These PPLs are within the desired range of PPLs from 145-160 dB that were predicted based on literature and previous data. Hence, the optimal radial distance of 8 ft. at 10^{o} from the centerline was subsequently used as the animal position to collect the hearing deficit data induced by ME.

A.2 Calibration of the CNGS System

The CNGS designed to generate continuous background noise was tested by collecting the sound pressure level (SPL) at selective distances from the speakers using the sound level meter. The setup configuration is illustrated in Figure 72, and the results are shown in Table 40.

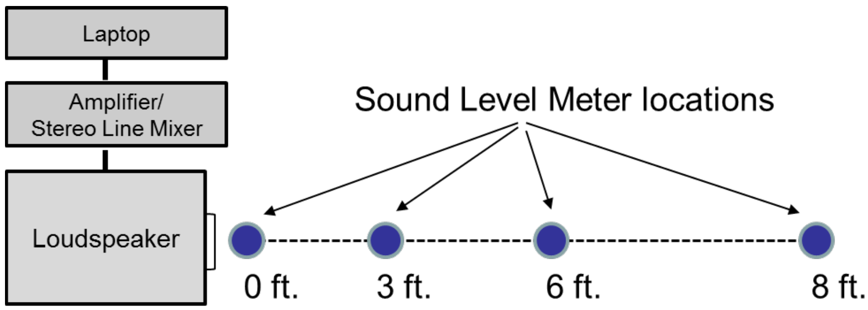

Figure 72. CNGS test configuration

In Table 40, the A-weighted SPLs recorded at the selective distances from the speaker are reported. Close to the speaker location (0 ft.), the maximum level of 105.8 dBA was recorded. The lowest SPL of 82 dBA was recorded at 8 ft., and the second maximum (88 dBA) was recorded at 3 ft. These latter levels correspond to peak levels of approximately, 114, and 122 dB PPL at 8 and 3 ft., respectively. It is therefore possible to produce the desired continuous noise levels of 90 and 100 dB PPL using the current CNGS. The positioning of the loudspeaker was optimized to produce the desired noise level at the animal ear.

Table 39. Sound levels recording using the CNGS

Distance (in ft.)	Fast time-weighting (in dBA)
0	105.8
3	87.0 – 88.0
6	83.0 – 84.0
8	82.0 – 82.9